Fall 2013

Effects of Dip-coated films on the Properties of Implantable Intracortical Microelectrodes

Salah Sommakia
Purdue University

Graduate School ETD Form 9
(Revised 12/07)

PURDUE UNIVERSITY
GRADUATE SCHOOL
Thesis/Dissertation Acceptance

This is to certify that the thesis/dissertation prepared

By Salah Sommakia

Entitled
EFFECTS OF DIP-COATED FILMS ON THE PROPERTIES OF IMPLANTABLE INTRACORTICAL MICROELECTRODES

For the degree of Doctor of Philosophy

Is approved by the final examining committee:

Jenna L. Rickus
Chair

Kevin J. Otto

Alyssa Panitch

James C. Clemens

To the best of my knowledge and as understood by the student in the *Research Integrity and Copyright Disclaimer (Graduate School Form 20)*, this thesis/dissertation adheres to the provisions of Purdue University's "Policy on Integrity in Research" and the use of copyrighted material.

Approved by Major Professor(s): Kevin Otto

Approved by: George R. Wodicka 11/26/2013
Head of the Graduate Program Date

EFFECTS OF DIP-COATED FILMS ON THE PROPERTIES OF IMPLANTABLE INTRACORTICAL MICROELECTRODES

A Dissertation

Submitted to the Faculty

of

Purdue University

by

Salah Sommakia

In Partial Fulfillment of the

Requirements for the Degree

of

Doctor of Philosophy

December 2013

Purdue University

West Lafayette, Indiana

To my uncle Ghazwan, who left us far too soon.

ACKNOWLEDGMENTS

The work presented in this dissertation could not have been achieved were it not for the kindness and encouragement of many, many individuals. First and foremost, I would like to thank my co-advisors, Dr. Kevin Otto and Dr. Jenna Rickus for taking me in, nurturing my scientific curiosity, and letting me go out on a limb with some of my ideas. Thank you for teaching me to think like a PhD, to step out of my comfort zone, and to face the challenges within me as well as the challenges without. Many thanks go out to my committee members, Dr. Jim Clemens and Dr. Alyssa Panitch, for their patience, support, and insights. Dr. Panitch's guidance and encouragement helped me immensely, from when I first started at Purdue, through the BIOMEDSHIP program, and up until my defense, and for that I am very grateful. Dr. Jamie Brugnano was always available for my seemingly endless queries, and was always willing to lend a me hand — and the occasional laboratory reagent. Dr. Sherry Voytik-Harbin deserves a special mention for her enthusiasm, spirit, and generosity. I learned great cell culture practices in her laboratory with Joanna Kuske who did most of the hands-on training; thank you both. Dr. Chris Rochet and his lab members, especially Dr. Kate Strathairn and Vartika Mishra, provided me with tissue samples for my cell culture studies. The great BME staff deserve a

huge thank you for all their support and hard work: the ever affable Bill Schoenlein for his constant encouragement and eagerness to help whenever I needed it; Dr. Allison Sieving and Dr. Marcia Pool for their dedication and friendship that made teaching BME labs fun; Sandy May for her meticulous organization and outstanding dedication that made navigating the graduate school bureaucracy so much easier; Dr. Andrew Brightman for his tireless advocacy for the department, his valuable advice, encouragement, and friendship; and Jim Jones and Megan Boing for so smoothly ensuring that everything behind the IT curtain worked flawlessly.

My Neuroprostheses Reseach Laboratory colleagues and friends were crucial to the accomplishment of this dissertation. Special thanks go to Janak Gaire for his training and assistance with surgeries; Matt McDermott for his advice on various chemistry techniques; Johnny Zhang for assistance with electrochemical measurements and MATLAB scripts; Dr. Andrew Woolley for confocal training and imaging advice; and Dr. Andrew Koivuniemi for discussions on rigorous statistics. Additionally, thanks to Roy Lycke, Hugh Lee, Andrew Ready, Ryan Verner, and Himanshi Desai for feedback and helpful discussions.

I am honored to have shared this journey with some great friends who provided me with feedback, support, inspiration, and genuine friendship. Dr. Trisha Eustaquio, Tarun Madangopal, Dr. David Jaroch, Dr. Aki Uchida, Camille Gaspard, Dr. Fatima Esseili, Dr. Wahbeh Qardaji, Yasmine Abraham, Dania Jaara, Abbas Abdallah, Dr. Elina Tzatzalos, Dr. Núria Royo, Dr. John Chap-

pelow, and Dr. Andrew Voyiadjis: thank you for walking with me along this path. Thanks to Dr. Don Werden for his invaluable advice and support, and to the graduate student group members for their support during rough times.

A special and deep thank you is due to my parents, Siba and Modar, for supporting and believing in me no matter what. I am who I am today because of their Herculean efforts. I could never thank them enough. Thanks to my brothers, Bassel and Hani, for playing along with their know-it-all older brother. A very deep thank you goes to my late uncle Ghazwan, my aunt Rima, and my cousins Sara and Rani, for receiving me into their house, life, and family like a son and a brother. I will always be grateful.

And finally, to the wonderful Michelle Stoller, for her limitless love and support. She was there for me through the darkest and toughest times, never giving up on me, even when I was ready to give up on myself. Michelle, I look forward to a life full of happiness with you.

TABLE OF CONTENTS

Page

LIST OF TABLES viii

LIST OF FIGURES ix

ABBREVIATIONS xiii

ABSTRACT xiv

1 RATIONALE AND SIGNIFICANCE 1

2 BACKGROUND 4

2.1 Common Electrode Array Designs 4

2.2 Progression of the reactive tissue response 8

2.3 Current approaches to improving electrode integration 18

3 SOL-GEL THIN FILM COATINGS FOR IMPLANTABLE INTRACORTICAL MICROELECTRODES 26

3.1 Introduction 26

3.2 Materials and methods 28

3.3 Results 31

3.4 Discussion 33

4 QUANTIFIABLE PROTEIN-ADSORPTION-CAUSED CHANGES IN ELECTRODE IMPEDANCE ARE PREVENTABLE USING DIP-COATED PEG 40

4.1 Introduction 40

4.2 Materials and methods 42

4.3 Results 45

4.4 Discussion 55

5 DIRECT CURRENT BIASING FOR THE RESTORATION OF SITE IMPEDANCE OF NEURAL MICROELECTRODES 60

Page

5.1 Introduction 60
5.2 Methods 63
5.3 Results 66
5.4 Discussion 73
6 CELLULAR RESPONSES TO MICROSCALE FOREIGN BODIES DIP-COATED WITH LPS AND PEG 75
6.1 Introduction 75
6.2 Methods 77
6.3 Results 82
6.4 Discussion 87
7 CONCLUDING REMARKS 94
7.1 Summary 94
7.2 Future Work 95
LIST OF REFERENCES 99
VITA 115

LIST OF TABLES

Table Page

4.1 Increase in resistance from baseline observed *in vivo* for No PEG vs. PEG treatment at 4 frequencies (mean ± standard error). 52

4.2 Increase in reactance from baseline observed *in vivo* for No PEG vs. PEG treatment at 4 frequencies (mean ± standard error). 54

4.3 Increase in total impedance from baseline *in vivo* for No PEG vs. PEG treatment at 4 frequencies (mean ± standard error). 55

LIST OF FIGURES

Figure Page

2.1 Examples of commonly used electrode arrays currently under investigation for use in neural prosthetic applications 4

2.2 Projected timeline of cellular responses to implanted electrodes in the CNS. Adapted from He and Bellamkonda [2008] 9

2.3 Immunofluorescence images showing some components of a glial scar around an electrode implanted in the cortex of a rat. Left image shows a layer of activated microglia; center image shows a layer of reactive astrocytes; right image shows decreased neuronal density. Scale bar = 100 μm. Modified from Biran et al. [2005] 16

2.4 Decline in electrical properties of implanted electrodes over time. Adapted from Vetter et al. [2004] 17

3.1 Fluorescence microscopy confirms the adherence of sol-gel coatings to microelectrodes. (A) Bright field image of probes to show their location. (B) Fluorescent micrograph of coated probes. Left probe is unlabeled control, right probe is fluorescently labeled. These images demonstrate that the silica sol-gels can be successfully applied to silicon-based microelectrodes. Additionally, these images confirm the ability to encapsulate molecules in the TMOS precursor to facilitate biomolecule delivery to the implantation site. Reprinted from Pierce et al. [2009] with permission. 32

3.2 (A) Representative cyclic voltammogram demonstrates changes in hysteresis curve. Cyclic voltammograms pre- and post-coating reveal an increase in current for each applied voltage of the sweep. This result indicates an increase in charge carrying capacity of the electrode site after application of the coating. (B) The average cathodic charge storage capacity (n = 92) increases after coating for all experimental sites. The increase in CV area is indicative of an increase in charge carrying capacity of the electrode following coating. Reprinted from Pierce et al. [2009] with permission. 34

Figure Page

3.3 Plots generated from EIS performed before and after coating show decreasing impedance losses with increasing frequency (n = 92). (A) Separated real and imaginary impedances show a resistance increase and reactance decrease following coating, with the most pronounced effects occurring at low frequency. (B) The total impedance shows a general decrease with the most pronounced effect also occurring for low frequency. The total impedance is dominated by the imaginary component. Reprinted from Pierce et al. [2009] with permission. . 35

3.4 (A) Representative Nyquist plot generated through electrochemical impedance spectroscopy demonstrates changes in impedance. Spectrograms obtained pre and post coating show a moderate decrease in impedance magnitude for all frequencies. (BŰD) Bar graphs showing average (n = 92) change in resistance (R), reactance (X), and total impedance (Z) following coating for (B) 100 Hz, (C) 1 kHz, and (D) 10 kHz. Resistance increases significantly for all frequencies. Reactance and total impedance decrease significantly at low frequencies, become unchanged near physiological frequencies (i.e. 1 kHz), and become significantly higher at high frequencies. The reactance increase at high frequency is much smaller in magnitude than the decrease seen at low frequency. Reprinted from Pierce et al. [2009] with permission. 36

4.1 (a) Total impedance magnitude spectrum for electrodes not pretreated with PEG before BSA application is higher than both the control and PEG treated electrodes. (b) Phase angle spectrum for electrodes not pretreated with PEG prior to BSA application shows a lower phase angle for lower and intermediate frequencies compared to the control, while the phase angle spectrum for electrodes pretreated with PEG exhibits smaller phase angles across all frequencies. 47

4.2 Nyquist plot for electrodes pretreated with PEG before BSA application is close to the control plot, with a slight shift to the left at lower frequencies, indicating a decrease in resistance. Nyquist plot for electrodes not pretreated with PEG before BSA shows a shift up and to the right, indicating increases in both resistance and reactance. . 48

Figure Page

4.3 Resistance: electrodes coated with BSA without PEG pretreatment exhibited considerable and statistically significant increases in resistance (real impedance) compared to uncoated controls at all frequency values studied. In contrast, electrodes treated with PEG prior to BSA application did not exhibit any significant increases in resistance compared to the control at all studied frequencies, and were all significantly lower compared to BSA coated electrodes. Control plot shown slightly offset to the left for clarity. Error bars represent the standard error of the means. 49

4.4 Reactance: for BSA coated electrodes, no change in reactance (imaginary impedance) was observed compared to uncoated control at 50Hz, whereas increases in reactance were observed at higher frequencies. PEG coated electrodes exhibited slight decreases in reactance compared to uncoated controls at frequencies greater than 50Hz. Control plot shown slightly offset to the left for clarity. Error bars represent the standard error of the means. 50

4.5 Total Impedance: for BSA coated electrodes, total impedance exhibited statistically significant increases compared to uncoated controls except at 50Hz. For electrodes treated with PEG prior to application in BSA, smaller but statistically significant decreases in total impedance were observed except at 10 kHz. Control plot shown slightly offset to the left for clarity. Error bars represent the standard error of the means. 51

4.6 *In vivo* increase in resistance from baseline. 53

4.7 *In vivo* increase in reactance from baseline. 54

4.8 *In vivo* increase in total impedance from baseline. 55

5.1 Effects of progressively increasing durations of DC biasing on total impedance (a), and resistance and reactance (b) 68

5.2 Nyquist plot of electrodes immersed overnight in multipurpose contact solution before DC biasing and after 10 seconds of DC biasing. 69

5.3 DC biasing returns electrode impedance at 1 kHz to baseline after exposure to protein and agar 71

5.4 Effects of DC biasing for 15 seconds on the 1 kHz impedance of electrodes acutely implanted into rat cortex, showing a reliable return to baseline. 72

Figure Page

6.1 Image quantification. Wells in 96 well plate (A) were imaged to produce a fluorescent image (B) and extract intensity profiles for each channel. The fluorescent image is pseudocolored to show neurons in red, astrocytes in green, and microglia in blue. Scale bar is 50 μm. For each examined region (examples shown within rectangles), three intensity profiles (C) are generated, and response indices calculated by summing the area under the graph corresponding to the chosen distances. 81

6.2 Microglia—interface. For the narrowest interface are, the only significant difference in the response index was between the PEG coated microwire and LPS coated microwire. For the wider interface areas, significant pairwise differences were observed between the LPS coated microwire and all the other microwires. Error bars represent standard errors of the mean. 83

6.3 Microglia—distant. For the closest distant bin (50-150um from edge of microwire), the response index for LPS coated microwire was significantly higher than all the other treatments. For the more distant bins, the only significant difference observed was between LPS coated microwire and PEG coated microwire in all 3 bins. Error bars represent standard errors of the mean. 84

6.4 Astrocytes—interface. In all examined interface areas, the astrocyte response index for LPS coated microwire was significantly higher than PEG coated and LPS+PEG coated microwire, but not uncoated microwire. Error bars represent standard errors of the mean. . . . 85

6.5 Astrocytes—distant. No significant differences were observed between the different treatments for the closest distant bin. For the middle two distant bins, a slightly significant difference was observed between LPS coated wire and LPS+PEG coated wire. Error bars represent standard errors of the mean. 86

6.6 Neurons. No significant differences in the neuron response index were observed between any of the treatments in interface or distant areas 88

ABBREVIATIONS

ICM	Intracotrical microelectrode
RTR	Reactive tissue response
PEG	Polyethylene glycol
HMWPEG	High molecular weight PEG
DC	Direct current
EIS	Electrochemical impedance spectroscopy
LPS	Lipopolysaccharide
TL4	Toll-like 4
SCI	Spinal cord injury
CNS	Central nervous system
SNR	Signal to Noise Ratio
BBB	Blood-brain barrier
PEDOT	Poly(3-4-ethylenedioxythiophene)
ECM	Extracellular matrix

ABSTRACT

Sommakia, Salah Ph.D., Purdue University, December 2013. Effects of Dip-coated films on the Properties of Implantable Intracortical Microelectrodes. Major Professor: Kevin J. Otto and Jenna L. Rickus.

The successful clinical use of implantable intracortical microelectrodes (ICMs) to treat certain types of deafness, blindness, and paralysis is limited by a reactive tissue response (RTR) of the brain. This RTR culminates in the formation of a tight glial scar and a loss of neuronal density around implanted ICMs, and is accompanied by a decrease in signal to noise ratio and an increase in impedance. While no comprehensive mechanistic understanding of the underlying biology is currently agreed upon in the field, a general consensus exists around a highly volatile acute RTR phase. During this acute phase, the electrical properties of ICMs do not always coincide with cellular responses, and the extent of initial injury appears to greatly influence the degree of the chronic RTR. While many electrode modifications and treatments are effective in the short term, the chronic RTR appears impervious to most interventions.

To better understand the acute phase of the RTR, this dissertation aims to investigate the effects of various dip-coated biomolecules on the electrical properties of ICMs and cellular responses to microscale ICM-like foreign bodies. We first present an examination of silica sol-gel thin films as a potential biomolecule

delivery platform which does not adversely affect the electrical properties of ICMs. The second study shows that adsorbed proteins, thought to play an important role in modulating the RTR, cause significant increases in electrode impedance. In contrast to prevalent electrical models of the electrode tissue interface which assume purely resistive impedance changes due to adsorbed proteins, our results show both resistive and capacitive changes. We also show that increases in impedance related to protein adsorption can be prevented by dip coating ICMs in an aqueous solution of high molecular weight polyethylene glycol (PEG). We then describe a method to clean electrode sites using direct current (DC) biasing, showing that DC biasing is capable of restoring electrode impedance following exposure to enzymatic cleaning solutions, proteins, phantom brains, and actual brain tissue. The final study in an in vitro mixed primary cortical cell culture model shows that lipopolysaccharide (LPS), a well-known ligand to toll-like 4 (TL4) receptors, dip-coated onto segments of metal microwire, can simulate localized inflammation around an implanted ICM. We observe elevated activation of glial cells in interface regions, and extending into more distant regions. This elevation in glial responses is not accompanied by a decrease in neuronal density. We additionally show that microwire dip-coated with a mixture of LPS and PEG exhibits significantly lower microglial and astrocyte responses.

These findings highlight the importance of adsorbed proteins, some of which are implicated in aggravating the reactive tissue response, but which we show

can result in significant increases in electrode impedance before the RTR even begins. These impedance changes can be prevented through the use of dip-coated PEG. Our cell culture data presents further evidence for the attractiveness of TL4 receptors as a target for intervention, and suggests that the loss of neuronal density observed in vivo is better explained by other mechanisms following device insertion than pure glial activation.

1. RATIONALE AND SIGNIFICANCE

Many traumatic injuries and degenerative diseases are currently incurable, but can be treated with varying degrees of success by implantable neural microelectrodes in the central nervous system. For example, Spinal Cord Injuries (SCI) occur at a rate of 11,000 cases per year in the U.S. and currently affect up to 400,000 Americans [Berkowitz et al., 1998] and are extremely costly to treat. Additionally, there are about 3.3 million Americans suffering from visual impairment [In et al., 2004] and about 750,000 affected by severe to profound hearing impairment [Mohr et al., 2001]. The lack of successful cures for sensory impairments and CNS injuries has stimulated research into using external devices to interface with the remaining healthy parts of the CNS, to create either a brain machine interface [Nicolelis et al., 2003] or a neural prosthesis capable of restoring or enhancing lost neural function. Such devices has been used with varying degrees of success to treat blindness [Maynard, 2001] and deafness [Lenarz et al., 2006, Loeb, 1990] and to enable bladder and muscle control in paralyzed patients [Grill, 2000]. For devices interfacing with the central nervous system, two distinct approaches exist. The first approach is to use surface electrodes that rest on top of the brain surface [Leuthardt et al., 2004]. Surface electrodes, however, are limited by the organization of cortical cells into dis-

tinct layers and columns within those layers, placing target neuron populations deep within the cortex. The second approach employs penetrating intracortical electrodes which offer unique abilities to target deep neuron populations with high specificity [Normann et al., 1999, Otto et al., 2005]. While intracortical implants have been shown to be feasible, they are unreliable in chronic settings. They encounter decreased signal to noise ratios (SNR), increased impedance and a loss of discrimination [Vetter et al., 2004]. The degradation in electrical characteristics of the electrode-tissue interface is correlated with a reactive response of brain tissue. The trauma of insertion initiates a cascade of events culminating in the formation of a glial scar around the electrode, isolating it from the surrounding healthy brain tissue. Various treatments have been investigated to mitigate this reactive tissue response, but no completely effective solution has been found.

The state of the art in the field holds that a highly volatile acute phase is susceptible to various interventions, but that beneficial effects are typically lost within a few weeks once the chronic response sets in. There is a lack of a detailed and comprehensive understanding of the relation between the biological components of the reactive tissue response and the changes in electrical properties of the implanted ICM, which do not always exhibit a consistent correlation. Many current studies into neurointegrative interventions are performed on non-functional electrodes for various reasons of cost-effectiveness and con-

venience, making it difficult to draw solid and accurate conclusions as to the efficacy of such interventions. This dissertation will attempt to shed some light on some of these unaddressed points. A background review of the literature will be presented in Chapter 2, surveying common electrode designs and their application, and attempt to summarize current knowledge about the progression of the reactive tissue response as well as various interventions. Chapter 3 will discuss silica-sol gel thin films as coatings for neural microelectrodes with potential bioactivity without adverse effect on electrode properties. Chapter 4 will discuss details of impedance changes to electrode properties following exposure to a model protein, and demonstrate how such changes can be prevented by applying a dip-coated film of high molecular weight polyethylene glycol (PEG). A preliminary *in vivo* study will also be presented, investigating how impedance increases *in vivo* can prevented by applying PEG topically into the brain and examining the implications. Chapter 5 will describe a method of cleaning electrode sites using relatively long duration direct current (DC) pulsing, suitable for acute experiments. Chapter 6 will investigate the cellular responses to ICM-like microscale foreign bodies in a primary mixed cortical cell culture model. Using lipopolysaccharide (LPS) to induce microglial activation, we simulate localized inflammation without the presence of blood brain barrier injury, and attempt to draw physiologically relevant conclusions from the behavior of the various cell types. Chapter 7 will summarize and offer conclusions, unanswered questions, and potential future work.

2. BACKGROUND

2.1 Common Electrode Array Designs

Factors such as cost and availability guide the choice of electrode array, but a basic understanding of each design's advantages and limitations is essential for long term studies, especially when the reactive tissue response to the implanted electrode is to be considered. Figure 2.1 shows examples of penetrating intracortical electrode arrays under investigation for neural prosthetic applications.

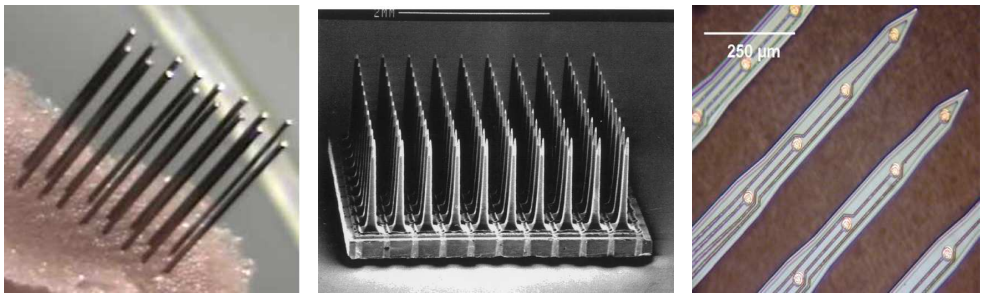

(a) Microwire Array; adapted from Williams et al. [2007]

(b) Utah Electrode Array; adapted from Normann et al. [1999]

(c) Michigan probe; adapted from Vetter et al. [2004]

Fig. 2.1. Examples of commonly used electrode arrays currently under investigation for use in neural prosthetic applications

2.1.1 Microwire

Microwire neural electrodes have been used since 1958, when Strumwasser reported the feasibility of using 80 μm diameter stainless steel wire for obtaining single neuron recordings lasting more than a week from awake, unrestrained animals [Strumwasser, 1958]. Current microwire-based electrodes are usually made of a conducting material such as gold [Yuen and Agnew, 1995], iridium [Liu et al., 1999], tungsten [Williams et al., 1999], or stainless steel [Nicolelis et al., 2003]. The microwire is coated with an insulating material, leaving the tip exposed to act the electrode site. They are usually arranged into arrays to cover a larger cortical area. The electrode counts of commonly utilized arrays have ranged from four [Yuen and Agnew, 1995] to more than 100 [Nicolelis et al., 2003]. While microwire arrays are relatively easy to construct, they are prone to bending during insertion, introducing uncertainty about the precise location of the microwires within the cortex [Edell et al., 1992]. Size considerations mean that blunt microwires, usually implanted in bundles [Cheung, 2007] can cause unacceptable levels of neuron displacement during insertion. These limitations necessitated the development of alternative electrode substrate materials and fabrication methods, paving the way for the next generation of silicon arrays.

2.1.2 Micromachined silicon-based electrode arrays

Silicon micromachining techniques have enabled the uniform production of microelectrodes with high electrode site counts and allow complex designs [Polikov et al., 2005], resulting in more design flexibility to counter the problem of the reactive tissue response. Photolithography methods applied to electrode fabrication enable great control over electrode size, shape and spacing. Smaller electrodes result in better spatial discrimination [Kipke et al., 2003] allowing the design of more sensitive electrodes. Additionally, electrode spacing has proven important in recent research into the effect of electrode depth within the brain on neural prosthetic control [Schwarz, 2004]. Among the many electrode array designs tested, two designs have emerged as de facto standards within the neural engineering community: the Utah electrode array (UEA), originally developed at the University of Utah, and the Michigan probe, originally developed at the University of Michigan.

Utah electrode array

The UEA is an array of sharpened conductive silicon shanks, that is fabricated from a single block of silicon through repeated steps of doping and etching. The silicon shanks are individually isolated, with the electrode site at the tip [Cheung, 2007]. The UEA has come a long way since Campbell et al. [1991] demonstrated its feasibility as a neural prosthetic device in 1991. It has

been recently employed in a BMI tested in a severely tetraplegic human patient [Hochberg et al., 2006]. A major drawback of the UEA is the location of the electrode sites at the tip of the silicon shanks, restricting control over the depth location of the electrode sites. Some attempts have been made to overcome this limitation through fabricating a UEA with graded shank lengths to permit excitation and recording at different depths [Badi et al., 2003].

Michigan array

The Michigan probe currently produced by the Center of Neural Communication Technology (CNCT) evolved from the original designs of Kensall Wise at the University of Michigan [Wise et al., 1970]. The advantage of Michigan probes is the reproducible fabrication of shanks with a high precision electrode placement [Cheung, 2007]. This layout allows for research into the electrical activity of different layers in the cortex and for the precise marking of the location of the electrode sites within the cortex [Townsend et al., 2002]. This kind of precise mapping of electrode location was not previously possible. While acute recording and stimulation with Michigan probes have been shown to be feasible [Hetke and Anderson, 2002, McConnell et al., 2007], there is interest in developing chronic applications. The chronic response of brain tissue has been studied extensively using Michigan probes. Many studies on treatments for integrating implantable electrodes with neural tissue are conducted using Michigan probes supplied by CNCT.

2.2 Progression of the reactive tissue response

The reaction of CNS tissue to implanted devices is physiologically unique due to the presence of the blood-brain barrier (BBB). The BBB consists of closely packed endothelial cells surrounded by astrocytic processes. This layer protects the brain from biochemical fluctuations in the periphery by restricting the passage of certain molecules, while allowing the passage of nutrients and oxygen [Shoichet et al., 2008]. Chronic BBB injury has been pinpointed as a major factor in the adverse brain tissue response to implanted microelctrodes[Saxena et al., 2013]. The response of brain tissue to implanted electrodes is an aggregate of many sub-responses involving many cell types in the brain, including glial cells, neurons, meningeal fibroblasts and blood macrophages. Over all, the tissue response can be divided into an acute and a chronic components. Figure 2.2 shows a hypothetical timeline of the response of various cell types in the CNS to an implanted electrode.

2.2.1 Acute (initial) response

Vascular damage, edema, and biofouling

The cortex has a high vascular density with small capillaries forming dense networks between larger, longitudinal vessels [Cavaglia et al., 2001]. The injury process following electrode insertion into the brain begins with the inevitable breach of the blood-brain barrier, releasing serum and blood cells into the in-

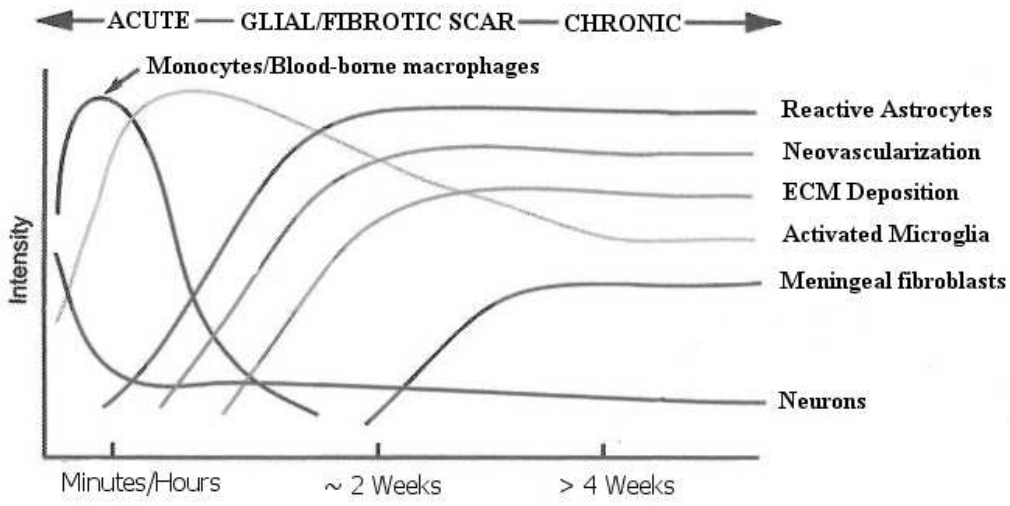

Fig. 2.2. Projected timeline of cellular responses to implanted electrodes in the CNS. Adapted from He and Bellamkonda [2008]

jury site [Clark et al., 1994]. Studies performed in live brain slices show that vascular damage in the CNS in response to electrode insertion can be classified into four categories: fluid displacement, vessel rupture, vessel severing and mechanical dragging by the device [Bjornsson et al., 2006]. Electrode insertion also damages neurons and glial cells, causing the immediate accumulation of cellular and myelin debris at the injury site [Fawcett and Asher, 1999, Polikov et al., 2005]. During insertion electrodes penetrate the meningeal surface carrying meningeal cells into the brain and allowing for their migration along the electrode shank [Krueger et al., 1986]. Migrating fibroblasts attempt to recreate the glia limitans, a layer of tightly meshed astrocytic processes and fibroblasts separating neurons in the brain from the pia mater [Ramer et al., 2001].

Vascular damage results in clot formation. Platelets adhere to collagen fibers from the broken endothelium of the damaged blood vessels, forming the initial hemostatic plug. They subsequently upregulate the high-affinity platelet integrin αIIbβ, which mediates further platelet aggregation [Ruggeri, 2002]. Once bound, platelets degranulate, releasing plasma coagulation factors which trigger the formation of a fibrin clot [Standeven et al., 2005]. Activated platelets also release signaling molecules such as platelet-derived growth factor (PDGF) [Deuel and Huang, 1984, Heldin, 1992], transforming growth factor-β (TGF-β) [Assoian et al., 1983] and vascular endothelial growth factor (VEGF) [Mohle et al., 1997, Papavassiliou et al., 1997]. These factors attract extravasated inflammatory blood-borne cells to the injury site, leading to the formation of brain

edema [Klatzo, 1987, Schilling and Wahl, 1997, 1999, Wahl et al., 1988]. Local edema increases pressure around the implantation site, resulting in the further neuronal displacement [Polikov et al., 2005]. Extravasated proteins contribute to the later inflammatory response; for example, thrombin has been suggested as a trigger for microglia [Choi et al., 2003, Hanisch et al., 2004, Moller et al., 2000] and astrocyte [Ehrenreich et al., 1993, Grabham and Cunningham, 1995, Suidan et al., 1997] activation. Protein adsorption, contributes to the immune response to implanted materials everywhere in the body, ultimately affecting device biocompatibility [Williams et al., 1985]. Adsorbed proteins have been implicated in increasing the levels of activated glia, especially microglia, at the device/tissue interface [Leung et al., 2008].

Activation of glial cells

Glial cells form the majority of the cells in brain, constituting about 75% of the total brain volume [Purves et al., 1997]. Previously thought to only provide structural support for neurons, glial cells have been found to provide growth cues to neurons during development, control the chemical environment in the brain and modulate electrical activity of neurons, among many other functions [Kettenmann and Ransom, 2005]. The main glial cells involved in the reactive tissue response to implanted electrodes that are discussed in this document are microglia and astrocytes. The exact details of glial activation are still

under investigation, but the phenotypical transformations that they undergo are well characterized.

Microglia While the question of the ontogeny of microglia is controversial, the most prevalent view holds that they arise from the prenatal arrival of blood-borne monocytes into the CNS [Kaur et al., 2001]. Microglia roam the brain acting as pathological event sensors, performing multiple functions including activation, proliferation and migration to the injury site [Kreutzburg, 1996]. In the absence of injury, ramified (resting) microglia exist in a highly branched state, constituting 5-10% of the total number of glial cells in the brain [Ling, 1981]. Following injury microglia interact with various cytokines adsorbed onto the implanted surface, as well as chemokines present in the vicinity of the injury site, and undergo activation. Activation is mediated through many factors such as ATP, toll-like receptor 4, and reactive oxygen species [Davalos et al., 2005, Okun et al., 2011, Qin et al., 2005, Tanga et al., 2005]. Microglial activation involves cell proliferation and the assumption of a compact ameboid morphology indistinguishable from macrophages [Fawcett and Asher, 1999]. Microglia begin to perform functions similar to macrophages including phagocytosis of foreign materials and upregulation of lytic enzymes to aid in the degradation of the foreign materials [Polikov et al., 2005]. Analysis of the glial sheath ex vivo around electrodes implanted in rat brains [Biran et al., 2005] and *in vitro* in primary rat cortex cultures [Polikov et al., 2006] shows that microglia form

the glial scar layer closest to the electrode surface, suggesting they are the first glial cell type to respond to implanted electrodes. They adhere to the surface of the electrode and act as a source for proinflammatory cytokines, such as IL1-β and TNF-α [Leung et al., 2008]. The accumulation of activated microglia may amplify the cytokine production cascade. Attenuating the production of these proinflammatory cytokines, either through prevention of microglial adhesion or direct intervention in the inflammatory pathways, may be a key factor to improving the neurointegration of chronically implanted electrode.

Astrocytes Astrocytes comprise 30-65% of glial cells in the CNS [Nathaniel and Nathaniel, 1981]. They possess a characteristic star shape with fine cellular processes, comprised of 8-10nm diameter filaments of polymerized glial fibrillary acidic protein (GFAP), considered to be a specific marker for astrocytes [Eng, 1985]. Following injury, astrocytes assume a reactive phenotype, undergoing dramatic biochemical and functional changes characterized by proliferation and hypertrophy through the upregulation of GFAP [Pekny and Nilsson, 2005]. This process is usually termed "reactive gliosis" [Norton et al., 1992]. Astrocyte activation initiates the chronic response and the formation of the glial scar, discussed in the following section. Astrocytic phenotype transformation also involves a switch from being conducive to neuronal growth towards being inhibitory [Davies et al., 1996].

2.2.2 Chronic (sustained) response

Formation of glial scar

The most prominent manifestation of the long-term response to implantable electrodes in the CNS is the formation of the glial scarâĂŤthe analogue of the fibrous encapsulation tissue observed in non-CNS tissue in response to non-degradable materials [Polikov et al., 2005]. In non-CNS tissue, fibrous encapsulation occurs when macrophages encounter a large non-degradable object that they are incapable of phagocytosing. In response, macrophages fuse into multinucleated foreign body giant cells and continue to secrete degradative factors such as superoxides and free radicals. In the CNS, the equivalent cells are microglia. Upon failing to phagocytose the implanted electrode, they persist in an activated state, further increasing neuronal damage). The main component of the glial scar, however, is not activated microglia, but reactive astrocytes bound by tight and gap junctions [Edell et al., 1992, Fawcett and Asher, 1999, Turner et al., 1999]. Pathological production of extracellular matrix components, such as laminin, collagen, and proteoglycans generally accompanies —and mediates— the formation of the glial scar in spinal cord and traumatic brain injury [Asher et al., 2001, Fitch and Silver, 2008, Liesi and Kauppila, 2002, McKeon et al., 1999]. A persistent glial scar forms as a response to the continued presence of the electrode within the brain [Biran et al., 2005, Rousche et al., 2001]. The *in vivo* formation of the glial scar exhibits great variabil-

ity between experiments. Even within the same experiment, some shanks of multi-shank probes elicit limited scarring while other shanks result in extensive scarring [Edell et al., 1992, Rousche and Normann, 1998]. The extent of the glial scarring is dependent on the amount of the initial damage done during insertion [Szarowski et al., 2003]. The chronic glial scar around an implanted electrode at 2 weeks is composed of reactive astrocytes 500–600 μm from the implanted electrode at about 2 weeks. Over time the area of the scar region decreases, but cells become more compact and tightly bound by weeks 6 to 12, with a thickness of 50–100 μm around the implant [Szarowski et al., 2003, Turner et al., 1999]. An *in vitro* model produced by Polikov et al. [2006] demonstrated a similar pattern of glial scar formation around microwires. The formation of the glial scar has been implicated as the cause for the dramatic increase of the impedance of implanted electrodes [Edell et al., 1992, Otto et al., 2006, Williams et al., 1999]. Observations of the total impedance magnitude of implanted electrodes over time reveal a marked jump at about 1 week post-implantation [Otto et al., 2006, Williams et al., 2007], displaying close temporal correlation to the formation of the tight junctions between the astrocytes in the glial scar. Proteins secreted by reactive astrocytes also play an important role in the ensuing neuronal response to electrode implantation. For example, reactive astrocytes also simultaneously produce type IV collagen and $\alpha 1$ laminin, leading to the formation of a basement membrane which blocks the neuron-outgrowth-promoting effects of $\gamma 1$ laminin secreted by resting astrocytes [Liesi and Kauppila, 2002].

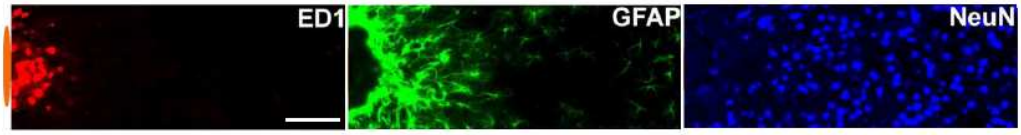

Fig. 2.3. Immunofluorescence images showing some components of a glial scar around an electrode implanted in the cortex of a rat. Left image shows a layer of activated microglia; center image shows a layer of reactive astrocytes; right image shows decreased neuronal density. Scale bar = 100 μm. Modified from Biran et al. [2005]

Figure 2.3 shows a representation of cellular distributions around an implanted electrodes 4 weeks after implantation, demonstrating minimally overlapping layers of activated microglia and reactive astrocytes, and a decline in neuronal density around the electrode.

Loss of neuronal density

The formation of the glial scar is accompanied by a loss of neural density in the vicinity of the implanted electode [Biran et al., 2005] and a decline in the recorded SNR over time [Vetter et al., 2004]. Reports of the size of this area of depleted neuronal density vary from about 1 μm to over 100 μm [Stensaas and Stensaas, 1976, Turner et al., 1999]. One explanation for this phenomenon is that insertion trauma causes neuronal death, leading some researchers to coin the term “kill zone”[Edell et al., 1992]. This explanation has been disputed by studies confirming the presence of neurons in the vicinity of the implanted

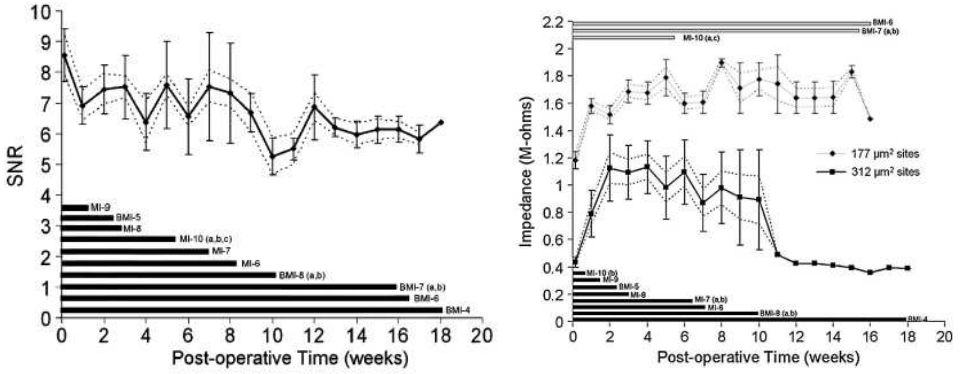

(a) Decline of SNR over time

(b) Gradual increase in impedance magnitude over time

Fig. 2.4. Decline in electrical properties of implanted electrodes over time. Adapted from Vetter et al. [2004]

electrode and the ability to record neural signals during the first week post-implantation [Biran et al., 2005, Williams et al., 1999]. This finding implies that neurons survive throughout the initial response. Several studies have reported a gradual decline in signal strength over time [Liu et al., 1999, Nicolelis, 2003, Vetter et al., 2004], suggesting that a gradual remodeling of neural tissue around the implanted electrode –where neurons are slowly displaced by migrating reactive microglia and astrocytes– is responsible for the decline in signal quality. Figure 2.4 shows the progressive decline of electrical properties of implanted electrodes. The left panel (Figure 2.4(a)) shows the decline in recorded SNR over time, while the right panel (Figure 2.4(b)) shows the gradual increase in impedance magnitude, with an abrupt increase between 7 and 10 days post-implantation.

2.3 Current approaches to improving electrode integration

Neurointegrative treatments can be implemented as a preventative method prior to electrode implantation. Preventative measures include electrode design elements, coating electrodes with conductive materials to improve their ability to deliver electrical charge beyond the glial scar or coating with biomimetic materials to suppress or eliminate the reactive tissue response. Neurointegrative treatments can also be applied during the implantation procedure (through local or intravenous delivery of anti-inflammatory drugs) or post-implantation by applying electrical fields of various strength to either guide neuron growth towards the electrode or to break up the disruptive glial scar layer. These approaches will be discussed in detail in the following sections.

2.3.1 Electrode design elements

One of the strongest efforts in current neuroprosthetic device development is research into ultrasmall electrodes and highly flexible materials to address mechanical mismatch between implanted electrodes and brain tissue. It has been shown that reducing electrode size and surface area results in smaller glial scars and improved neuronal integration [Kozai et al., 2012a, Seymour and Kipke, 2007, Skousen et al., 2011]. Smaller and more flexible electrodes have their disadvantages, most notable that they are difficult to insert through the pia and into the brain. Some potential solutions have been to use degradable

insertion shuttles [Kozai and Kipke, 2009], mechanically adaptive electrode materials [Harris et al., 2011] or a combination of both [Lewitus et al., 2011]. Dissolvable insertion shuttles, however, might subject their flexible cargo to substantial fluid forces [Rakuman et al., 2013]. Recent findings have suggested that material density might be as important as its stiffness [Lind et al., 2013].

2.3.2 Electrode enhancing treatments

The need for higher currents to stimulate neurons in the brain, in addition to the formation of the glial scar and the accompanying increase in impedance, necessitated the development of electrode materials capable of delivering higher amounts of electrical charge per unit surface area , a property known as charge injection capacity [Cogan, 2008]. A trade-off exists between the selectivity of neural electrodes (the ability to record from and stimulate a small number of neurons) and their sensitivity (the ability to pick up weak neural activity in the presence of thermal noise and signal loss through shunt pathways) [Ludwig et al., 2006]. A common approach to address this issue is to modify the electrode surface by adding a layer of a different material to either increase the charge injection capacity or increase the surface area to lower the impedance. The goal of such modifications is to increase the sensitivity while retaining a small enough electrode size to maintain acceptable sensitivity. The most prevalent method to enhance an electrode's electrical properties is the use of conductive polymers. Poly(3,4-ethylenedioxythiophene) (PEDOT) codeposited with Polystyrene Sul-

fonate (PSS) onto electrode sites of Michigan probes results in an electrochemically stable, fuzzy film with an impedance two orders of magnitude lower than native electrodes [Cui and Martin, 2003, Cui and Zhou, 2007, Yang and Martin, 2004]. More recent research has further validated the use of PEDOT as a micro-neural material for electrostimulation [Wilks et al., 2009], allowing for miniaturization of electrode site size without sacrificing sensitivity [Ludwig et al., 2011]. The superior electrical properties and electrochemical stability of PEDOT have made it a favorite candidate among the conductive polymers for use in neural electrodes. Chronic tests of PEDOT *in vivo* show that PEDOT-coated sites outperform uncoated electrode sites in SNR metrics(Ludwig et al., 2006). PEDOT-coated electrodes, however, exhibit impedance fluctuations, attributable to the delamination of the films from the electrode sites, leading to the investigation of more stable PEDOT films, such as PEDOT nanotubes [Abidian and Martin, 2009, Abidian et al., 2009, 2010]. PEDOT can also be polymerized in living neural tissue, depositing in the extracellular spaces and forming 'fingers' which protrude far enough into the neural tissue to potentially extend past any fibrous tissue attempting to encapsulate the electrode [Richardson-Burns et al., 2007]. Some studies have attempted to decorate PEDOT films with biological molecules to further improve its integration with neural tissue [Cui and Martin, 2003, Green et al., 2009]. While these treatments achieve improved electrical properties *in vivo*, they are typically limited to the electrode site area. In the most common electrode designs, electrode sites cover only a small por-

tion of the total area of electrode. Other neruointegrative treatments focus on covering the entire electrode surface as described in the following sections.

2.3.3 Biomimetic coatings

There are two main approaches to designing coatings that mimic the local ECM in the CNS. The first approach aims to encourage neuron attachment to the electrode, while the second approach aims to manipulate glial cells in an attempt to attenuate glial scar formation [Polikov et al., 2005].

Several studies have attempted to create surfaces more conducive to neural growth by incorporating or immobilizing cell adhesion molecules. A common approach is the use of multipeptide fragments of laminin for the purpose of modulating neural attachment and growth. The coating methods employed include covalent immobilization on dextran-coated surfaces [Massia et al., 2004], covalent immobilization on amino-modified glass (Kam et al., 2002), self-assembling peptide nanofibers [Tysseling-Mattiace et al., 2008, Wu et al., 2006], copolymerization with conductive polymers [Cui et al., 2001, Stauffer and Cui, 2006], electrostatic layer-by-layer deposition [He et al., 2006], microcontact printing [James et al., 2000, St. John et al., 1997], fiber templating within a hydrogel [Yu and Shoichet, 2005], and covalent binding to silica sol-gel [Jedlicka et al., 2006, 2007a].

These studies present *in vitro* results showing that coatings containing whole laminin (He and Bellamkonda, 2005), laminin sequences YIGSR [Cui et al.,

2001, Yu and Shoichet, 2005] or IKVAV [Jedlicka et al., 2007a, Massia et al., 2004, Yu and Shoichet, 2005] result in improved neuron and neuron-like cell (PC12) growth. The incorporation of the laminin fragment RGD, however, resulted at best in a non-specific effect on multiple cell types [Zhang et al., 2005] and at worst a preferential adhesion affinity for non neuronal cells [Kam et al., 2002]. More recently, the immobilization of a neuron specific adhesion molecule, L1, on a silicon substrate electrodes was investigated and showed improved neural adhesion *in vitro* [Azemi et al., 2008] and *in vivo* [Azemi et al., 2011].

Kam et al. have taken the converse approach, studying the effects of peptide sequences on astrocyte adhesion [Kam et al., 2002]. Their results showed that YIGSR and IKVAV have no effect on astrocyte growth and adhesion *in vitro*, but that the Neural Cell Adhesion Molecule (NCAM) sequence KHIFSDDSSE causes increased astrocyte growth compared to fibroblasts. Since NCAM is known to have an inhibitory effect on astrocyte proliferation following injury [Sporns et al., 1995]. Kam et al. argue that immobilizing the KHIFSDDSSE sequence to a neural electrode could attenuate the intensity of the resulting glial scar *in vivo*. The effect of this NCAM-modified surface on neurons was not investigated, and there was no *in vivo* follow up.

While these *in vitro* studies show potential for biomimetic coatings, *in vivo* studies have yet to show an unambiguous improvement in the reactive tissue response when such coatings are used. Cui et al. [2003] have shown that the incorporation of YIGSR in polypyrrole coatings result in more neuron survival at

the electrode site compared to control sites. He et al. [2006] have demonstrated that electrostatically deposited laminin results in a less intense glial scar. Neither of these studies, however, show a concrete and satisfactory improvement of electrode performance over a long time scale, and much research remains to be done in this field.

2.3.4 Drug elution

A different approach to neurointegrative coatings is to use drug elution to attenuate the inflammatory response to the implanted electrode. Such additives include neuropeptides such as α-melanocyte-stimulating hormone (α-MSH) and synthetic glucocorticoids such as methylprednisolone and dexamethasone [He and Bellamkonda, 2008, Li et al., 2005]. Peripheral injections of dexamethasone starting at the day of injury and continuing for 6 days have been shown to result in a profound attenuating effect on both the initial and sustained tissue responses [Spataro et al., 2005]. The systemic delivery of such anti-inflammatory compounds risks significant side effects, however, leading to research into drug elution techniques for the local delivery of these agents to the injury site. Ravi Bellamkonda's research group has demonstrated the feasibility of local anti-inflammatory drug delivery. Using a nitrocellulose-based coating for the sustained *in vivo* release of dexamethasone [Zhong and Bellamkonda, 2007] and α-MSH [Zhong and Bellamkonda, 2005] they showed a weakened tissue response over a four week period. Kim and Martin have demonstrated a

successful system for *in vitro* dexamethasone release from an alginate hydrogel matrix [Kim and Martin, 2006]. Wadhwa et al. [2006] have implemented a system for the electrochemically-controlled release of dexamethasone *in vitro* from polypyrrole films, while Abidian et al. [2006] have implemented a similar system for dexamethasone release from PEDOT and polypyrrole. A limitation of controlled drug release is that it is not sustainable over the long term, typically lasting days to weeks. To counter this limitation, He et al. [2007] immobilized α-MSH onto the silicon surface of neural electrodes resulting in an anti-inflammatory surface that elicited a significantly weaker tissue response.

Using a different approach to mitigate the reactive tissue response, Winter et al. [2007] have implemented a system for the controlled release of nerve growth factor (NGF) from a polyethylene glycol-polylactic acid (PEGPLA) hydrogel. This *in vitro* study showed that NGF-loaded hydrogel coatings on neural microelectrodes can sustain the release of NGF for 1 week with little effect on the electrical properties of the electrodes a significant positive effect on the survival and neurite extension of PC-12 cells.

While there is an extensive body of literature describing the reactive brain tissue response to implantable electrodes, there is no completely successful treatment regime currently in place. Sheafs of published literature currently show that any efficacy displayed by a particular treatment only lasts for a month at most. This places a huge obstacle to the further implementation of intracortical microelectrode-based neural prostheses. As shown by Szarowski et al.

[2003], the extent of the glial scar depends greatly on the extent of the acute damage, demonstrating the need to modulate the initial response, especially edema and the attachment and activation of microglia.

One important factor affecting the extent of the reactive tissue response, demonstrated by Seymour and Kipke [2007] is electrode size. The many advantages of silicon-based microelectrodes, including ease of fabrication and reliable large-scale production, make them indispensable in neuroprosthetic research at this point, despite their non-optimal size. Neurointegrative coatings must be designed in such a way that they do not exacerbate neuronal displacement, yet have enough coverage to treat the entire device shank, rather than just the electrode site.

3. SOL-GEL THIN FILM COATINGS FOR IMPLANTABLE INTRACORTICAL MICROELECTRODES

3.1 Introduction

The complexity underlying the RTR to implanted ICMs means that approaches towards mitigating it will likely entail multiple modalities, including immobilized biomimetic biomolecules, locally released anti-inflammatories, and systemically delivered drugs. Current drug delivery platforms are dominated by hydrogels [Kim and Martin, 2006, Winter et al., 2007], which, while well established, are large in scale in comparison to ICMs, and might exacerbate neuronal displacement effects. Some electrically conductive electrode coatings, such as PEDOT and carbon nanotubes, are capable of drug loading and delivery [Abidian et al., 2006, 2007]. They are, however, typically deposited only on the electrode sites, and cover only a small fraction of the indwelling part of the device. While some success has been demonstrated with direct grafting of bioactive molecules onto the substrate of the ICM device shanks [Azemi et al., 2008, 2011], such approaches can require multiple steps and the use of complicated chemical techniques.

One promising approach to mitigating the reactive tissue response is to coat the microelectrodes in a porous silica thin film using the sol-gel method. The sol-gel technique allows for single-pot synthesis at ambient conditions. Dip coated thin films of ultraporous silica exhibit a flat surface morphology, with pore size and surface features of <25 nm, and a thickness of approximately 100 nm [Jedlicka et al., 2006]. With the incorporation of short peptide chains into the silane precursor, peptide-presenting sol-gel silica thin films can be made with precise control over density of the presented peptides [Jedlicka et al., 2007a,b]. These peptide-presenting silica thin films have been shown to be excellent substrates for neuronal growth [Jedlicka et al., 2006, 2007a]. In addition, sol-gel thin films are a viable drug delivery platform, achievable through the controlled release of drugs encapsulated within the porous film [Radin and Ducheyne, 2007, Radin et al., 2009]. This coating technique thus has the potential to combine biomimetic material modification with localized drug delivery, but it is necessary to first establish the effects of such sol-gel thin films on the electrical properties of the microelectrodes. The purpose of this study is to explore the feasibility of applying sol-gel silica thin film coatings to silicon-based microelectrodes. Determining this feasibility includes verifying the adhesion of the coating to the probes, as well as ensuring that the coatings do not significantly detriment the electrode's electrical properties. This characterization is an important step toward developing these coatings towards better *in vivo* neurointegration of implantable ICMs.

3.2 Materials and methods

3.2.1 Coating technique

Sol-gel silica thin film were prepared as previously described in Jedlicka et al. [2006]. Briefly, the precursor sol was prepared by mixing 3.8 mL tetramethylorthosilicate (TMOS) (Sigma-Aldrich, St. Louis, MO) with 850 mL ddH2O, and subsequently adding 0.55 mL of 0.04N HCl to catalyze hydrolysis. The precursor was then sonicated for approximately 15 min. The sonicated mixture was filtered using a 0.2mm Whatman syringe filter. A solution was then mixed consisting of 300μL of the filtered TMOS mixture, 700 μL of sterile-filtered, pH6.0, 0.2M phosphate buffer, and 100 μL of methanol. The thin films were produced by dip coating the shanks of six single-shank silicon substrate microelectrodes (NeuroNexus Technologies, Ann Arbor, MI) at a constant rate of 35mm/s into this final solution. Each of the six electrodes evaluated in this study had 16 individual iridium sites with a site area of 703 μm^2, for a total of 96 coated electrode sites. The films were allowed to gel for approximately 1 minute in air at room temperature, and then stored in phosphate buffer for use.

3.2.2 Evaluation of coating

The presence and evenness of the sol-gel silica thin films on the electrodes were evaluated by incorporating a fluorescent label into the coating. This was achieved by adding a saturating quantity of fluorescein sodium salt to the phos-

phate buffer before coating, resulting in a silica thin film with uniform fluorescent label throughout. An electrode was coated in non-fluorescent sol-gel as a control to ensure that the coating itself did not autofluoresce. To ensure that fluorescence of the labeled probe was not due to surface adhesion of the fluorescein, coated and uncoated control probes were dipped in a fluorescein sodium salt solution identical to that used to coat the fluorescent probe, except that TMOS was replaced with an equal volume of phosphate buffer. Fluorescent images were obtained 1 hour after coating using a Leica DM-IRB fluorescence microscope. Images of the fluorescently labeled probes were collected at a 525 nm wavelength emission using 490 nm excitation. Fluorescence in images of the coated electrodes with fluorescein label was compared against the control electrodes, which were not labeled. To evaluate stability of the coating, an established phantom brain model was utilized [Chen et al., 2004]. A single shank, acute Michigan electrode was coated in the fluorescently labeled sol-gel and imaged as described above. The probe was then inserted repeatedly into the brain model and then imaged again. Stability was assessed by continued fluorescence following insertion in the phantom brain.

3.2.3 Electrical characterization

Electrochemical impedance spectroscopy (EIS) and cyclic voltammetry (CV) measurements were collected using an Autolab potentiostat PGSTAT12 (Eco-Chemie, Utrecht, The Netherlands) with built in frequency analyzer (Brinkman,

Westbury, NY). A three electrode setup was utilized for *in vitro* experiments, with the coated NeuroNexus acute, single-shank electrodes serving as the working electrode. A calomel electrode (Fisher Scientific,Waltham, MA)was used as a reference electrode, and a platinum wire as the counter electrode. Measurements were performed in 1x PBS at room temperature. EIS and CV were preformed prior to and 1 day following application of the thin film coatings. To perform EIS, a 25mV RMS sine wave was applied to electrode sites with frequencies ranging logarithmically from 0.1 to 10 kHz. CV was performed by sweeping a voltage linearly from-0.6 to +0.8V at a scanning rate of 1 V/s. Sites with broken or poor connections, detected by having a maximum current in cyclic voltammograms below 1 nA, were excluded from the data set. The impedance data gathered from EIS were averaged across all sites. The impedances were separated into resistive and reactive components, and were compared for the pre-coated and post-coated probes at all measured frequencies. Changes in resistance, reactance, and impedance magnitude were evaluated using t-tests with $p<0.05$ indicating statistical significance. Current values from cyclic voltammograms were likewise averaged across all electrode sites. The charge carrying capacity was calculated by integrating the cathodic current density curve generated by the cyclic voltammogram and dividing by the sweep rate, and was compared before and after coating.

3.3 Results

Fluorescent imaging shows fluorescence on the electrode coated with the labeled sol-gel but not on the control (Figure 3.1), indicating adherence of the sol-gel film to the electrode. The majority of the coating fluoresced uniformly; however, there were patches of increased fluorescence, suggestive of local coating irregularities or clumps within a thin, even film. Absence of fluorescence on the control probe demonstrates that the coating is not auto-fluorescent, and that the fluorescence of the labeled probe is due to encapsulation within the pores of the sol-gel film, rather than adhesion on the film's external surface. In addition, uncoated probes dipped in the fluorescein solution displayed no fluorescence (data not shown), indicating that the fluorescence seen in the experimental probe was not due to surface adhesion of the label directly onto the probe surface. The stability of the coating on the probe was confirmed through continued florescence after inserting the probe into a phantom brain (data not shown). The coating appeared unaltered after insertion into the model, demonstrating adherence of the coating to the probe given similar mechanical stresses during surgical insertion.

The results of cyclic voltammetry show moderate changes in the voltammograms post-coating (Figure 3.2A), with larger current magnitudes observed for all voltages along the sweep. Cathodic charge storage capacity post-coating ex-

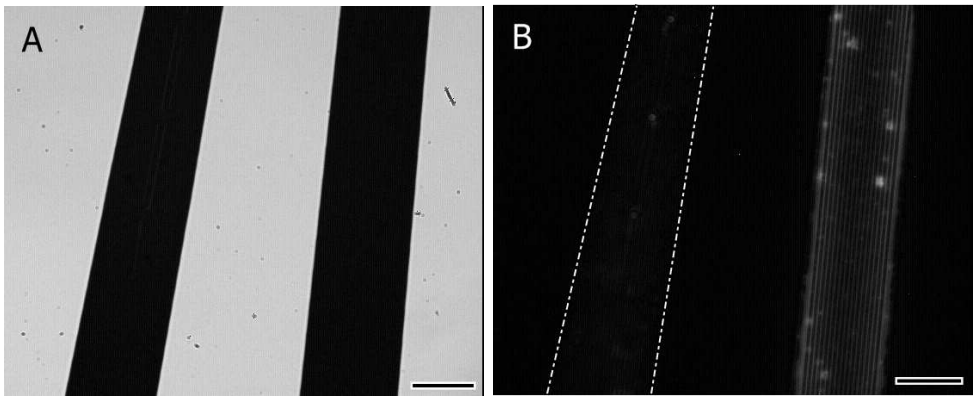

Fig. 3.1. Fluorescence microscopy confirms the adherence of sol-gel coatings to microelectrodes. (A) Bright field image of probes to show their location. (B) Fluorescent micrograph of coated probes. Left probe is unlabeled control, right probe is fluorescently labeled. These images demonstrate that the silica sol-gels can be successfully applied to silicon-based microelectrodes. Additionally, these images confirm the ability to encapsulate molecules in the TMOS precursor to facilitate biomolecule delivery to the implantation site. Reprinted from Pierce et al. [2009] with permission.

hibited a statistically significant increase (p<0.001) compared to pre-coated values (Figure 3.2B).

Comparison of the resistance and reactance as a function of frequency reveals an increase in resistance and a decrease in reactance (Figure 3.3A).The impedance magnitude pre and post coating demonstrates a decrease in impedance after coating at all frequencies tested (Figure 3.3B). Nyquist plots of the electrochemical impedance spectroscopy data exhibit a shift in the impedance curve towards increased resistance and decreased reactance, particularly at low frequencies (Fig. 4A). At low frequencies, both the resistive and reactive changes are more pronounced, with the reactance dominating the total impedance. Comparing the impedances at the individual frequencies of 100 Hz, 1 kHz, and 10 kHz (Fig. 4B–D), the resistance increases significantly across all frequencies (p<0.001), whereas the reactance is significantly decreased at 100 Hz (p<0.001), becomes unchanged around 1 kHz (p=0.1156), and is significantly increased at 10 kHz (p<0.001). The 100 Hz decrease is much larger in magnitude than the 10 kHz increase.

3.4 Discussion

A key consideration in coating an electrode is how the coating material affects the electrical properties of the electrode. If a coating that aims to mitigate

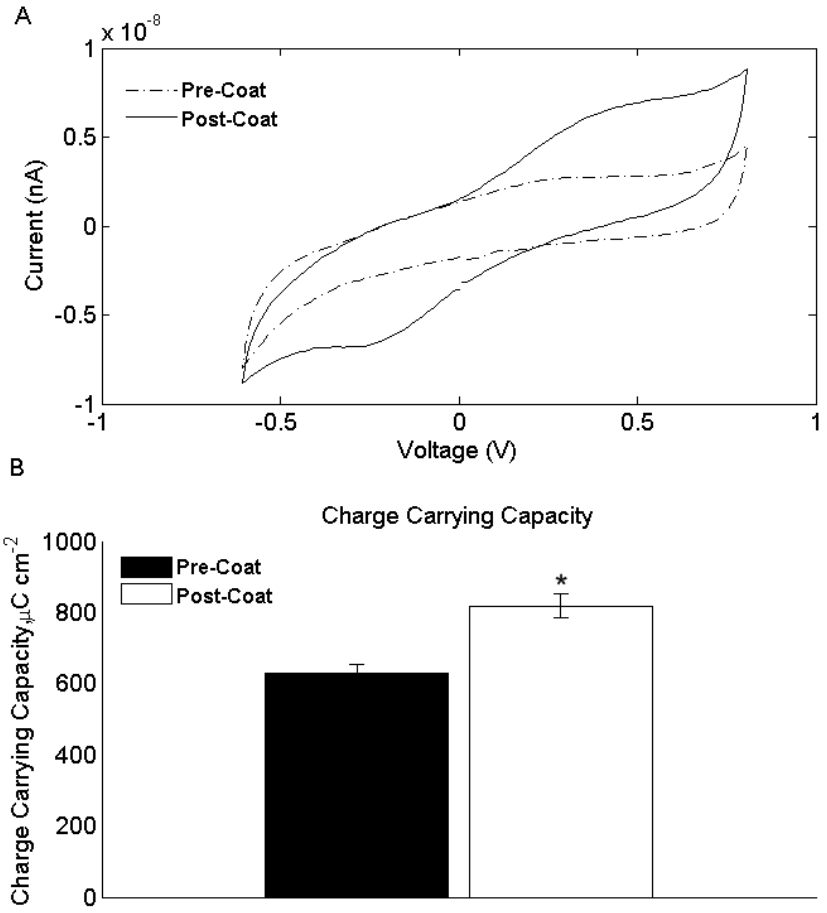

Fig. 3.2. (A) Representative cyclic voltammogram demonstrates changes in hysteresis curve. Cyclic voltammograms pre- and post-coating reveal an increase in current for each applied voltage of the sweep. This result indicates an increase in charge carrying capacity of the electrode site after application of the coating. (B) The average cathodic charge storage capacity (n = 92) increases after coating for all experimental sites. The increase in CV area is indicative of an increase in charge carrying capacity of the electrode following coating. Reprinted from Pierce et al. [2009] with permission.

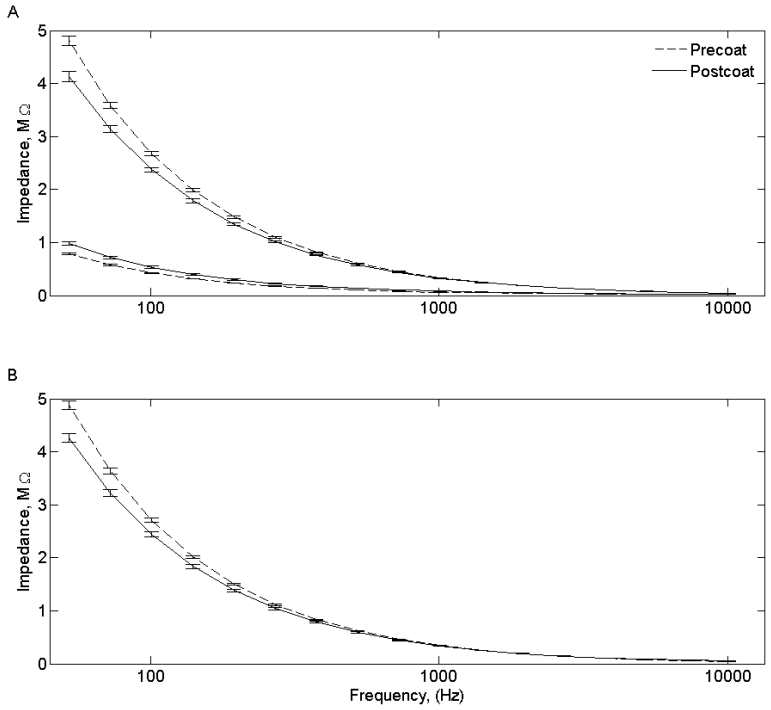

Fig. 3.3. Plots generated from EIS performed before and after coating show decreasing impedance losses with increasing frequency (n = 92). (A) Separated real and imaginary impedances show a resistance increase and reactance decrease following coating, with the most pronounced effects occurring at low frequency. (B) The total impedance shows a general decrease with the most pronounced effect also occurring for low frequency. The total impedance is dominated by the imaginary component. Reprinted from Pierce et al. [2009] with permission.

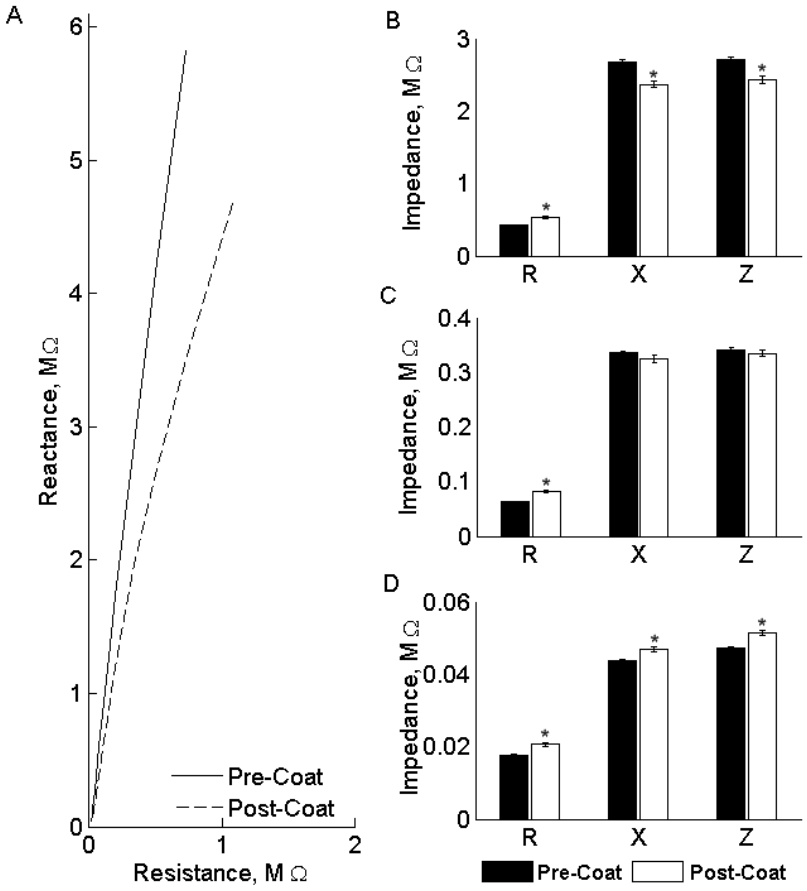

Fig. 3.4. (A) Representative Nyquist plot generated through electrochemical impedance spectroscopy demonstrates changes in impedance. Spectrograms obtained pre and post coating show a moderate decrease in impedance magnitude for all frequencies. (BŰD) Bar graphs showing average (n = 92) change in resistance (R), reactance (X), and total impedance (Z) following coating for (B) 100 Hz, (C) 1 kHz, and (D) 10 kHz. Resistance increases significantly for all frequencies. Reactance and total impedance decrease significantly at low frequencies, become unchanged near physiological frequencies (i.e. 1 kHz), and become significantly higher at high frequencies. The reactance increase at high frequency is much smaller in magnitude than the decrease seen at low frequency. Reprinted from Pierce et al. [2009] with permission.

the RTR results in detrimental changes to the electrical properties of the electrode, this coating would be of little practical value. The cyclic voltammetry results from our study demonstrate an overall increase in charge carrying capacity for coated electrode sites. Increasing charge carrying capacity corresponds to an increase in sensitivity for recording and allows for higher stimulation currents while minimizing voltage excursions [Wilks et al., 2009]. The increase in charge carrying capacity may be due in part to the decrease in impedance; however, it should be noted that the charge carrying capacity changes may be overestimated since the original site area was used for its calculation, but the porous coating likely increases the surface area across which charge transfer can occur. The results of EIS show a general decrease in site impedance, with impedance magnitude at the physiologically relevant frequency of 1 kHz being essentially unchanged from a bare electrode. Decreases in site impedance will increase the sensitivity of the electrodes, allowing for the detection of weaker signals across larger distances. Such decreases in impedance following the application of a non-conductive coating may be a result of increased capacitive charge transfer. Similar effects upon application of thin film coatings have been noted in the literature [Zhong and Bellamkonda, 2007]. The trends seen in the reactance and total impedance support the idea that these impedance decreases are a result of increased capacitance caused by charge separation due to introduction of the layer of thin, nonconductive silica. Because a capacitor's impedance is largest at small frequencies and decreases with increasing capacitance, an in-

crease in capacitance of the electrode interface would account for the reactance trend. Additionally, an increase in interfacial capacitance is consistent with the observed increase in charge carrying capacity. The resistance increased for all frequencies, as would be expected for an insulating layer. The electrical properties of sol-gel produced silica are highly dependent upon the material properties that result from the synthesis and treatment conditions of the film. While thick coatings of sol-gel silica sintered and densified by heat treatment substantially increase the total impedance [Hamdy et al., 2007, Pepe et al., 2006], high porosity silica xerogels and aerogels have dielectric constants in the range of 2.1–3.95. Our results demonstrate that the dip-coated, ambient-dried thin film silica sol-gel coatings do not adversely affect the electrical characteristics of the implantable electrodes, and may in fact provide beneficial electrical properties. A major advantage of the sol-gel silica is the potential for simple biofunctionalization schemes. Together these features will allow the sol-gel silica coatings to be used as a platform material for the mitigation of the RTR without causing significant detriment to the functionality of the probes.

The modest changes in the electrical properties of the probes should increase signal-to-noise ratio and improve the quality of neural recordings. These effects will likely be small, and the primary advantage of the coating is its use as a future platform for biochemical modulation of the electrode tissue interface. The impedance decreases observed in this study are much smaller than those caused by films or nanotube structures of poly(pyrrole) (PPy) or poly(3,4-

ethylenedioxythiophene) (PEDOT), for which changes are one or more orders of magnitude [Abidian et al., 2006, Wilks et al., 2009]. Likewise, the charge carrying capacity increase is much more subtle than that caused by PPy or PEDOT. Although less advantageous electrically than conductive polymers, sol-gel coatings provide a number of beneficial properties. While polymer nanotubes can deliver only small molecules, sol-gel materials can deliver a wide range of biomolecules. In addition, the rate of release can be finely tuned by adjusting the precursor silane to catalyst ratio [Avnir et al., 2006]. Another important point of contrast between silica sol-gel coatings and conducting polymer coatings is the physical scale. While sol-gel coatings have a total thickness of approximately 100 nm, coatings of conductive polymer nanotubes have a thickness ranging from 2 to 8.3 μm [Abidian and Martin, 2008].

The results of this study demonstrate the feasibility of applying silica sol-gel materials to microelectrodes. The potential clinical applications that depend on stable chronic recording from the cortex make the mitigation of the RTR a crucial issue. Our finding that silica sol-gel thin films can be coated onto ICMs without adversely affecting the electrical properties of the ICMs, combined with potential application of silica-sol gels as a combinatorial drug releasing and biomolecules presenting platform make silica thin films an interesting research avenue in the quest for alleviating chronic RTR.

4. QUANTIFIABLE PROTEIN-ADSORPTION-CAUSED CHANGES IN ELECTRODE IMPEDANCE ARE PREVENTABLE USING DIP-COATED PEG

4.1 Introduction

Failure of intracortical microelectrodes (ICMs) associated with the formation of a dense glial scar and loss of neuronal density typically manifests as increased impedance and decreased signal to noise ratios. *In vivo* impedance monitoring is a common tool to assess the functionality of implanted ICMs, and is used to infer the progression of the reactive tissue response to implanted ICMs [Vetter et al., 2004, Williams et al., 1999, 2007]. Recent research showing that changes in electrical properties do not always perfectly correlate with cellular responses implicates additional abiotic factors [Prasad and Sanchez, 2012, Prasad et al., 2012]. *In vitro* testing in 3D gel constructs revealed that the different glial cells have different impedance profiles when adhered to the surface of a microelectrode [Frampton et al., 2010]. While adsorbed proteins have been implicated in the biological response(Leung et al., 2008), their effects on the electrical impedance of ICMs have not been described with impedance spectroscopy. The prevalent electrical circuit model of the tissue electrode in-

terface assumes that adsorbed proteins result in purely resistive impedance changes [Otto et al., 2006, Williams et al., 2007] but there is not sufficient empirical verification of this assumption.

Another important question in this regard is whether any detrimental changes to the electrical characteristics of neural microelectrodes can be prevented using simple and cost effective approaches. For implantable devices in other biological systems, protein-resistant treatments are commonplace [Bluestein et al., 2010, Li and Henry, 2011, Salacinski et al., 2001]. One of the most common materials used to enhance the biocompatibility of biomedical implants is polyethylene glycol (PEG). Due to its hydrophilic nature, it prevents the adsorption of proteins by reducing access to the more hydrophobic surface onto which proteins prefer to bind [Michel et al., 2005]. Typically PEG is chemically grafted onto a substrate and very reliably reduces protein adsorption [Muthusubramaniam et al., 2011, Sharma et al., 2004a,b]. Current approaches in intracortical implant biocompatibility incorporate PEG as a scaffold for thick drug eluting hydrogels [Lu et al., 2009, Rao et al., 2011, Winter et al., 2007], which might exacerbate neuronal displacement.

This chapter will present an analysis of changes in ICM impedance following immersion in a model protein solution mimicking *in vivo* brain protein concentration. Total impedance, as well as resistance and reactance, will be analyzed at different points across the frequency spectrum to elucidate the contribution of adsorbed proteins to the impedance changes affecting electrode performance.

We will show that a dip-coated film of high molecular weight PEG (HMWPEG) prevents changes in impedance upon immersion in protein solution, and that *in vivo* application of PEG in an acute setting reduces the magnitude of impedance increase resulting from electrode insertion into tissue.

4.2 Materials and methods

4.2.1 Electrochemical measurements

Electrochemical measurements of 16-channel single shank Michigan electrode arrays (CNCT, Ann Arbor, MI) were made using an Autolab potentiostat PG-STAT12 with a built-in frequency response analyzer (EcoChemie, Utrecht, The Netherlands). A three-electrode cell configuration was used with the microelectrode site functioning as the working electrode, a large-area Pt wire functioning as the counter electrode, and an Accumet, gel-filled, KCl saturated calomel electrode (Thermo Fischer Scientific, Fair Lawn, NJ) functioning as the reference electrode. For each electrode array, Cyclic voltammetry (CV) was performed by sweeping the applied voltage from -0.6 to +0.8 V at a scanning rate of 1 V/s to determine sites with broken or poor connections, designated as those sites exhibiting a maximum current below 1 nA. These sites were discarded from the analysis, thus yielding a total of 30 functional sites on 3 different electrode arrays .

Electrochemical impedance spectroscopy (EIS), using the PGSTAT12, was used to measure the impedance of the electrode sites with the application of 16 sequentially applied sinusoidal waves at logarithmically spaced frequencies ranging from 46 Hz to 10 kHz, with an amplitude of 25 mVRMS. For each electrode, impedance spectroscopy was performed in PBS following each of three different treatments: a) no treatment, b) immersion in a 10% solution of bovine serum albumin (BSA) (Sigma-Aldrich, St. Louis, MO) in PBS, the concentration of which was chosen to mimic protein concentration in rat cerebral cortex [Banay-Schwartz et al., 1992], and c) immersion in a 20% solution of 4000MW PEG (Alfa-Aesar, Ward Hill, MA), air-drying for one minute, then immersion in BSA. An additional volume of 100 μL of PEG was further applied directly onto the microelectrode shank as it was immersed in BSA to mimic a topical application. Electrodes were rinsed with deionized water and anodically cleaned between the different treatments using 10 second long DC pulses, as previously described in Sommakia et al. [2009]. Impedance and phase spectra and Nyquist plots were generated for all treatment groups. Comparisons of the resistance, reactance and total impedance were done at 50 Hz, 100 Hz, 1 kHz, and 10 kHz.

4.2.2 Acute surgery

The laboratory animal protocol for this work was approved through the Purdue Animal Care and Use Committee (West Lafayette, IN, USA), and conforms to the guidelines of the US National Institutes of Health. Two male Sprague

Dawley rats (Harlan Laboratories, Indianapolis, IN) were used for this preliminary study. Each rat was anesthetized with 2% isofluorane, then transferred to a stereotactic frame and maintained with 0.5–1% isofluorane delivered through a nose cone. The head was shaved and swabbed with ethanol, and an eye lubricating ointment applied. Lidocaine was injected subcutaneously at multiple positions in the head, and then a midline incision approximately 2cm long was made along the cranium with a scalpel. The underlying pericranium was removed to expose the skull. A single burr hole was made with a dental drill towards the back of the head, slightly anterior to the ears, and a stainless steel bone screw with attached to a segment of platinum wire was threaded into it to serve as a counter electrode. Bilateral craniotomies about 2.5 mm in diameter were made with a dental drill, approximately 2.5 mm anterior to Bregma and 2 mm lateral to the midline. For each craniotomy, a slit was made in the dura using surgical microscissors. One craniotomy serving as control was wetted with 0.9% sterile saline before electrode insertion, while the other craniotomy was wetted with 20% w/v solution of 4000MW PEG prior to electrode insertion. An acute Michigan probe was used for this experiment, with its 1 kHz impedance in PBS measured immediately before insertion. The control craniotomy was done first, with the electrode connected to Autolab potentiostat. The electrode was held in a magnet-stabilized micromanipulator, and manually inserted into the cortex. Five minutes after insertion, EIS was measured in a two-electrode setup. The electrode was then removed, rinsed with MilliQ water, and cleaned

by applying a DC bias of 1.5 V for 10 seconds as described in Sommakia et al. [2009] and Chapter 5. After verifying the return of the 1 kHz impedance to baseline, the electrode was immersed in a 20% solution of 4000MW PEG in MilliQ water for 1 minute and allowed to dry for 2 minutes. The electrode was then replaced in the micromanipulator and inserted into the cortex in the other craniotomy wetted with PEG, and EIS was performed again.

4.2.3 Statistical analysis

Statistical analysis was done using the SAS 9.3 statistical package (SAS Institute, Cary, NC). A general linear model (GLM) procedure was used to perform a one way ANOVA with block to remove variations between the different electrodes by treating electrodes as a statistical block. Tukey post-hoc tests were used to identify statistically significant differences between the groups at a significance level of α<0.05. Plots were generated using MATLAB (The MathWorks Inc., Natick, MA).

4.3 Results

4.3.1 Analysis of impedance changes with model protein solution and PEG *in vitro*

Figure 4.1(a) shows the magnitude spectrum for electrodes dipped into BSA without pretreatment with PEG is higher than the magnitude spectrum for un-

coated controls for all frequencies, indicating an overall increase in impedance. In contrast, the magnitude spectrum for electrodes treated with PEG prior to BSA immersion shows more congruence with the magnitude spectrum of the control. Figure 4.1(b) shows the phase spectrum for non-PEG treated electrodes immersed in BSA exhibits lower phase angles at the lower end of the frequency spectrum, and the difference is most pronounced in the middle of the spectrum between 200–500 Hz. For electrodes pretreated with PEG prior to BSA immersion, the phase angle is also lower than the controls, but higher than the non-PEG electrodes, at the low frequency end of the spectrum. At higher frequencies, the phase angle of non-PEG electrodes approaches that of the controls, whereas the PEG treated electrodes exhibit a reduced phased angle at frequencies higher than approximately 2 kHz.

Figure 4.2 shows the Nyquist plots for the different treatments. The Nyquist plot for electrodes not treated with PEG prior to BSA immersion appears shifted up and the right compared to the controls, indicating both increased resistance and reactance, with the most pronounced divergence occurring toward the middle of the plot. In contrast, the plot for electrodes pretreated with PEG shows more congruence with the control in the middle of the plot and slight divergence at the lower end of the plot, corresponding to the higher frequencies.

Figure 4.3 shows changes in the real component of the impedance, i.e. resistance, relative to the control at four frequency values across the spectrum.

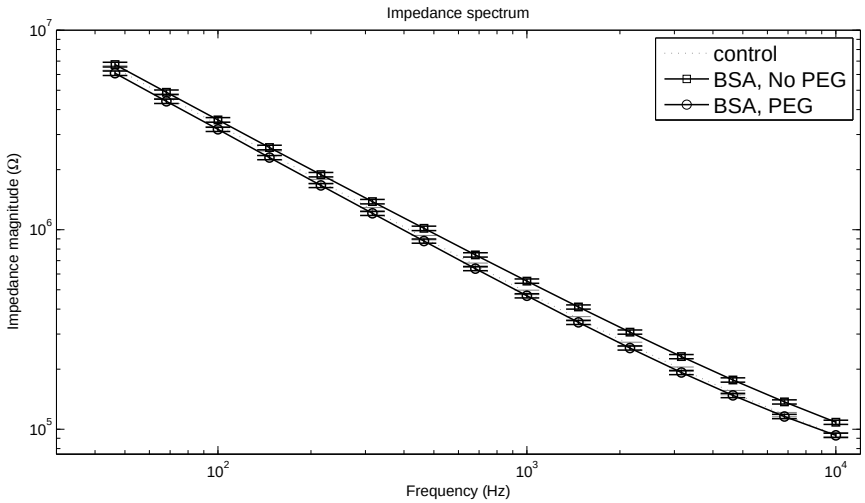

(a) Magnitude spectrum (Bode plot)

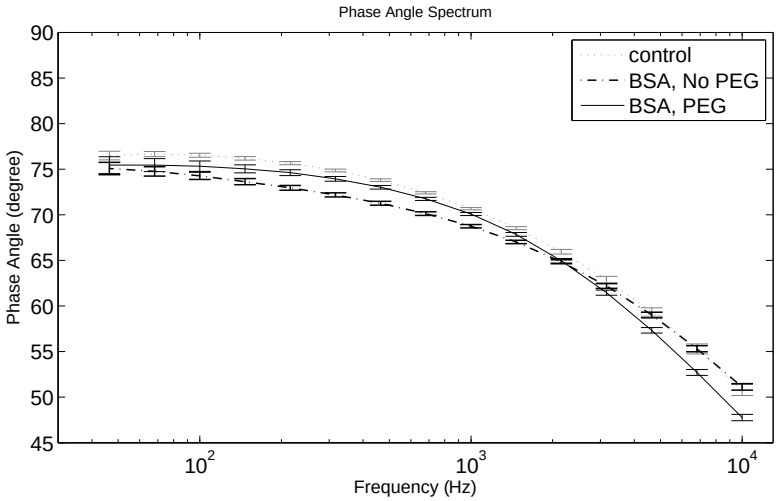

(b) Phase spectrum (Bode plot)

Fig. 4.1. (a) Total impedance magnitude spectrum for electrodes not pretreated with PEG before BSA application is higher than both the control and PEG treated electrodes. (b) Phase angle spectrum for electrodes not pretreated with PEG prior to BSA application shows a lower phase angle for lower and intermediate frequencies compared to the control, while the phase angle spectrum for electrodes pretreated with PEG exhibits smaller phase angles across all frequencies.

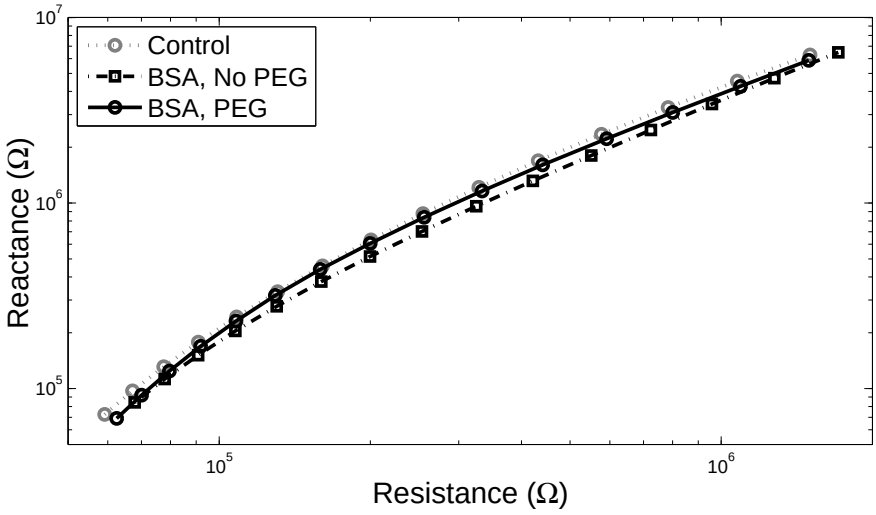

Fig. 4.2. Nyquist plot for electrodes pretreated with PEG before BSA application is close to the control plot, with a slight shift to the left at lower frequencies, indicating a decrease in resistance. Nyquist plot for electrodes not pretreated with PEG before BSA shows a shift up and to the right, indicating increases in both resistance and reactance.

Electrodes immersed in BSA without PEG pretreatment exhibited highly statistically significant increases in the resistance compared to the uncoated control at examined frequencies. The highest impedance increase relative to control was in the middle of the frequency spectrum, specifically at 1 kHz, with a 30.7% increase in resistance. At 50Hz, the increase in resistance in resistance for the BSA coated electrodes without PEG pretreatment was 14.5%, at 100Hz, the resistance increase was 23.9%, and 10 kHz, the resistance increase was 17%. The electrodes pretreated with PEG prior to BSA immersion, on the other hand, did not exhibit any significant differences in resistance compared to the uncoated

controls at all examined frequencies.

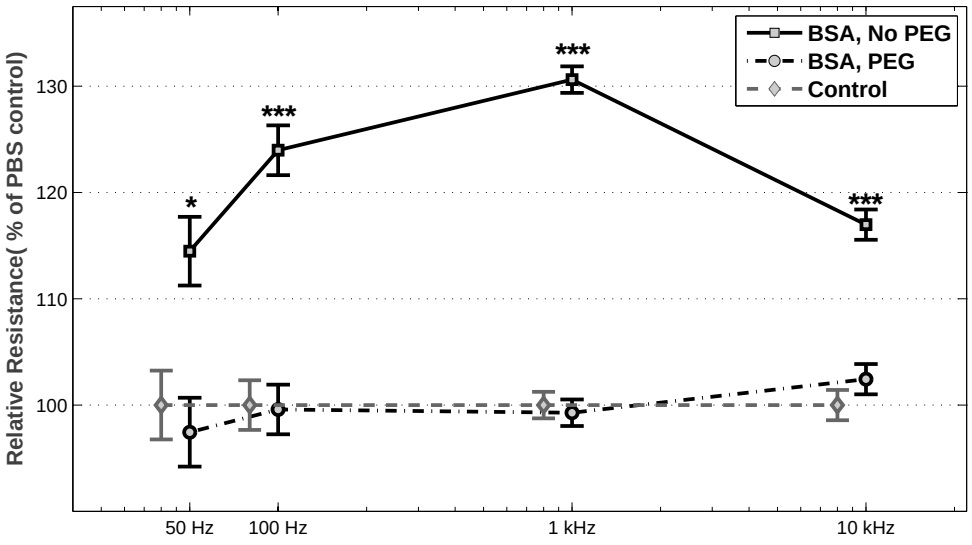

Fig. 4.3. Resistance: electrodes coated with BSA without PEG pretreatment exhibited considerable and statistically significant increases in resistance (real impedance) compared to uncoated controls at all frequency values studied. In contrast, electrodes treated with PEG prior to BSA application did not exhibit any significant increases in resistance compared to the control at all studied frequencies, and were all significantly lower compared to BSA coated electrodes. Control plot shown slightly offset to the left for clarity. Error bars represent the standard error of the means.

Figure 4.4 shows changes in the imaginary component of the impedance, i.e. reactance, relative to the control at four frequency values. For electrodes not pretreated with PEG prior to immersion in BSA, no significant increase in reactance was observed at 50 Hz or 100 Hz, while increases of 4%, 12% and

15% were observed at 100 Hz, 1 kHz and 10 kHz, respectively. In contrast, electrodes pretreated with PEG prior to immersion in BSA exhibited modest decreases in the reactance relative to control at all frequencies (-6.3% at 50Hz, -6.3% at 100Hz, -4.2% at 1 kHz, and -4.8% at 10 kHz).

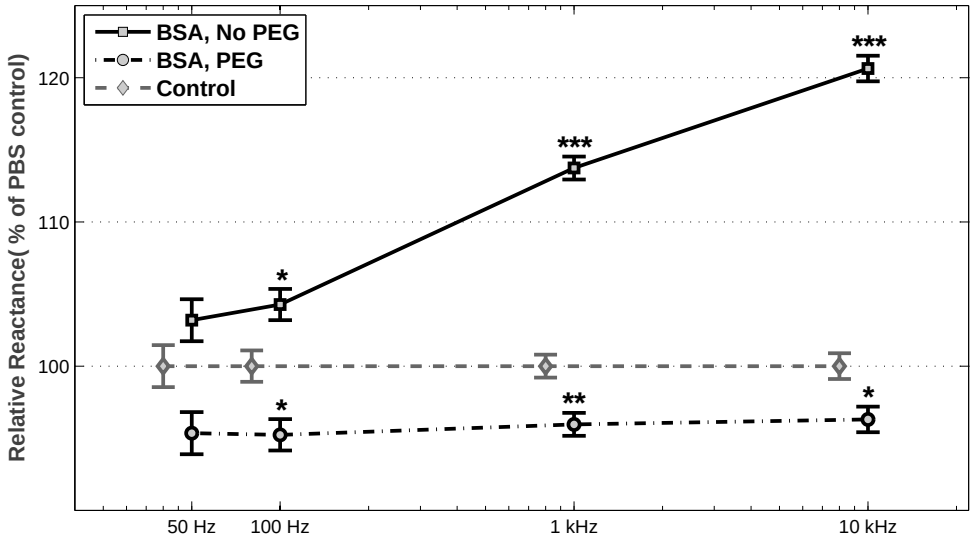

Fig. 4.4. Reactance: for BSA coated electrodes, no change in reactance (imaginary impedance) was observed compared to uncoated control at 50Hz, whereas increases in reactance were observed at higher frequencies. PEG coated electrodes exhibited slight decreases in reactance compared to uncoated controls at frequencies greater than 50Hz. Control plot shown slightly offset to the left for clarity. Error bars represent the standard error of the means.

Figure 4.5 shows the changes in total impedance relative to the control at four frequency values. For electrodes not pretreated with PEG prior to BSA im-

mersion, no significant difference in total impedance was observed at 50Hz, but progressive increases in the impedance were observed at the higher frequencies (4.5% at 100hz, 13.5% at 1 kHz, 15.3% at 10 kHz). For electrodes pretreated with PEG prior to BSA immersion, modest decreases in total impedance were observed at the lower frequencies (-5.8% at 50Hz, -5.6% at 100 Hz, -3.9% at 1 kHz), while no significant difference in the total impedance compared to the control was observed 10 kHz.

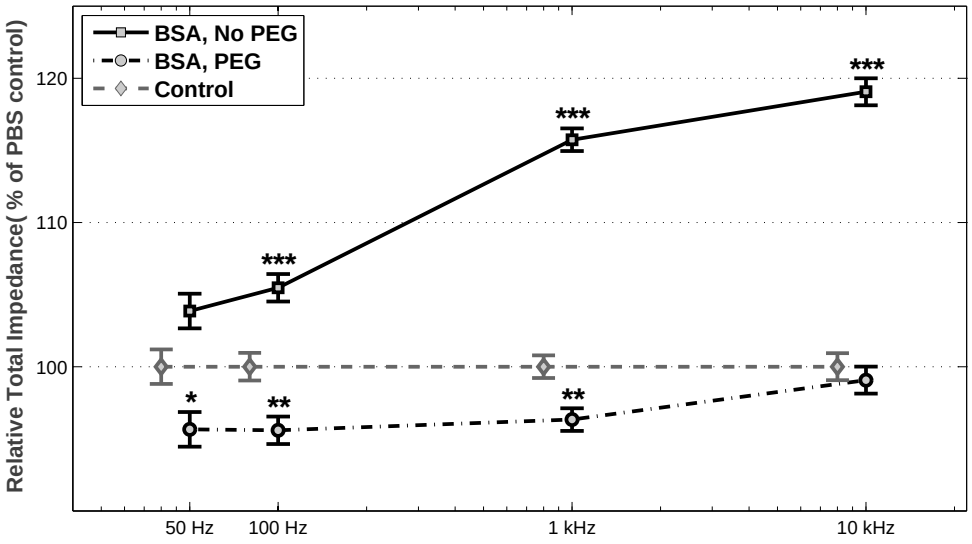

Fig. 4.5. Total Impedance: for BSA coated electrodes, total impedance exhibited statistically significant increases compared to uncoated controls except at 50Hz. For electrodes treated with PEG prior to application in BSA, smaller but statistically significant decreases in total impedance were observed except at 10 kHz. Control plot shown slightly offset to the left for clarity. Error bars represent the standard error of the means.

4.3.2 Preliminary analysis of impedance changes with and without PEG *in vivo*

Figure 4.6 shows the percent increase of the real component of the impedance, i.e. resistance, between the *in vitro* baseline and the *in vivo* measurement at four frequency values across the spectrum. In both cases of PEG treatment or non-treatment, the resistance increased significantly when measured *in vivo* compared to the *in vitro* baseline. Insertion into the cortex without PEG treatment, however, resulted in a larger increase from baseline compared to insertion with PEG treatment. The increases compared to baseline are presented in table 4.1.

Table 4.1
Increase in resistance from baseline observed *in vivo* for No PEG vs. PEG treatment at 4 frequencies (mean ± standard error).

	50 Hz	100 Hz	1 kHz	10 kHz
No PEG	69.1±4.6%	112.2±5.9%	218.7±11%	305±15.8%
PEG	49±4.6%	56.6±5.9%	142.5±11%	215.2±15.8%
	p=0.0033	p<0.0001	p<0.0001	p<0.0001

Figure 4.7 shows the percent increase of the imaginary component of the impedance, i.e. reactance, between the *in vitro* baseline and the *in vivo* measurement at four frequency values across the spectrum. In both cases of PEG treatment or none-treatment, the reactance increased significantly when mea-

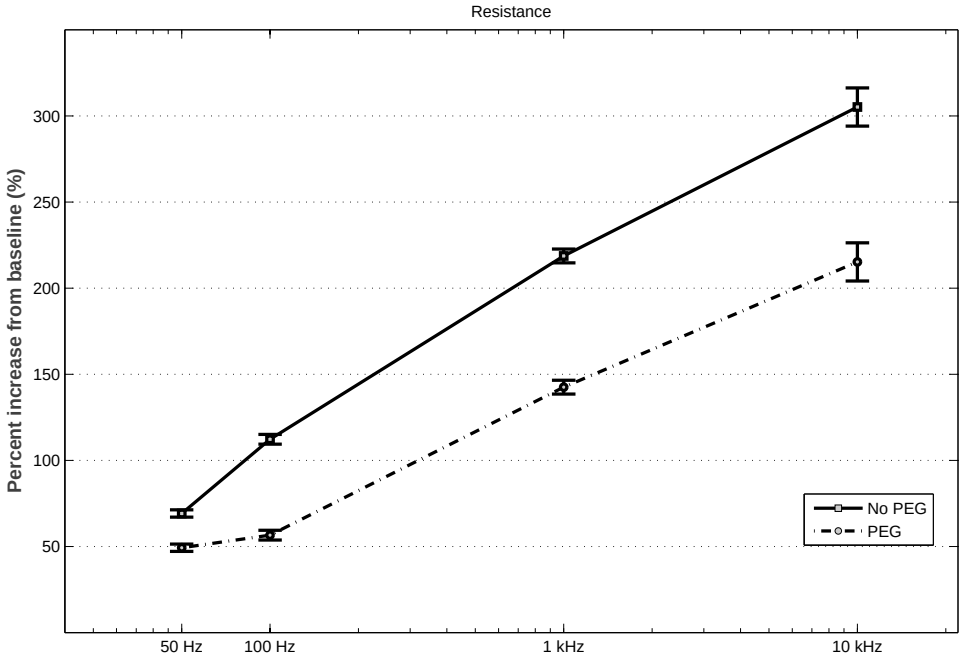

Fig. 4.6. *In vivo* increase in resistance from baseline.

sured *in vivo* compared to the *in vitro* baseline. Insertion into the cortex without PEG treatment, however, resulted in a larger increase from baseline compared to insertion with PEG treatment. The magnitudes of the increases in reactance were smaller than those for the resistance. The increases compared to baseline are presented in table 4.2.

Figure 4.8 shows the percent increase of the total impedance between the *in vitro* baseline and the *in vivo* measurement at four frequency values across the spectrum. In both cases of PEG treatment or none-treatment, the total

Table 4.2
Increase in reactance from baseline observed *in vivo* for No PEG vs. PEG treatment at 4 frequencies (mean ± standard error).

	50 Hz	100 Hz	1 kHz	10 kHz
No PEG	49.7±2%	53.7±2.7%	75.7±3.1%	157±7.3%
PEG	30.4±2%	32.2±2.7%	42.2±3.1%	91.8±7.3%
	p=0.0033	p<0.0001	p<0.0001	p<0.0001

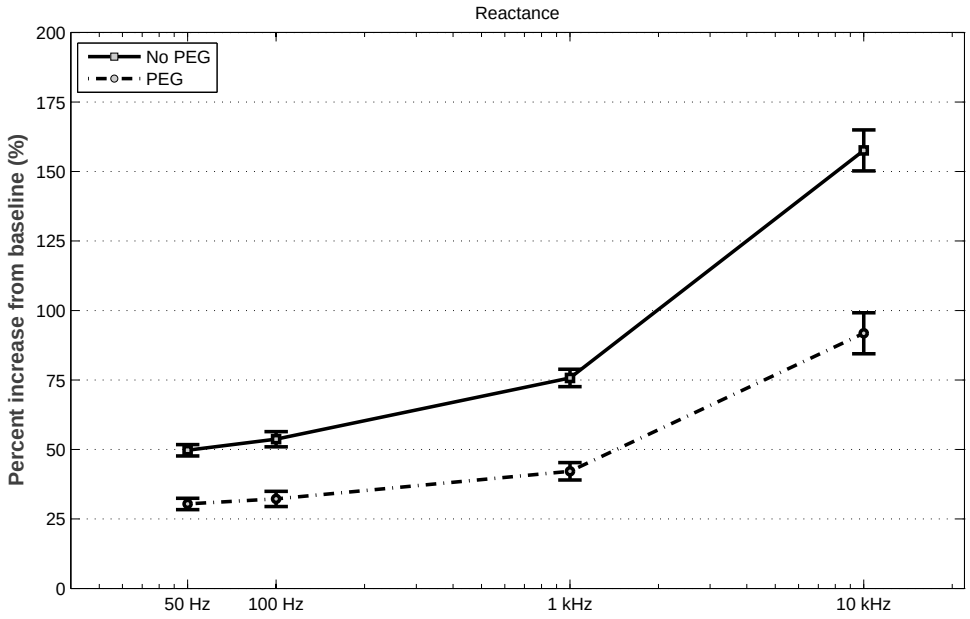

Fig. 4.7. *In vivo* increase in reactance from baseline.

impedance increased significantly when measured *in vivo* compared to the *in vitro* baseline. Insertion into the cortex without PEG treatment, however, resulted in a larger increase from baseline compared to insertion with PEG treatment. The increases compared to baseline are presented in table 4.2.

Table 4.3
Increase in total impedance from baseline *in vivo* for No PEG vs. PEG treatment at 4 frequencies (mean ± standard error).

	50 Hz	100 Hz	1 kHz	10 kHz
No PEG	52.3±2.1%	58.7±2.9%	98.9±4%	222.5±11%
PEG	31.5±2.1%	34.2±2.9%	57.5±4%	154.2±11%
	$p = 0.0033$	$p < 0.0001$	$p < 0.0001$	$p < 0.0001$

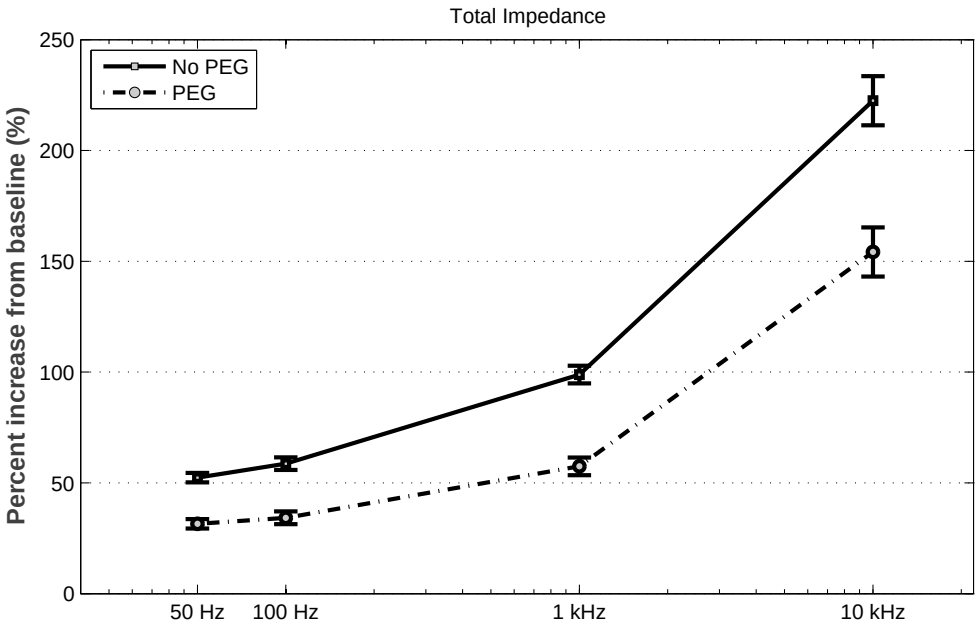

Fig. 4.8. *In vivo* increase in total impedance from baseline.

4.4 Discussion

4.4.1 Rationale

The *in vivo* reactive tissue response is an aggregate of amplified biological processes that begin with device insertion and accompanying trauma. The in-

dwelling implant acts as a nucleation site/sink for various proinflammatory proteins, as well as substrate for cell attachment [Leung et al., 2008]. A quantification of the effects of immediate protein adhesion onto neural electrodes on the electrical properties of the microelectrodes does not exist in the literature. Countering the effects of protein adsorption onto neural microelectrodes is important inasmuch as it actually improves device performance, particularly as inferred by its electrical properties. Current efforts in combating the reactive tissue response focus on targeting and quantifying the cellular component of the reactive tissue response. A potential alternative might be to quantify and target molecular and extracellular components.

4.4.2 Explanation of results

As seen from the impedance and phase angle spectra and the Nyquist plots, the quantitative effects on electrode impedance are not easily discernible by examining log-plot Bode and Nyquist plots. We therefore examined the relative resistance, reactance, and total impedance at various points across the frequency spectrum to better understand how protein adsorption affects the electrical properties of neural microelectrodes, and how attempts to mitigate protein adsorption might affect electrode performance.

Our first finding was that readily apparent and significant increases in resistance at all examined frequencies occur immediately upon exposure to a pro-

tein solution at a concentration mimicking *in vivo* concentrations. Furthermore, significant increases in the reactance are observed at higher frequencies, including the physiologically relevant 1 kHz. The aggregate impedance effect is that of a significant increase at frequencies higher than 50Hz. These observed *in vitro* changes in impedance might not exactly match *in vivo* changes, given the difference in protein composition in the brain, and the presence of additional biomolecules with widely varying degrees of hydrophobicity, such as lipids and polysaccharides [Margolis and Margolis, 1974, Norton et al., 1975, O'Brien and Sampson, 1965, Pease, 1966]. This finding of changes in both resistive and capacitive component following protein adsorption challenges current assumptions inherent in prevalent electrical circuit models of the device tissue interface. Such models typically assume that protein adsorption causes purely resistive changes in impedance [Otto et al., 2006, Williams et al., 2007]. We demonstrate that the exposure of microelectrodes to a protein solution results in both resistive and capacitive changes in impedance, rather than purely resistive changes. These findings suggest a need for the reexamination of assumptions upon which prevalent electrical circuit models for the tissue electrode interface are built.

Our study further demonstrates that treating electrodes with a PEG film via dip coating prior to immersion in a protein solution negates these increases in impedances at physiologically relevant frequencies. That the reactance exhibits slight decreases for electrodes pretreated with PEG supports our work-

ing hypothesis that the PEG film forms a hydrated layer close to the electrode surface that prevents proteins from accessing the surface of the electrode, while simultaneously avoiding detrimental effects on charge transfer at the electrode-electrolyte layer. As expected, electrode insertion into the brain results in a considerable increase in impedance, both resistive and capacitive, as predicted by electrode tissue interface models [Otto et al., 2006, Williams et al., 2007]. The addition of an aqueous solution of HMWPEG by dip-coating onto the microelectrode and directly into the craniotomy resulted in a reduction in the magnitude of the increase from baseline. Because cellular responses in the brain are not observed until several hours post implantation [Kozai et al., 2012b], this suggests that a considerable portion of the immediate impedance increase comes from biomolecules with hydrophobic properties that come into contact with the electrode surface and hinder charge transfer. The presence of free HMWPEG entering the brain simultaneously with the electrode appears to confer some degree of protection from the effects of aforementioned biomolecules. While grafted microscale antifouling coatings that prevent cellular adhesion *in vitro* do not result in significant improvement to the cellular composition of the chronic electrode tissue interface [Gutowski et al., 2013], the effects of such coatings on the electrical behavior of functional electrodes has not been tested. Applying higher molecular weight PEG in solution has been shown to improve cellular and behavioral recovery in traumatic brain injury [Koob and Borgens, 2006, Koob et al., 2005, 2008], due to its hydrophilicity achieving membrane

sealing effects. It is possible that this property of HMWPEG can be similarly effective in disrupting deposition of proteins and other molecules at the electrode vicinity. It has been suggested that cellular, specifically microglial, responses do not consistently correlate to electrode performance [Prasad et al., 2012]. Our findings, in conjunction to these observations from the literature, suggest the importance of future studies to correlate *in vivo* electrode performance with molecular and extracellular components of the reactive tissue response.

5. DIRECT CURRENT BIASING FOR THE RESTORATION OF SITE IMPEDANCE OF NEURAL MICROELECTRODES

5.1 Introduction

Acute experiments using penetrating silicon-shank intracortical microelectrodes (ICMs) have been successfully used to study electrophysiology in the central nervous system [Crea et al., 2009, Hoa et al., 2008, McConnell et al., 2007, Niu et al., 2013, Snyder et al., 2008]. The major advantage of penetrating ICMs is the high specificity conferred by their small size scale and their ability to reach physiologically relevant neuron populations inside the cortex [Anderson et al., 1989, Drake et al., 1988]. These properties simultaneously constitute a disadvantage because the insertion procedure causes localized injury to neural tissue and the blood brain barrier, including cell lysis and blood vessel permeabilization [Saxena et al., 2013]. This injury results in the extravasation of blood borne protein and cells and the accumulation of a diverse range of molecules on the electrode surface [Fawcett and Asher, 1999, He and Bellamkonda, 2008, Leung et al., 2008]. The smaller size of the electrically active sites on neural microelectrodes makes them geometrically more susceptible to accumulation of cellular and extracellular biomolecules. This effect is also true

when exposing such electrodes *in vitro* to model protein solutions and phantom brains for the sake of various tests. This accumulation of proteins, cell debris, and other biomolecules can result in an increase in the impedance of the electrode site. Increases in impedance can be detrimental to *in vivo* recording sensitivity and to electrode assessment in other *in vitro* tests [Vetter et al., 2004, Williams et al., 2007].

Protein removal from surfaces is a time and labor intensive process, most commonly involving various surfactants and electrophoresis techniques [Green et al., 2001, Magnani et al., 2004, Vinaraphong et al., 1995]. Ultrasonic cavitation (sonication) is another common alternative which functions by creating oscillating nanobubbles at the surface. These cavitations exert drag and shear forces that remove adsorbed proteins [Maisonhaute et al., 2002a,b]. The brittle mechanics of silicon [Stieglitz et al., 2000], however, limit the use of ultrasonic cavitation. Piranha solution etching is the most robust method of removing organic residues [Verhaverbeke and Christenson, 2001], but Piranha solution is a volatile and potentially explosive material, and cannot be safely used to quickly clean electrodes within a surgical setting. NeuroNexus, a prominent manufacturer of silicon-shank microelectrodes, recommends soaking electrodes in a multipurpose contact lens cleaner for a few hours. This recommendation restricts the reuse of an acute electrode in same day experiments, and, as we will demonstrate in this paper, soaking microelectrodes in contact lens solution results in substantial increases in electrode site impedance.

One approach that has been shown to successfully, albeit temporarily, restore recording capabilities to encapsulated chronic microelectrodes is DC biasing at voltages outside the water window [Johnson et al., 2005, Otto et al., 2006]. Application of DC voltages above 0.8 V in an electrochemical cell results in the electrolysis of water and the production of hydrogen gas [Holladay et al., 2009]. Similar approaches have been used to remove metal oxide layers by holding a constant potential at a relatively voltage high in a strong acid solution [Robblee et al., 1983]. Similarly, we posit that DC voltages applied to electrode sites of an iridium microelectrode in an electrochemical cell with an aqueous electrolyte will result in the decomposition of water at the electrode-electrolyte surface and the production of hydrogen gas bubbles. We hypothesize that these bubbles would exert forces on adsorbed biomolecules somewhat similar to those forces exerted by nanobubbles in sonication, with similar results. In this paper we demonstrate the utility of using DC anodic cleaning to restore the impedance of silicon microelectrodes following exposure to various biomolecules. We will show that applying a DC voltage to an electrode for as little as 2 seconds results in a significant and considerable decrease in impedance, and that pulses of over 10 seconds are sufficient to achieve a stable impedance value. We demonstrate the use of this technique to clean electrodes placed in protein solution, phantom agar brain, and rat brain tissue.

5.2 Methods

5.2.1 Electrochemical measurement and DC biasing

Electrochemical measurements of acute 16-channel single shank Michigan electrode arrays (NeuroNexus Inc., Ann Arbor, MI) were made using an Autolab potentiostat PG-STAT12 with a built-in frequency response analyzer (Eco-Chemie, Utrecht, The Netherlands). Both two- and three-electrode cell configurations were used with the microelectrode site functioning as the working electrode and a large-area Pt wire functioned as the counter electrode. For the three-electrode configuration, an Accumet, gel-filled, KCl saturated calomel electrode (Thermo Fischer Scientific, Fair Lawn, NJ) functioned as the reference electrode. Measurements were performed in 1x PBS at room temperature. To determine sites with broken or poor connection, cyclic voltammetry (CV) was performed by sweeping the applied voltage from -0.6 to +0.8 V at a scanning rate of 1 V/sec . Sites exhibiting a maximum current below 1 nA were discarded from the analysis. Electrochemical impedance spectroscopy (EIS), using the PGSTAT12, was used to measure the impedance of the electrode sites with the application of 16 sequentially applied sinusoidal waves at logarithmically spaced frequencies ranging from 46 Hz to 10 kHz, with an amplitude of 25 mV RMS. For the DC biasing, the PG-STAT12 was instructed to apply a constant voltage of 1.5 V for a set duration.

5.2.2 DC duration study

To study the effect of DC biasing duration, electrodes were placed with the silicon shank in Equate brand multipurpose contact solution (Walmart, Bentonville, AR) overnight, then removed and rinsed with MilliQ water, as per instruction from the NeuronexusNeuroNexus website. Electrodes were then placed in three-electrode cell described above and EIS was performed to obtain the baseline impedance. A 1.5 V DC voltage was applied for 2 seconds, and the impedance was measured again. This procedure of paired consecutive DC biasing and EIS was repeated eight times, for a total DC biasing time of 16 seconds.

5.2.3 *In Vitro* biomolecule models

To demonstrate the efficacy of DC biasing at restoring electrode impedance following exposure to biomolecules, two models were employed. Model protein solution was a 10% weight/volume bovine serum albumin (Sigma-Aldrich, St. Louis, MO) in MilliQ water, prepared as described previously [Sommakia et al., 2009]. Phantom brains were prepared by mixing 1% agar (Sigma Aldrich, St. Louis, MO) in 1x PBS on a heated magnetic stirrer until well dissolved, and allowed to set for 2 hours at room temperature then overnight at 4 degrees. For each model, EIS measurements were performed to measure baseline impedance. The electrode was then affixed to a manipulator and immersed in

the BSA solution or inserted in the phantom brain. Electrodes were held in BSA for 5 minutes and in agar for 15 minutes. Electrodes were then removed and placed back into the three-electrode cell. EIS was performed to measure impedance, and then DC biasing at 1.5 V was performed for 15 seconds, and EIS performed again. Efficacy of DC biasing method was evaluated by examining the 1 kHz impedance, which is a typical metric for evaluating microelectrodes [Cogan, 2008].

5.2.4 DC biasing following acute *in vivo* implant

To demonstrate the efficacy of DC biasing at restoring electrode impedance during acute surgeries, DC biasing was performed during the course of acute surgeries. The laboratory animal protocol for this work was approved through the Purdue Animal Care and Use Committee (West Lafayette, IN, USA), and conforms to the guidelines of the US National Institutes of Health. Briefly, male Sprague Dawley rats (Harlan Laboratories, Indianapolis, IN) undergoing acute surgeries are anesthetized with 2% isofluorane and placed into a stereotactic frame. A subcutaneous injection of 0.5 ml of Lidocaine was administered, and then a midline incision was made along the cranium with a scalpel. A 2 mm diameter craniotomy was made with a dental drill, approximately 2.5 mm anterior to Bregma and 2 mm lateral to the midline. A slit in the dura was made using microscissors, and the electrode inserted into the brain with a magnet-stabilized micromanipulator. Once the experiment was concluded, the electrode

was withdrawn from the brain and rinsed in MilliQ water. EIS was performed in a two-electrode configuration at the surgical site, after which DC biasing was applied at 1.5 V for 15 seconds, and the EIS performed again.

5.2.5 Data Analysis

Experiments were run in triplicate except for the *in vivo* acute surgery, which was performed in duplicate. EIS data was extracted using a custom MATLAB (MathWorks, Natick, MA) function. Statistical analysis was performed using the SAS statistical package (SAS Institute, Cary, NC). A generalized linear model procedure was used to perform a one-way ANOVA with blocking to remove the effect of variations between electrodes and extract the least square means of the treatments. Post-hoc Tukey tests were performed to determine the pairwise differences between the treatments to a significance level of $\alpha = 0.05$. Graphs were plotted using MATLAB.

5.3 Results

5.3.1 Effects of Duration of DC biasing

Figure 5.1 shows the effect of the duration of DC biasing at 1.5 V on electrodes that have been placed in contact solution overnight. Figure 5.1(a) shows the effect of DC biasing on the Total impedance magnitude at 1 kHz. Without any DC biasing, these electrodes exhibit an average 1 kHz impedance of

3456.8 kΩ. Applying a 1.5 V DC bias for 2 seconds reduces the average 1 kHz impedance to 1181.2 kΩ (p<0.0001, compared to uncleaned), a decrease of 65%. A total of 4 seconds of cumulative DC biasing reduces the average 1 kHz impedance to 901.05 kΩ (p=0.0048 compared to 2 sec), a total decrease of 74% from the impedance of uncleaned electrodes. Additional DC biasing for durations longer than 4 seconds slightly reduces the 1 kHz impedance, with no statistically significant difference observed until 12 seconds of cumulative DC biasing, where the 1 kHz impedance is 661.2 kΩ (p=0.031). The observed mean 1 kHz impedance over time can be fitted to an exponential decay function (Rsquare value).

Analyzing the reactance and resistance separately as shown in Figure 5.1(b) reveals that the reactance follows an extremely similar pattern to the total impedance at 1 kHz. Uncleaned electrodes with a 1 kHz reactance of 3211 kΩ drops down to 1134.2 kΩ with 2 sec of DC biasing at 1.5 V, a decrease of 64% (p<0.0001). Cumulative DC biasing for 4 seconds reduces the reactance to 865.9 kΩ, a decrease of 73% from the uncleaned electrodes. Additional DC biasing slightly reduces the reactance, but a statistically significant difference does not occur again until 12 seconds of cumulative DC cleaning, where the reactance is observed to be 636 kΩ. The resistance at 1 kHz changes in a slightly different manner. DC biasing for 2 seconds results in a decrease from 1238.7 kΩ to 327.5 kΩ, representing a decrease of 73%. Unlike the reactance, DC biasing longer than 2 seconds did not result in significant decreases in the resistance.

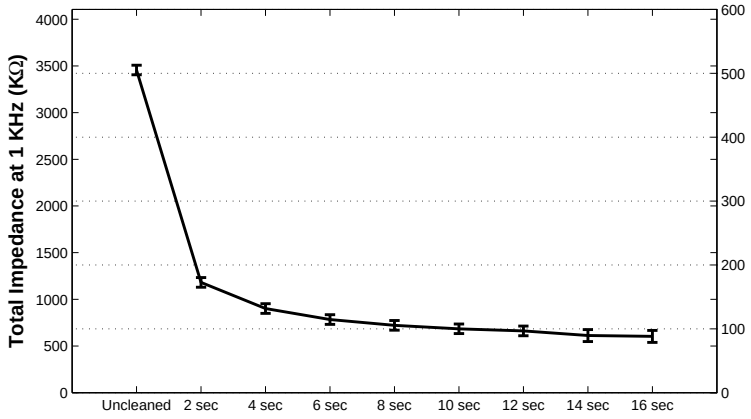

(a) Total impedance vs. DC biasing duration

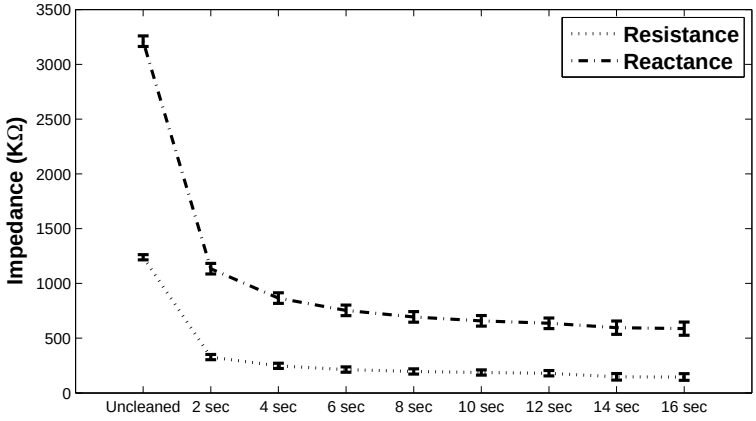

(b) Resistance and reactance vs. DC biasing duration

Fig. 5.1. Effects of progressively increasing durations of DC biasing on total impedance (a), and resistance and reactance (b)

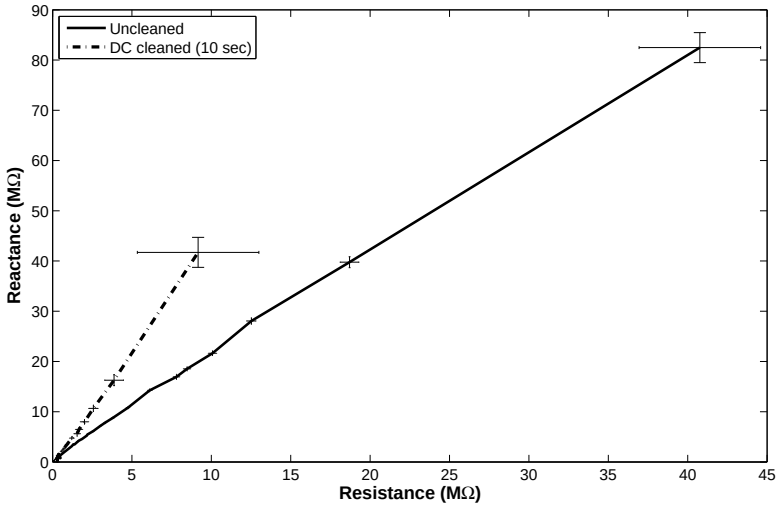

Fig. 5.2. Nyquist plot of electrodes immersed overnight in multipurpose contact solution before DC biasing and after 10 seconds of DC biasing.

5.3.2 Effects of DC biasing on the components of the impedance

The Nyquist plot shown in Figure 5.2 shows a comparison between the impedance of electrodes placed overnight in multipurpose contact solution before and after 10 seconds of DC biasing. A shift to the left and up is observed after cleaning, indicating a decrease in both the resistance and the reactance at all frequencies. The slope of the line approximately doubles after cleaning, indicating that changes to the resistive component of the impedance are stronger than the capacitive components.

5.3.3 Effects of DC biasing following model biomolecule adsorption

Figure 5.3(a) shows that a set of electrodes immersed in BSA experienced a statistically significant increase of 17% (from Z=491.7 $\pm$ 4.9 kΩ to Z=573.13 $\pm$ 4.54 kΩ) in the 1 kHz impedance compared to baseline (p<0.0001). After DC biasing for 15 seconds at 1.5 V, the 1 kHz impedance returned to a value statistically identical to the baseline impedance (Z=481.9 $\pm$ 4.54 kΩ).

Figure 5.3(b) shows that a different set of electrodes inserted into an agar phantom brain experience a statistically significant increase of 20.2% (from Z= 340.16 $\pm$ 5.5 to Z= 409.27 $\pm$ 5.58 kΩ) compared to baseline (p<0.0001). After DC biasing at 1.5 V for 15 seconds, the 1 kHz impedance returned to a value indistinguishable from baseline impedance (Z=339.29 $\pm$ 5.77 kΩ).

5.3.4 Effects of DC biasing following *in vivo* exposure to brain tissue

Figure 5.4 shows that electrodes inserted into rat cortex during an acute surgery experience a statistically significant increase of 33% (from Z=480.59 $\pm$ 12.15 to 639.61 $\pm$ 12.15 kΩ) in the 1 kHz impedance compared to baseline. After DC biasing for 15 seconds at 1.5 V, the 1 kHz impedance returned to a value statistically identical to the baseline (Z=470 $\pm$ 12.15 kΩ).

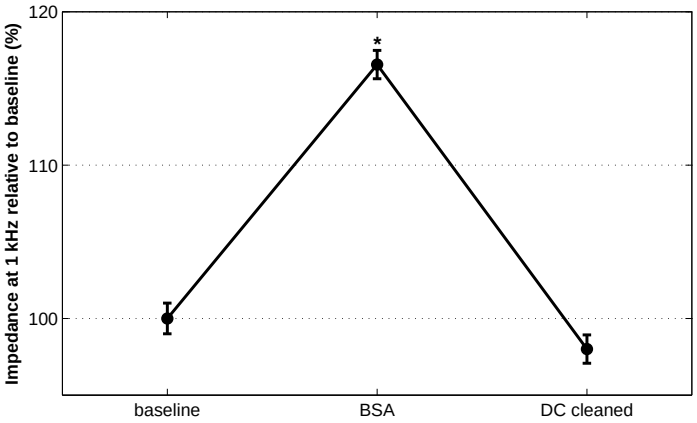

(a) Effects of DC biasing for 15 seconds on electrodes immersed in a 10% w/v BSA solution on the 1 kHz impedance, showing a reliable return to baseline

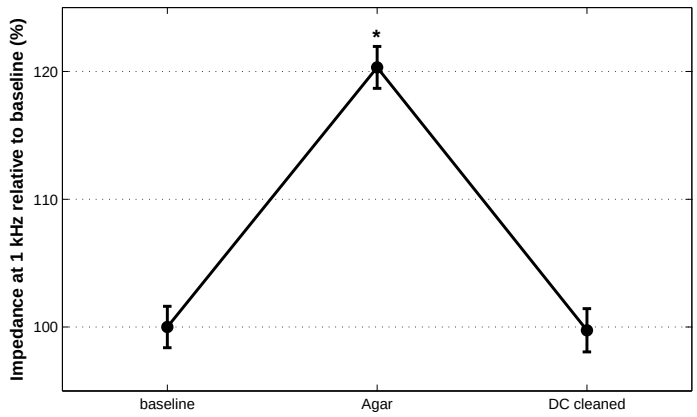

(b) Effects of DC biasing for 15 seconds on electrodes inserted into agar phantom brain on the 1 kHz impedance, showing a reliable return to baseline.

Fig. 5.3. DC biasing returns electrode impedance at 1 kHz to baseline after exposure to protein and agar

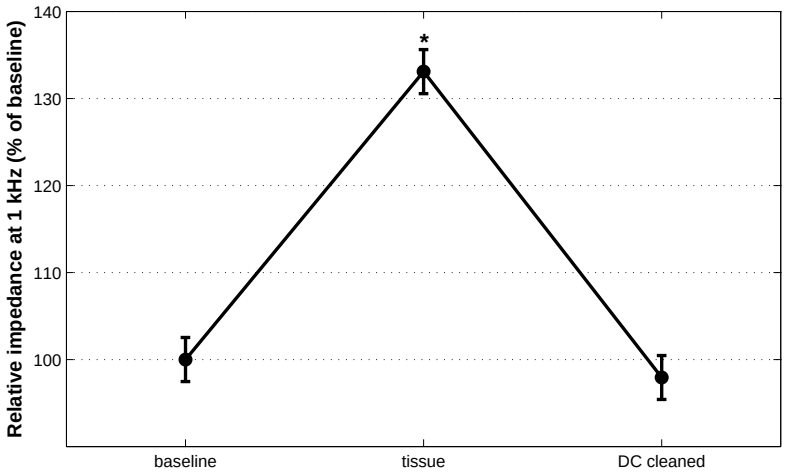

Fig. 5.4. Effects of DC biasing for 15 seconds on the 1 kHz impedance of electrodes acutely implanted into rat cortex, showing a reliable return to baseline.

5.4 Discussion

The use of neural microelectrodes with lower impedance is a common approach to improving recording sensitivity [Keefer et al., 2008, Ludwig et al., 2011]. While tissue and extracellular components are the major culprits in degrading recording quality for chronic electrodes, the time scale in most acute experiments is not long enough for these tissue responses to develop [Kozai et al., 2012b]. In such experiments, increases in the electrode impedance will be the result of adsorbed protein and other biomolecules from brain tissue. Most common cleaning procedures are time intensive, and cannot practically be performed within the confines of an acute experiment. In this chapter we described an alternative cleaning method using DC biasing to restore electrode impedance following exposure to a variety of biomolecules and brain tissue. Concerns about altering the chemical composition of the electrode are not realized with DC biasing at 1.5 for durations of less than 20 seconds, as observed by the 1 kHz impedance approaching asymptotic values. Typically, oxidation of iridium to form activated iridium oxide (AIROF) is achieved by repetitive voltage cycling in sulfuric acid [Burke and Whelan, 1984, Robblee et al., 1983, Zerbino et al., 1978], so it is unlikely that activated iridium oxide layers would form on electrodes cleaned by DC biasing in PBS. We have not investigated the effect of holding DC bias on a microelectrode for durations longer than 20 seconds, since durations under 20 seconds appear to be sufficient to return electrodes exposed

to biological solutions to baseline values. The drawback of this method is that the cleaning effect of the DC biasing is likely to be confined to the surface of the electrode site, and would not be useful to remove adsorbed molecules elsewhere on the electrode shank. We propose that this method is a useful approach to cleaning electrodes during acute experiments with multiple insertions for the same electrode. It could also be used as an adjunct cleaning step for chronic electrodes pre-implantation, either prior to or following sterilization.

6. CELLULAR RESPONSES TO MICROSCALE FOREIGN BODIES DIP-COATED WITH LPS AND PEG

6.1 Introduction

The biological pathways governing the progression of the RTR to ICMs are not well characterized. Dural and blood vessel damage appears to be a major factor contributing to the RTR [Saxena et al., 2013]. This RTR has been shown to be non-uniform and depth related [Woolley et al., 2013], with stronger scarring closer to the surface of the brain. Recent work has shown that transdural implants elicit a much higher response that implants dwelling completely within the brain [Markwardt et al., 2013]. These findings collectively suggest that the introduction of dural fibroblasts, blood borne cells, and proteins into the brain activates inflammatory pathways, and that this activation is strongest at the site of injury to these structures. Potential mechanisms include accumulation of reactive oxygen species and activation of toll-like receptor 4 (TL4) [Potter et al., 2013, Ravikumar et al., 2013]. The complexity underlying *in vivo* conditions and obscuring biological mechanisms can be somewhat controlled by using *in vitro* cell culture models. The most widely used model was described by Polikov et al. [2006, 2009] using microscale foreign bodies in primary mixed

neural cultures. This model has been widely applied to test biocompatibility of various materials as neural interfaces [Achyuta et al., 2010, Ereifej et al., 2013, Tien et al., 2013]. While this model relies on modifying culture media to achieve a globally elevated activation state, we posit that the model can be slightly modified by dip coating in lipopolysaccharide (LPS) to simulate an inflammatory microenvironment localized around the foreign body placed in the cell cultures. LPS is a known upregulator of microglial activation through TL4 binding [Lehnardt et al., 2003, Tzeng et al., 2005], and as such is an attractive option for modifying the Polikov model to test cellular responses to specific, localized targeting of TL4 receptors.

Previous research in the neurotrauma field has also found that, due its surfactant properties, soluble PEG can induce membrane sealing of damaged cells and reduce edema. This has been shown to significantly improve recovery from both spinal cord and traumatic brain injuries by inducing cellular and behavioral recovery [Koob and Borgens, 2006, Koob et al., 2008]. In this regard, a non-grafted dip-coated PEG film is a technically and economically attractive option to achieve both antifouling and membrane sealing. Our hypothesis is that a dip-coated layer of high molecular weight PEG will exhibit sufficient short term stability, simultaneously preventing adverse changes in electrical properties of microelectrodes as well as and modulating cellular responses in response to microelectrodes *in vitro*. Given the importance of the early stages

of the injury response in shaping the later chronic stages, this approach might prove highly beneficial *in vivo*.

6.2 Methods

6.2.1 Cell culture and microwire placement

The experimental procedures complied with the Guide for the Care and Use of Laboratory Animals and were approved by The Purdue Animal Care and Use Committee (PACUC). Forebrains from E17 embryonic rat pups were received suspended in 5 mL of Solution 1 (NaCl 7.24g/L; KCl 0.4g/L; NaH2PO4 0.14g/L; Glucose 2.61g/L; Hepes 5.96g/L; MgSO4 0.295 g/L; BSA 3 g/L) in a 50 mL centrifuge tube. Under sterile conditions, the tissue was gently triturated with an added 18 μL of trypsin solution (Sigma-Aldrich, St. Louis, MO) (7.5mg/mL in 0.9% saline). Following 20 minute incubation in a 37°C water bath, 100 μL of trypsin inhibitor/DNAse solution (Sigma-Aldrich, St. Louis, MO) (2.5 mg/mL trypsin inhibitor, 400 μg/mL DNAse in 0.9% saline) was added and tissue was again gently triturated. The tissue was then centrifuged at 1,000 rpm for 5 minutes at room temperature and supernatant was poured off. Cells were re-suspended in 16 mL of Hibernate-E (Brainbits, Springfield, IL) and triturated again. Cells were filtered through a cell strainer and centrifuged at 1,400 rpm for 5 min at room temperature. Supernatant was poured off and cells were re-suspended in a culture medium consisting of Dulbecco's modified

Eagle's Medium (DMEM) with 10% Fetal Bovine Serum (FBS) and 10% horse serum (HS). The cells were then seeded in 96 well plates at a density of 500,000 cells/cm2, and cultured for 7 days at 37°C and 5% CO2, with the cell media being replaced every 48 hours. At day 7 *in vitro*, lengths of 50 μm-diameter tungsten microwire (California Fine Wire Co., Grover Beach, CA) were autoclaved then cut into small segments of 5-7 mm in length using carbide scissors. The microwire segments were treated by dip coating with one of four treatments: LPS (50 ng/mL) only, PEG (20% aqueous solution, 4000 MW) only, a 1:1 mixture of LPS and PEG, or uncoated. In each well, one segment of microwire was dropped into the medium and allowed to sink to the bottom of the well. The plates were then placed in the incubator for an additional 7 days. Figure 6.1(A) shows wells with microwire.

6.2.2 Cell fixing and labeling

At day 14 *in vitro*, the cultures were fixed with 4% paraformaldehyde for 10 minutes, rinsed 3x with Hepes Buffered Hank's saline (HBHS) (in g/L; 7.5 g NaCl, 0.3 g KCl, 0.06 g KH2PO4, 0.13 g Na2HPO4, 2 g Glucose, 2.4 g HEPES, 0.05 g MgCl2:6H2O, 0.05 g MgSO4:7H2O, 0.165 g CaCl2, 90 mg NaN3, at pH 7.4), then permeabilized with 0.2% Triton-X (Sigma-Aldrich, St. Louis, MO). The cultures were then blocked with 10% normal goat serum (Jackson Immunoresearch, West Grove, PA) for 1 hour, after which primary antibodies were added. These antibodies include beta-3-tubulin (β-3-tub) (Covance, Princeton,

NJ), which labels neurons; Glial Fibrillary Acidic Protein (GFAP) (Millipore, Billerica, MA), which labels astrocytes; and Ionized Calcium binding adaptor molecule 1 (Iba-1) (Wako, Osaka, Japan), and the cultures incubated in a 4°C refrigerator overnight. The wells were then aspirated, rinsed in HBHS 3x, and the following secondary antibodies were added: Alexa Fluor 488 Goat anti-mouse, Alexa Fluor 555 Goat anti-chicken, and Alexa Fluor 635 Goat anti-rabbit (Invitrogen, Carlsbad, CA). After a 2 hour incubation at room temperature, the secondary antibodies were rinsed 3x with HBHS, and a final volume of 100 μL of HBHS was left in the wells for imaging.

6.2.3 Image acquisition and analysis:

With the microwire still attached to the bottom of the Fluorescent images of 512x512 pixels with obtained on a confocal microscope fitted with a long working distance 10x air objective using Fluoview software (Olympus, Center Valley, PA). The different channels were imaged sequentially, and noise reduction was achieved by applying a Kalman filter built into the acquisition software to 3 scans for each channel. Each plate was imaged using the same set of imaging parameters (laser power, aperture, acquisition time) to ensure uniformity. Source images were imported into ImageJ (ImageJ, U. S. National Institutes of Health, Bethesda, MD) and visually inspected and rotated to place the microwire in a vertical orientation, as shown in Figure 6.1(B). When possible, two adjacent rectangular selections, 480 pixels high by 240 pixels wide (equivalent

to 994 μm by 496 μm), were made with the long edge running on the center of the microwire. If that was not possible due to excessive proximity to wall of the well, only a single rectangular selection was made facing the interior of the well. From these selections, intensity profiles of average brightness of each vertical line were generated, as shown in Figure 6.1(C). Microwire segments were also imaged in three empty wells, and an average intensity profile was obtained and subtracted from the intensity profile generated from cell-containing wells. Three response indices (one per cell type) for each region were obtained by summing the area underneath the intensity profile line between the distance points corresponding to the defined region , and dividing by 10000. Statistical analysis was performed using the SAS 9.3 statistical package (SAS Institute Inc., Cary, NC) . A general linear model (GLM) procedure was used perform to a one way ANOVA with block, to remove the effects of variations between the plates by treating the plates as a statistical block. Post hoc Tukey tests were used to determine statistical significance between the treatment groups at a significance level of α<0.05. Plots were generated using MATLAB (The MathWorks Inc., Natick, MA).

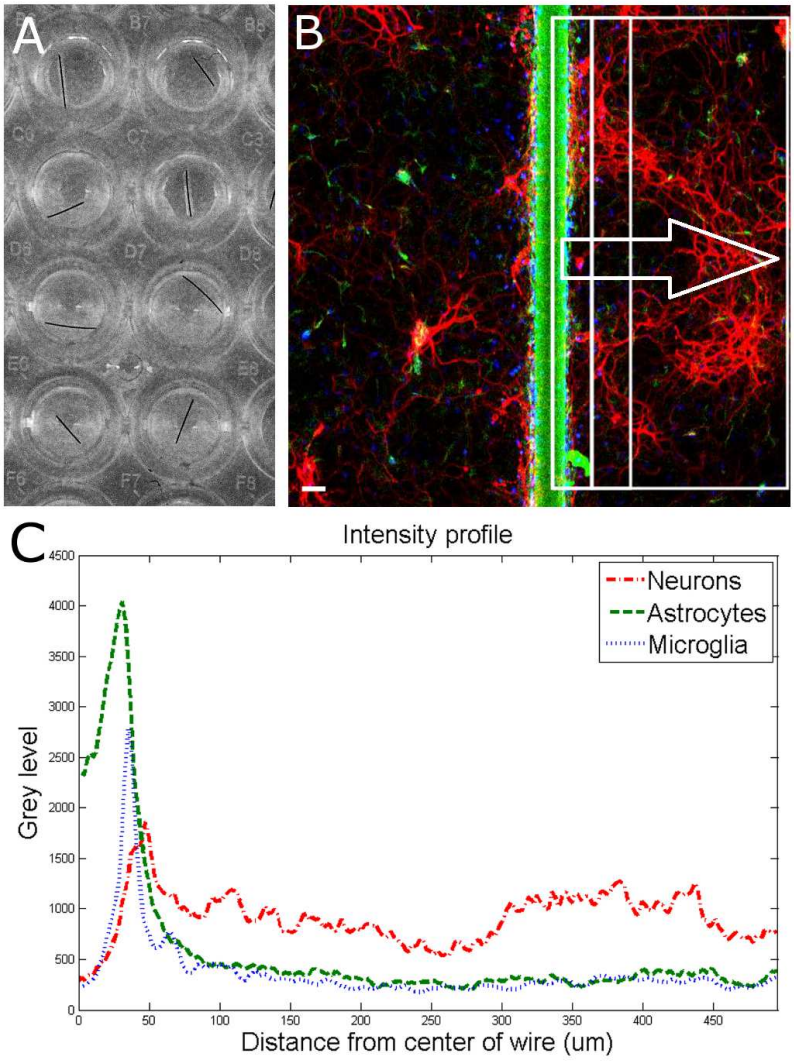

Fig. 6.1. Image quantification. Wells in 96 well plate (A) were imaged to produce a fluorescent image (B) and extract intensity profiles for each channel. The fluorescent image is pseudocolored to show neurons in red, astrocytes in green, and microglia in blue. Scale bar is 50 μm. For each examined region (examples shown within rectangles), three intensity profiles (C) are generated, and response indices calculated by summing the area under the graph corresponding to the chosen distances.

6.3 Results

6.3.1 Microglia

As shown in Figure 6.2, in the interface area containing only the microwire, the only significant difference in the microglial response index was between the PEG coated microwire and LPS coated microwire (RI=1.37 vs. 2.2, p=0.007). For the interface area containing the microwire and extending over an adjacent 25um, significant pairwise differences were observed between the LPS coated microwire (RI=5.84) and the other microwires (uncoated RI=4.92, p=0.041; PEG RI=4.26, p<0.0001; LPS+PEG RI=4.82, p=0.022) . For a wider interface area containing the microwire and extending over the adjacent 50um, these pairwise differences get stronger between the LPS coated microwire (RI=8.27) and the other microwires (uncoated RI=6.58, p=0.0007; PEG RI=5.8, p<0.0001; LPS+PEG RI=6.4, p=0.0002).

Figure 6.3 shows the microglial responses at more distant regions. For the closest distant bin extending from 50 to 150um from edge of microwire, the response index for LPS coated microwire (RI=5.62) was significantly higher than all the other treatments (uncoated RI=4.21, p=0.0001; PEG RI=3.71, p<0.0001; LPS+PEG RI=3.91, p<0.0001). For the next three distant 100um wide bins, the only significant difference observed was between LPS coated microwire and PEG coated microwire in all 3 bins. The calculated RI are as follows: for the bin

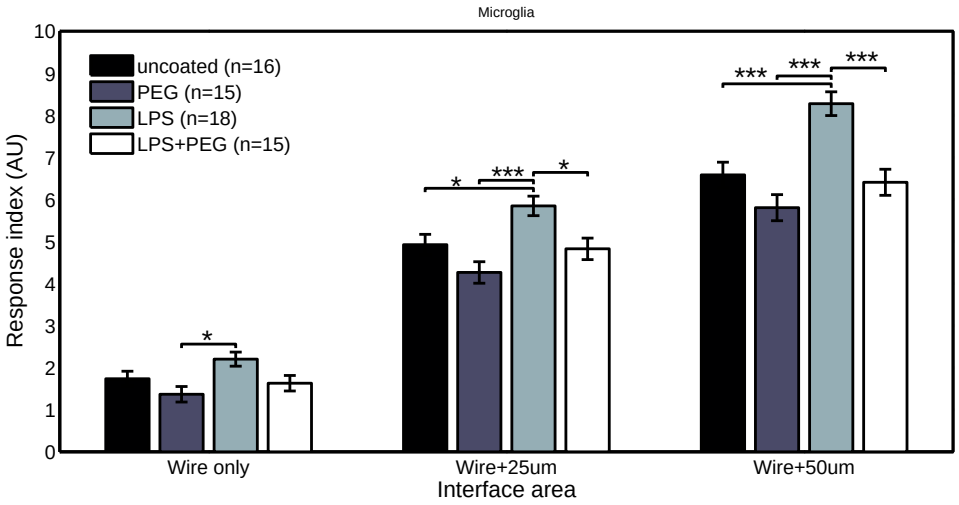

Fig. 6.2. Microglia—interface. For the narrowest interface are, the only significant difference in the response index was between the PEG coated microwire and LPS coated microwire. For the wider interface areas, significant pairwise differences were observed between the LPS coated microwire and all the other microwires. Error bars represent standard errors of the mean.

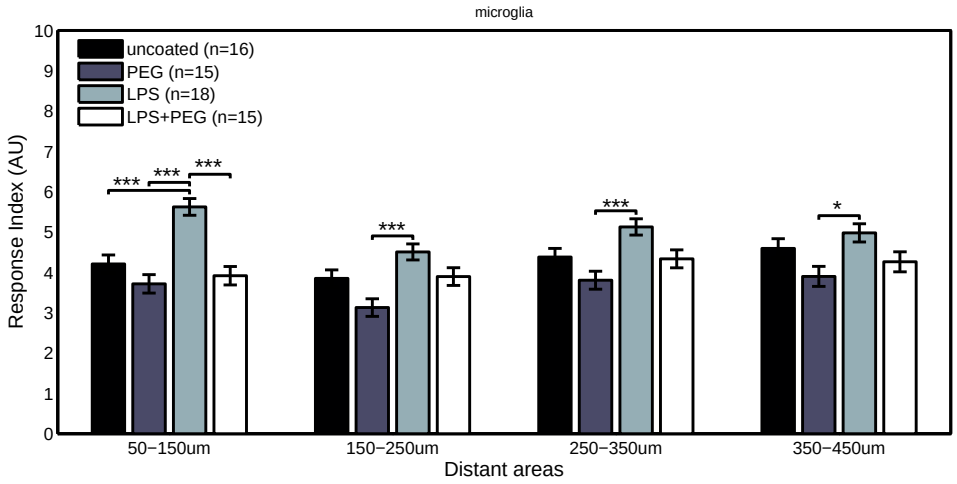

Fig. 6.3. Microglia—distant. For the closest distant bin (50-150um from edge of microwire), the response index for LPS coated microwire was significantly higher than all the other treatments. For the more distant bins, the only significant difference observed was between LPS coated microwire and PEG coated microwire in all 3 bins. Error bars represent standard errors of the mean.

extending from 150 to 250um from edge of microwire: LPS RI=4.5 vs. PEG 3.12, p=0.0001; for the bin extending 250 to 350um from edge of microwire: RI= 5.12 vs. 3.8, p=0.0003; for the bin extending 350 to 450um from edge of microwire): RI=4.98 vs. 3.9, p=0.01.

Figure 6.4 shows the astrocyte response index at interface areas. For the interface area containing only the microwire, the astrocyte response index for LPS coated microwire (RI=3.33) was significantly higher than PEG coated and LPS+PEG coated microwire (PEG RI=2.59, p=0.015; LPS+PEG RI=2.63, p=0.02).

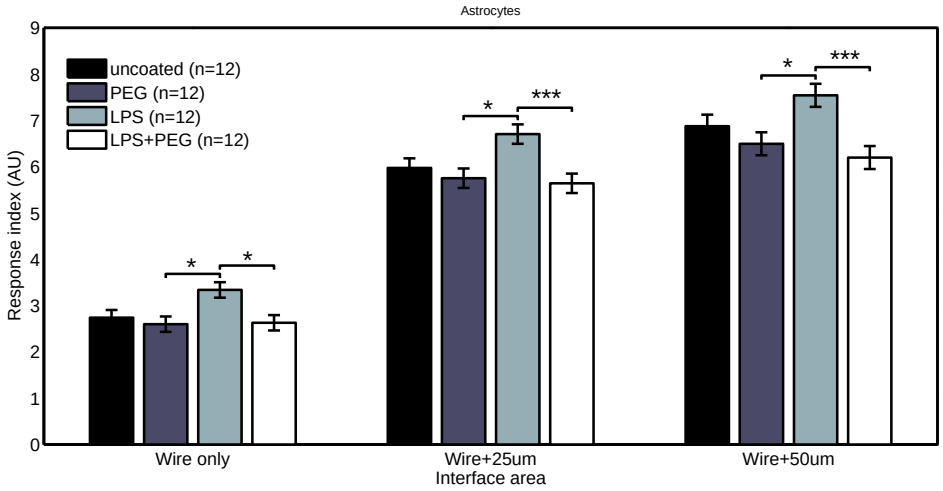

Fig. 6.4. Astrocytes—interface. In all examined interface areas, the astrocyte response index for LPS coated microwire was significantly higher than PEG coated and LPS+PEG coated microwire, but not uncoated microwire. Error bars represent standard errors of the mean.

For the interface area containing the microwire and extending an adjacent 25um, the same pairwise difference were observed, but with a stronger difference between the LPS coated microwire (RI=6.7) and the LPS+PEG coated microwire (PEG RI=5.75, p=0.012; LPS+PEG RI=5.64, p=0.0045). For the interface area containing the microwire and extending an adjacent 50μm, the same observation of the LPS astrocyte response index being higher than both PEG and LPS+PEG was noticed (LPS RI=7.54, PEG RI=6.49, p=0.02; LPS+PEG RI=6.19, p=0.002).

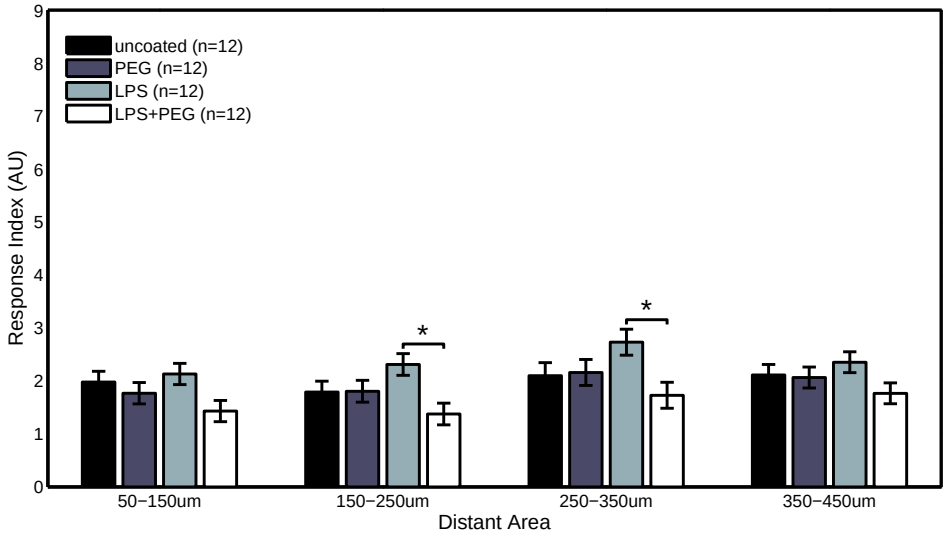

Fig. 6.5. Astrocytes—distant. No significant differences were observed between the different treatments for the closest distant bin. For the middle two distant bins, a slightly significant difference was observed between LPS coated wire and LPS+PEG coated wire. Error bars represent standard errors of the mean.

Figure 6.5 shows the astrocyte response index at distant areas. No significant differences were observed between the different treatments for the closest distant bin extending from 50 to 150um from edge of microwire. For the middle two distant bins, a slightly significant difference was observed between LPS coated wire and LPS+PEG coated wire bin 2 (150-250um from edge of wire): LPS RI=2.31, LPS+PEG RI=1.37, p=0.012; bin 3 (250-350um from edge of wire): LPS RI=2.73, LPS+PEG RI=1.73, p=0.03.

Figure 6.6 shows the neuron response index in interface(a) and distant(b) regions, respectively. No significant differences in the neuron response were found between any of the treatment conditions in either interface or distant region. In contrast to microglia and astrocytes, where the response index was higher in distant areas in comparison to the widest interface area examined, the neuron response index in distant areas was roughly equal to that in the widest interface area examined.

6.4 Discussion

6.4.1 Validity of study:

To test the effects of such a dip coated PEG film on the cellular responses to implanted electrodes, we modified a robust and frequently replicated *in vitro* mixed cortical culture model pioneered by Polikov et al. [2006, 2009]. The main drawback of *in vitro* models is their inability to accurately mimic *in vivo* microenvironments. In this particular model of primary cortical cell cultures, the cells exist in isolation from supporting vasculature, extra-cellular brain tissue components, and meninges. These aforementioned structures are heavily damaged during microelectrode insertion, which has been shown to strongly the chronic response of the brain to implanted microelectrodes [Markwardt et al., 2013, Saxena et al., 2013]. The original model developed by Polikov et al. [2006]

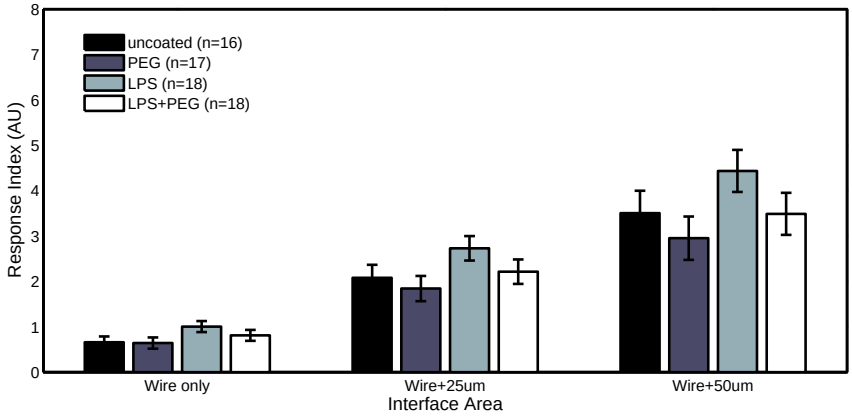

(a) Neurons—interface

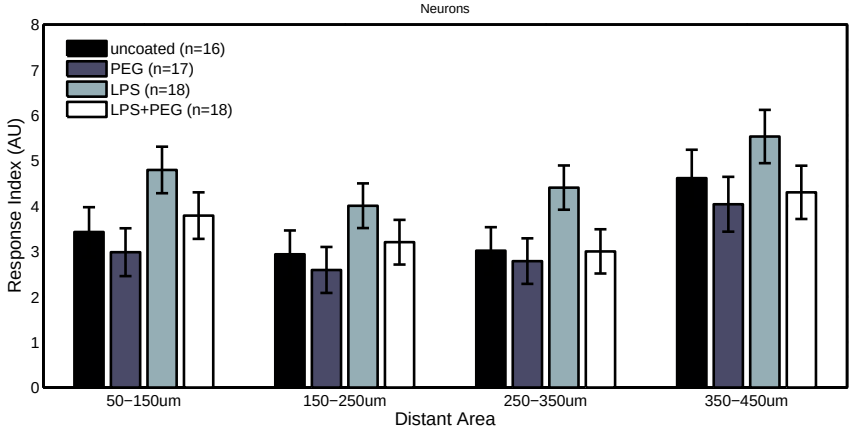

(b) Neurons—distant

Fig. 6.6. Neurons. No significant differences in the neuron response index were observed between any of the treatments in interface or distant areas

did not elicit a consistent glial scar, and it was necessary to alter the composition of the culture media to place all glial cells in the culture in an elevated reactive state, thereby ensuring a consistent glial scar [Polikov et al., 2009]. By coating LPS directly onto microwire, we are able to create a localized inflammatory microenvironment that more closely mimics the reality of an indwelling cortical implant, rather than placing the glial cells in the culture in a globally activated state. This localized inflammatory microenvironment enables us to examine distance related effects on the cultured cells. For the LPS+PEG condition, concerns about cross contamination and the potential to disrupt the dip coated PEG film led to the decision of codepositing PEG and LPS via dip-coating from a single pot. Because PEG has been shown to be an excellent rapid drug release platform [Avula et al., 2013, Craig, 2002], we were confident that our codeposition of PEG and LPS would not hinder the exposure of the cells to LPS.

While a morphological examination of the glial cells in this model to determine the degree of activation is difficult, we can infer the degree of activation from the overall fluorescence levels. Iba-1 and GFAP are upregulated in microglia and astrocytes, respectively, in the activated state. Similar image analysis approaches have been used *in vitro* [Achyuta et al., 2010, Polikov et al., 2009, Tien et al., 2013] and *in vivo* [Azemi et al., 2011, Potter et al., 2013] to analyze responses to microelectrodes and microscale foreign bodies.

6.4.2 Analysis of cellular responses:

Microglia:

When examining the microglial response in a narrow interface region comprising only the area under the microwire, we observe a three tiered response; where a significant difference exists between the LPS only and the PEG only treatments, but not between the other conditions. This tiered response might be attributed to the difference between increased activation caused by the LPS and reduced cellular adhesion caused by PEG. As the examined interface area gets wider, we see a progressive increase in Iba-1 fluorescence in response to the LPS coated wire compared to the other treatments. This increase in Iba-1 fluorescence might be explained by elevated activation of microglia through amplification of inflammatory pathway precipitated by TL4 binding. The observed elevation of Iba-1 fluorescence persists in the next 100μm wide distant region, again indicating an extended inflammatory response, potentially mediated by secreted cytokines produced by activated microglia but dissipates in further distant regions, reverting to a tiered response, where the only significant pairwise difference is between LPS and PEG. This tiered response can again be attributed to distinct pathway amplification between the two treatments; the difference appearing only between the increased upregulation of microglial activation due to LPS and the reduced microglial activation due to PEG.

Astrocytes

In interface regions of carrying width, the astrocyte response also exhibits a three tiered response, where an elevated astrocyte response is observed with LPS, and a reduction occurs with both PEG conditions (with LPS and without). In the distant regions, the first and fourth 100um wide distant bin do not exhibit any differences between the different treatments, but we observe a difference between LPS and LPS+PEG in the middle two 100um wide bins, but surprisingly no difference between LPS and PEG in these distant areas. A potential explanation is that the astrocytes are exhibiting a dose dependent response to LPS. Under this explanation, the increased activation in the interface area for the LPS only treatment results in both astrocyte migration from distant regions and increased overall activation; delivering the LPS with PEG results in astrocyte migration without an accompanying equivalent increase in activation, resulting in a depletion of distant astrocytes; while PEG only results in even less astrocyte activation in interface areas, which in turn does not signal migration of distant astrocytes. Because we did not directly test for whether LPS was acting through direct binding to receptors on astrocyte surfaces, we are merely discussing correlative effects. It is unclear whether the astrocyte response is due to direct action by LPS, or if it they are reacting to cytokines and chemokines secreted by microglia. While astrocytes are not typically thought to express TL4 receptors, there is some evidence to the contrary [Bowman et al.,

2003]. Additionally, while GFAP-positive astrocytes are observed in primary cultures, a considerable portion of them differentiate *in vitro* from astrocyte precursors [Abney et al., 1981]. It is possible that due to these culture conditions that the astrocyte response is altered from normally developing astrocytes *in vivo*.

Neurons

No significant differences were detected in neuron response to any of the treatments, in either interface or distant regions. While not statistically significant, a coupling between neuron and astrocyte response can be noticed, where slightly higher (but not significantly different) neuron growth was observed for the LPS treatment. Neuronal growth has been consistently shown to occur on a supporting substrate of astrocytes [Noble et al., 1984, Tomaselli et al., 1988]. In contrast to the microglia and astrocytes, where the response in the widest interface bin was considerably higher than the first adjacent distant bin, the neuron response in that distant bin was comparable to that in the wide interface bin, and we did not observe a decline in neuron density over distance. One explanation mirrors the concern expressed earlier about the maturity of the astrocytes, where immature astrocytes in culture provided a better substrate for neuron outgrowth compared to mature astrocytes [Smith et al., 1990]. An alternative explanation is that elevated glial activation is not, in and of itself, neurotoxic or neurodegenerative within a foreign body reactive tissue response paradigm. If

the latter explanation is correct, then the loss of neural density *in vivo* following implantation of a microelectrode might be better explained by displacement of neurons following insertion trauma and edema which fail to reoccupy depleted zones because of the glial scar formation, or that *in vivo* neurotoxicity occurs due to direct contact between neurons and extrabrain components.

6.4.3 Conclusion

We have shown that microglial response in a primary mixed cortical culture can be manipulated by dip-coating microscale foreign bodies. Microglial response can be increased by coating the surface of the foreign body with LPS, and this increase can be prevented by codepositing LPS and PEG. As described in Chapter 2, we hypothesize that the film of high molecular weight PEG, while allowing for LPS release, presents a hydrated physical barrier that disrupts cytokine, chemokines and adsorbed protein gradients that typically guide pathological responses. Astrocyte response also increased for LPS coated foreign bodies, but it is unclear whether this response is directly mediated by LPS or whether it is caused by other microglia-secreted factors. Neuron response was not negatively correlated with microglial response, raising questions about the mechanisms of chronic *in vivo* neuronal density loss .

7. CONCLUDING REMARKS

7.1 Summary

Implantable ICMs are a promising technique for treating a wide range of neurological deficiencies, but they face many challenges to becoming a viable candidate for human clinical use. The major challenge faced by such devices is their unreliability in chronic use. The causes of this unreliability are not completely understood, but a major suspect is the glial scar formed around the implanted electrode. While much research has been conducted into the progression of the reactive tissue response, no definitive solution has yet emerged.

The work presented in this dissertation highlights several important aspects potentially salient to the progression of the reactive tissue response. Chapter 3 presented an analysis of silica sol-gel dip-coated thin-films for intracortical electrodes, emphasizing the need to preserve electrical properties when developing neurointegrative and bioactive coatings for intracortical microelectrodes. Chapter 4 described the effects of adsorbed protein on the electrical properties of microelectrodes, and demonstrated the utility of dip-coated high molecular weight PEG in preventing such adsorption induced changes. PEG was also shown to reduce acute impedance increases in preliminary in vivo exper-

iments, suggesting a role for hydrophobic molecular components in influencing impedance changes during the acute phase of the reactive tissue response. Chapter 5 reported a method to restore electrode impedance following exposure to a variety of solutions in vitro and to brain tissue.

While the previous chapters focused on impedance measurements in response to exposure to protein and tissue, and approaches for prevention and cleaning, chapter 6 examined the cellular responses to microscale foreign objects in a primary mixed cortical cell culture model simulating localized inflammation using LPS dip-coated onto the microwires. The observed responses support a role suggested in recent literature for TL4 receptors in the reactive tissue response, but also show that neuronal density in this model is not negatively correlated with microglial activation, indicating mechanisms for neuronal density loss other than glial activation. The results also suggest that dip-coated films of high molecular weight PEG have the potential to disrupt gradients of molecules involved in the reactive tissue response.

7.2 Future Work

The results from this dissertation provide some insights to approach several gaps in the current literature that might be of interest for future work.

The first gap is a lack of a comprehensive understanding of the biological pathways and cascades governing the progression of the reactive tissue response. Systemically delivered drugs or drug eluting coatings requires knowl-

edge of the biological pathway involved to ensure efficient treatment. Most information about the reactive of brain cells to injury comes from the spinal cord and traumatic brain injury literature, which while certainly relevant and important, does not have to contend with the effects of a chronically indwelling implant. It has been shown that stab wounds made with inserted electrodes do not typically result in a glial scar compared to an implanted electrode [Biran et al., 2005], and that a major contributor to the reactive tissue response is the chronic injury to the blood brain barrier [Saxena et al., 2013]. Only recently have efforts been made to examine specific receptors and cytokines involved in the reactive tissue response. TL4 receptors have been the target of several recent publications [Potter et al., 2013, Ravikumar et al., 2013], while other work involved some investigation of upregulation of gene expression of neurotoxic cytokine transcripts using qRT-PCR [Karumbaiah et al., 2012, 2013, Saxena et al., 2013].

A second gap involves understanding the composition of the glial scar, and how that composition relates to the failure of implanted microelectrodes. The typical method of assessing glial scar extent is to examine fluorescence intensity of cell surface markers associated with glial cells like microglia, astrocytes, or oligodendrocytes. The glial scar, however, is not only composed of cells but also of deposited extracellular matrix biomolecules, such as proteoglycans, laminin, and collagen. As shown in this dissertation, biomolecules have a considerable effect on the properties of neural microelectrodes, and potentially on the pro-

gression of the reactive tissue response. While a recent study by Barrese et al. [2013] that retrospectively analyzed large sets of chronic data confirmed that the acute biological response is not necessarily correlated to electrical performance, the majority of chronic failures in that study were due to biological factors.

With the goal of identifying various extracellular proteins and receptors involved in the reactive tissue response, a systematic genomic and proteomic approach is preferable to ad hoc examinations of individual proteins or cytokines. This might be possible by collecting slices of tissue containing the entire device and encapsulation tissue as described by Woolley et al. [2011, 2012, 2013], and using DNA or protein microarray technologies which enable the analysis of thousands of parameters in a single experiment [Heller, 2002, Templin et al., 2002]. Such an approach would be an immense leap over current piecemeal approaches if successful at identifying molecular components of the glial scar and/or genes involved in its formation.

Another gap in the literature concerns the biphasic nature of the reactive tissue response. While consistent reports appear in the literature on the volatility of the acute response and the intransigence of the chronic response to various treatments, it is unclear as to why this discrepancy exists and why treatments that affect the acute response are not effective against the chronic response. It is possible that systematic genomic and proteomic data mining techniques examining the glial scar over an extended timeline might be able to shed light on this

question. Recent reports detailing the role of transmeningeal implants [Barrese et al., 2013, Markwardt et al., 2013, Woolley et al., 2013] suggest the importance of migrating away from the paradigm of wired implants and towards wireless systems. With constant advances in that field, it is very possible that such devices might be realized in the near future. Even so, a detailed understanding of the composition of the glial scar and the biological switches controlling the progression of the reactive tissue response are avoid designs and approaches that would still be susceptible to degradation and failure due to the reactive tissue response.

LIST OF REFERENCES

LIST OF REFERENCES

M. R. Abidian and D. C. Martin. Experimental and theoretical characterization of implantable neural microelectrodes modified with conducting polymer nanotubes. *Biomaterials*, 29(9):1273–1283, 2008.

M. R. Abidian and D. C. Martin. Multifunctional Nanobiomaterials for Neural Interfaces. *Advanced Functional Materials*, 19(4):573–585, 2009.

M. R. Abidian, D. H. Kim, and D. C. Martin. Conducting-polymer nanotubes for controlled drug release. *Adv. Mater*, 18:405–409, 2006.

M. R. Abidian, L. G. Salas, A. Yazdan-Shahmorad, T. C. Marzullo, D. C. Martin, and D. R. Kipke. In-vivo Evaluation of Chronically Implanted Neural Microelectrode Arrays Modified with Poly (3,4-ethylenedioxythiophene) Nanotubes. *2007 3rd International IEEE/EMBS Conference on Neural Engineering*, pages 61–64, May 2007.

M. R. Abidian, K. A. Ludwig, T. C. Marzullo, D. C. Martin, and D. R. Kipke. Interfacing Conducting Polymer Nanotubes with the Central Nervous System: Chronic Neural Recording using Poly(3,4-ethylenedioxythiophene) Nanotubes. *Advanced Materials*, 21(37):3764–3770, 2009.

M. R. Abidian, J. M. Corey, D. R. Kipke, and D. C. Martin. Conducting-Polymer Nanotubes Improve Electrical Properties, Mechanical Adhesion, Neural Attachment, and Neurite Outgrowth of Neural Electrodes. *Small*, 6(3):421–429, 2010.

E. R. Abney, P. P. Bartlett, and M. C. Raff. Astrocytes, ependymal cells, and oligodendrocytes develop on schedule in dissociated cell cultures of embryonic rat brain. *Developmental biology*, 83(2):301–310, 1981.

A. K. H. Achyuta, V. S. Polikov, A. J. White, H. G. P. Lewis, and S. K. Murthy. Biocompatibility Assessment of Insulating Silicone Polymer Coatings Using an in vitro Glial Scar Assay. *Macromolecular Bioscience*, 10(8):872–880, 2010.

D. J. Anderson, K. Najafi, S. J. Tanghe, D. A. Evans, K. L. Levy, J. F. Hetke, X. L. Xue, J. J. Zappia, and K. D. Wise. Batch fabricated thin-film electrodes for stimulation of thecentral auditory system. *Biomedical Engineering, IEEE Transactions on*, 36(7):693–704, July 1989.

R. A. Asher, D. A. Morgenstern, L. D. F. Moon, and J. W. Fawcett. Chondroitin sulphate proteoglycans: inhibitory components of the glial scar. *Progress in brain research*, 132:611–619, 2001.

R. K. Assoian, A. Komoriya, C. A. Meyers, D. M. Miller, and M. B. Sporn. Transforming growth factor-beta in human platelets. Identification of a major storage site, purification, and characterization. *Journal of Biological Chemistry*, 258(11):7155–7160, 1983.

D. Avnir, T. Coradin, O. Lev, and J. Livage. Recent bio-applications of sol–gel materials. *Journal of Materials Chemistry*, 16(11):1013–1030, 2006.

M. N. Avula, A. N. Rao, L. D. McGill, D. W. Grainger, and F. Solzbacher. Modulation of the foreign body response to implanted sensor models through device-based delivery of the tyrosine kinase inhibitor, masitinib. *Biomaterials*, 34(38): 9737–9746, 2013.

E. Azemi, W. R. Stauffer, M. S. Gostock, C. F. Lagenaur, and X. T. Cui. Surface immobilization of neural adhesion molecule L1 for improving the biocompatibility of chronic neural probes: In vitro characterization. *Acta Biomaterialia*, 2008.

E. Azemi, C. F. Lagenaur, and X. T. Cui. The surface immobilization of the neural adhesion molecule L1 on neural probes and its effect on neuronal density and gliosis at the probe/tissue interface. *Biomaterials*, 32(3):681–692, 2011.

A. N. Badi, T. R. Kertesz, R. K. Gurgel, C. Shelton, and R. A. Normann. Development of a Novel Eighth-Nerve Intraneural Auditory Neuroprosthesis. *The Laryngoscope*, 113(5):833, 2003.

M. Banay-Schwartz, A. Kenessey, T. DeGuzman, A. Lajtha, and M. Palkovits. Protein content of various regions of rat brain and adult and aging human brain. *Age*, 15(2):51–54, 1992.

J. C. Barrese, N. Rao, K. Paroo, C. Triebwasser, C. Vargas-Irwin, L. Franquemont, and J. P. Donoghue. Failure mode analysis of silicon-based intracortical microelectrode arrays in non-human primates. *Journal of neural engineering*, 10(6):66014, 2013.

M. Berkowitz, O. K.O., D. L. Kruse, and C. Harver. *Spinal Cord Injury: An Analysis of Medical and Social Costs*. Demos Medical Publishing, 1998.

R. Biran, D. C. Martin, and P. A. Tresco. Neuronal cell loss accompanies the brain tissue response to chronically implanted silicon microelectrode arrays. *Experimental Neurology*, 195(1):115–126, 2005.

C. S. Bjornsson, S. J. Oh, Y. A. Al-Kofahi, Y. J. Lim, K. L. Smith, J. N. Turner, S. De, B. Roysam, W. Shain, and S. J. Kim. Effects of insertion conditions on tissue strain and vascular damage during neuroprosthetic device insertion. *J. of Neural Eng*, 3(3):196–207, 2006.

D. Bluestein, K. B. Chandran, and K. B. Manning. Towards non-thrombogenic performance of blood recirculating devices. *Annals of biomedical engineering*, 38(3):1236–56, Mar. 2010.

C. C. Bowman, A. Rasley, S. L. Tranguch, and I. Marriott. Cultured astrocytes express toll-like receptors for bacterial products. *Glia*, 43(3):281–91, Sept. 2003.

L. D. Burke and D. P. Whelan. A voltammetric investigation of the charge storage reactions of hydrous iridium oxide layers. *Journal of electroanalytical chemistry and interfacial electrochemistry*, 162(1):121–141, 1984.

P. K. Campbell, K. E. Jones, R. J. Huber, K. W. Horch, and R. A. Normann. A silicon-based, three-dimensional neural interface: manufacturingprocesses for an intracortical electrode array. *Biomedical Engineering, IEEE Transactions on*, 38(8):758–768, 1991.

M. Cavaglia, S. M. Dombrowski, J. Drazba, A. Vasanji, P. M. Bokesch, and D. Janigro. Regional variation in brain capillary density and vascular response to ischemia. *Brain Research*, 910(1-2):81–93, 2001.

Z.-J. Chen, G. T. Gillies, W. C. Broaddus, S. S. Prabhu, H. Fillmore, R. M. Mitchell, F. D. Corwin, and P. P. Fatouros. A realistic brain tissue phantom for intraparenchymal infusion studies. *Journal of neurosurgery*, 101(2):314–322, 2004.

K. C. Cheung. Implantable microscale neural interfaces. *Biomedical Microdevices*, 9:923–938, 2007.

S. H. Choi, E. H. Joe, S. U. Kim, and B. K. Jin. Thrombin-induced microglial activation produces degeneration of nigral dopaminergic neurons in vivo. *Journal of Neuroscience*, 23(13):5877–5886, 2003.

R. S. Clark, J. K. Schiding, S. L. Kaczorowski, D. W. Marion, and P. M. Kochanek. Neutrophil accumulation after traumatic brain injury in rats: comparison of weight drop and controlled cortical impact models. *J Neurotrauma*, 11(5):499–506, 1994.

S. F. Cogan. Neural Stimulation and Recording Electrodes. *Annual Review of Biomedical Engineering*, 10(1), 2008.

D. Q. M. Craig. The mechanisms of drug release from solid dispersions in water-soluble polymers. *International Journal of Pharmaceutics*, 231(2):131–144, 2002.

K. N. Crea, M. N. Shivdasani, R. E. Argent, S. J. Mauger, G. D. Rathbone, S. J. O'Leary, and A. G. Paolini. Acute cochlear nucleus compression alters tuning properties of inferior colliculus neurons. *Audiology and Neurotology*, 15(1):18–26, 2009.

X. T. Cui and D. C. Martin. Electrochemical deposition and characterization of poly (3, 4-ethylenedioxythiophene) on neural microelectrode arrays. *Sensors & Actuators: B. Chemical*, 89(1-2):92–102, 2003.

X. T. Cui and D. D. Zhou. Poly (3, 4-Ethylenedioxythiophene) for Chronic Neural Stimulation. *Neural Systems and Rehabilitation Engineering, IEEE Transactions on*, 15(4):502–508, 2007.

X. T. Cui, V. a. Lee, Y. Raphael, J. A. Wiler, J. F. Hetke, D. J. Anderson, and D. C. Martin. Surface modification of neural recording electrodes with conducting polymer/biomolecule blends. *Journal of biomedical materials research*, 56 (2):261–72, Aug. 2001.

X. T. Cui, J. Wiler, M. Dzaman, R. A. Altschuler, and D. C. Martin. In vivo studies of polypyrrole/peptide coated neural probes. *Biomaterials*, 24(5):777–787, 2003.

D. Davalos, J. Grutzendler, G. Yang, J. V. Kim, Y. Zuo, S. Jung, D. R. Littman, M. L. Dustin, and W. B. Gan. ATP mediates rapid microglial response to local brain injury in vivo. *Nature Neuroscience*, 8:752–758, 2005.

S. J. A. Davies, P. M. Field, and G. Raisman. Regeneration of Cut Adult Axons Fails Even in the Presence of Continuous Aligned Glial Pathways. *Experimental Neurology*, 142(2):203–216, 1996.

T. F. Deuel and J. S. Huang. Platelet-derived growth factor. Structure, function, and roles in normal and transformed cells. *Journal of Clinical Investigation*, 74(3):669, 1984.

K. L. Drake, K. D. Wise, J. Farraye, D. J. Anderson, and S. L. BeMent. Performance of planar multisite microprobes in recordingextracellular single-unit intracortical activity. *Biomedical Engineering, IEEE Transactions on*, 35(9): 719–732, 1988.

D. J. Edell, V. V. Toi, V. M. McNeil, and L. D. Clark. Factors influencing the biocompatibility of insertable siliconmicroshafts in cerebral cortex. *Biomedical Engineering, IEEE Transactions on*, 39(6):635–643, 1992.

H. Ehrenreich, T. Costa, K. A. Clouse, R. M. Pluta, Y. Ogino, J. E. Coligan, and P. R. Burd. Thrombin is a regulator of astrocytic endothelin-1. *Brain Res*, 600 (2):201–207, 1993.

L. F. Eng. Glial fibrillary acidic protein (GFAP): the major protein of glial intermediate filaments in differentiated astrocytes. *J Neuroimmunol*, 8(4-6): 203–214, 1985.

E. S. Ereifej, S. Khan, G. Newaz, J. Zhang, G. W. Auner, and P. J. VandeVord. Comparative assessment of iridium oxide and platinum alloy wires using an in vitro glial scar assay. *Biomedical Microdevices*, pages 1–8, 2013.

J. W. Fawcett and R. A. Asher. The glial scar and central nervous system repair. *Brain Research Bulletin*, 49(6):377–391, 1999.

M. T. Fitch and J. Silver. CNS injury, glial scars, and inflammation: Inhibitory extracellular matrices and regeneration failure. *Experimental neurology*, 209 (2):294–301, 2008.

J. P. Frampton, M. R. Hynd, M. L. Shuler, and W. Shain. Effects of Glial Cells on Electrode Impedance Recorded from Neural Prosthetic Devices In Vitro. *Annals of Biomedical Engineering*, 38(3):1031–1047, Jan. 2010.

P. Grabham and D. D. Cunningham. Thrombin Receptor Activation Stimulates Astrocyte Proliferation and Reversal of Stellation by Distinct Pathways: Involvement of Tyrosine Phosphorylation. *Journal of Neurochemistry*, 64(2): 583–591, 1995.

R. A. Green, N. H. Lovell, and L. A. Poole-Warren. Cell attachment functionality of bioactive conducting polymers for neural interfaces. *Biomaterials*, 30 (22):3637–3644, 2009.

R. J. Green, T. J. Su, J. R. Lu, and J. R. P. Webster. The displacement of preadsorbed protein with a cationic surfactant at the hydrophilic SiO2-water interface. *The Journal of Physical Chemistry B*, 105(38):9331–9338, 2001.

W. M. Grill. Electrical Activation of Spinal Neural Circuits: Application to Motor-System Neural Prostheses. *Neuromodulation*, 3(2):97–106, 2000.

S. M. Gutowski, K. L. Templeman, A. B. South, J. C. Gaulding, J. T. Shoemaker, M. C. LaPlaca, R. V. Bellamkonda, L. A. Lyon, and A. J. García. Host response to microgel coatings on neural electrodes implanted in the brain. *Journal of Biomedical Materials Research Part A*, 2013.

A. S. Hamdy, D. P. Butt, and A. A. Ismail. Electrochemical impedance studies of sol–gel based ceramic coatings systems in 3.5% NaCl solution. *Electrochimica acta*, 52(9):3310–3316, 2007.

U. K. Hanisch, D. van Rossum, Y. Xie, K. Gast, R. Misselwitz, S. Auriola, G. Goldsteins, J. Koistinaho, H. Kettenmann, and T. Moller. The Microglia-activating Potential of Thrombin: THE PROTEASE IS NOT INVOLVED IN THE INDUCTION OF PROINFLAMMATORY CYTOKINES AND CHEMOKINES. *Journal of Biological Chemistry*, 279(50):51880, 2004.

J. P. Harris, J. R. Capadona, R. H. Miller, B. C. Healy, K. Shanmuganathan, S. J. Rowan, C. Weder, and D. J. Tyler. Mechanically adaptive intracortical implants improve the proximity of neuronal cell bodies. *Journal of neural engineering*, 8(6):66011, 2011.

W. He and R. V. Bellamkonda. *Indwelling Neural Implants*, chapter A Molecula, pages 151–175. Frontiers in Neuroengineering. CRC, 2008.

W. He, G. C. McConnell, and R. V. Bellamkonda. Nanoscale laminin coating modulates cortical scarring response around implanted silicon microelectrode arrays. *J Neural Eng*, 3:316–326, 2006.

W. He, G. C. McConnell, T. M. Schneider, and R. V. Bellamkonda. A novel anti-inflammatory surface for neural electrodes. *Advanced Materials*, 19(21):3529, 2007.

C. H. Heldin. Structural and functional studies on platelet-derived growth factor. *EMBO J*, 11(12):4251–4259, 1992.

M. J. Heller. DNA microarray technology: devices, systems, and applications. *Annual review of biomedical engineering*, 4(1):129–153, 2002.

J. F. Hetke and D. J. Anderson. *Handbook of Neuroprosthetic Methods*, chapter Silicon mi, pages 163–191. CRC, 2002.

M. Hoa, Z. Guan, G. Auner, and J. Zhang. Tonotopic responses in the inferior colliculus following electrical stimulation of the dorsal cochlear nucleus of guinea pigs. *Otolaryngology–Head and Neck Surgery*, 139(1):152–155, 2008.

L. R. Hochberg, M. D. Serruya, G. M. Friehs, J. A. Mukand, M. Saleh, A. H. Caplan, A. Branner, D. Chen, R. D. Penn, and J. P. Donoghue. Neuronal ensemble control of prosthetic devices by a human with tetraplegia. *Nature*, 442: 164–171, 2006.

J. D. Holladay, J. Hu, D. L. King, and Y. Wang. An overview of hydrogen production technologies. *Catalysis Today*, 139(4):244–260, 2009.

S. In, N. Congdon, B. O'Colmain, C. C. Klaver, R. Klein, B. Munoz, D. S. Friedman, J. Kempen, H. R. Taylor, and P. Mitchell. Causes and Prevalence of Visual Impairment Among Adults in the United States. *Archives of Ophthalmology*, 122(4):477–485, 2004.

C. D. James, R. Davis, M. Meyer, A. Turner, S. Turner, G. Withers, L. Kam, G. Banker, H. G. Craighead, M. Issacson, and Others. Aligned microcontact printing of micrometer-scale poly-L-Lysinestructures for controlled growth of cultured neurons on planar microelectrode arrays. *Biomedical Engineering, IEEE Transactions on*, 47(1):17–21, 2000.

S. S. Jedlicka, J. L. McKenzie, S. J. Leavesley, K. M. Little, T. J. Webster, J. P. Robinson, D. E. Nivens, and J. L. Rickus. Sol-gel derived materials as substrates for neuronal differentiation: effects of surface features and protein conformation. *Journal of Materials Chemistry*, 16(31):3221–3230, 2006.

S. S. Jedlicka, K. M. Little, D. E. Nivens, D. Y. Zemlyanov, and J. L. Rickus. Peptide ormosils as cellular substrates. *Journal of Materials Chemistry*, 17 (48):5058–5067, 2007a.

S. S. Jedlicka, J. L. Rickus, and D. Y. Zemlyanov. Surface analysis by X-ray photoelectron spectroscopy of sol-gel silica modified with covalently bound peptides. *The journal of physical chemistry. B*, 111(40):11850–7, Oct. 2007b.

M. D. Johnson, K. J. Otto, and D. R. Kipke. Repeated voltage biasing improves unit recordings by reducing resistive tissue impedances. *Neural Systems and Rehabilitation Engineering, IEEE Transactions on*, 13(2):160–165, 2005.

L. Kam, W. Shain, J. N. Turner, and R. Bizios. Selective adhesion of astrocytes to surfaces modified with immobilized peptides. *Biomaterials*, 23(2):511–515, 2002.

L. Karumbaiah, S. E. Norman, N. B. Rajan, S. Anand, T. Saxena, M. Betancur, R. Patkar, and R. V. Bellamkonda. The upregulation of specific interleukin (IL) receptor antagonists and paradoxical enhancement of neuronal apoptosis due to electrode induced strain and brain micromotion. *Biomaterials*, 33(26):5983–5996, 2012.

L. Karumbaiah, T. Saxena, D. Carlson, K. Patil, R. Patkar, E. A. Gaupp, M. Betancur, G. B. Stanley, L. Carin, and R. V. Bellamkonda. The impact of chronic blood–brain barrier breach on intracortical electrode function. *Biomaterials*, 34(33):8061–8074, 2013.

C. Kaur, A. J. Hao, C. H. Wu, and E. A. Ling. Origin of microglia. *Microscopy Research and Technique*, 54(1):2–9, 2001.

E. W. Keefer, B. R. Botterman, M. I. Romero, A. F. Rossi, and G. W. Gross. Carbon nanotube coating improves neuronal recordings. *Nature nanotechnology*, 3(7):434–439, 2008.

H. Kettenmann and B. R. Ransom. *Neuroglia*. Oxford University Press, USA, 2005.

D. H. Kim and D. C. Martin. Sustained release of dexamethasone from hydrophilic matrices using PLGA nanoparticles for neural drug delivery. *Biomaterials*, 27(15):3031–3037, 2006.

D. R. Kipke, R. J. Vetter, J. C. Williams, and J. F. Hetke. Silicon-substrate intracortical microelectrode arrays for long-term recording of neuronal spike activity in cerebral cortex. *Neural Systems and Rehabilitation Engineering, IEEE Transactions on [see also IEEE Trans. on Rehabilitation Engineering]*, 11(2):151–155, 2003.

I. Klatzo. Pathophysiological aspects of brain edema. *Acta Neuropathologica*, 72(3):236–239, 1987.

A. O. Koob and R. B. Borgens. Polyethylene glycol treatment after traumatic brain injury reduces beta-amyloid precursor protein accumulation in degenerating axons. *Journal of Neuroscience Research*, 83(8):1558–1563, 2006.

A. O. Koob, B. S. Duerstock, C. F. Babbs, Y. Sun, and R. B. Borgens. Intravenous Polyethylene Glycol Inhibits the Loss of Cerebral Cells after Brain Injury. *Journal of Neurotrauma*, 22(10):1092–1111, 2005.

A. O. Koob, J. M. Colby, and R. B. Borgens. Behavioral recovery from traumatic brain injury after membrane reconstruction using polyethylene glycol. *Journal of Biological Engineering*, 2:9, 2008.

T. D. Y. Kozai and D. R. Kipke. Insertion shuttle with carboxyl terminated self-assembled monolayer coatings for implanting flexible polymer neural probes in the brain. *Journal of neuroscience methods*, 184(2):199–205, 2009.

T. D. Y. Kozai, N. B. Langhals, P. R. Patel, X. Deng, H. Zhang, K. L. Smith, J. Lahann, N. A. Kotov, and D. R. Kipke. Ultrasmall implantable composite microelectrodes with bioactive surfaces for chronic neural interfaces. *Nature materials*, 11(12):1065–1073, 2012a.

T. D. Y. Kozai, A. L. Vazquez, C. L. Weaver, S.-G. Kim, and X. T. Cui. In vivo two-photon microscopy reveals immediate microglial reaction to implantation of microelectrode through extension of processes. *Journal of neural engineering*, 9(6):66001, 2012b.

G. W. Kreutzburg. Microglia: A sensor for pathological events in the CNS. *Trends in Neuroscience*, 19:312–318, 1996.

S. Krueger, J. Sievers, C. Hansen, M. Sadler, and M. Berry. Three morphologically distinct types of interface develop between adult host and fetal brain transplants: Implications for scar formation in the adult central nervous system. *The Journal of Comparative Neurology*, 249(1):103–116, 1986.

S. Lehnardt, L. Massillon, P. Follett, F. E. Jensen, R. Ratan, P. A. Rosenberg, J. J. Volpe, and T. Vartanian. Activation of innate immunity in the CNS triggers neurodegeneration through a Toll-like receptor 4-dependent pathway. *Proceedings of the National Academy of Sciences*, 100(14):8514–9, July 2003.

T. Lenarz, H. H. Lim, G. Reuter, J. F. Patrick, and M. Lenarz. The Auditory Midbrain Implant: A New Auditory Prosthesis for Neural Deafness-Concept and Device Description. *Otology & Neurotology*, 27(6):838, 2006.

B. K. Leung, R. Biran, C. J. Underwood, and P. A. Tresco. Characterization of microglial attachment and cytokine release on biomaterials of differing surface chemistry. *Biomaterials*, 29(23):3289–3297, 2008.

E. C. Leuthardt, G. Schalk, J. R. Wolpaw, J. G. Ojemann, and D. W. Moran. A brain-computer interface using electrocorticographic signals in humans. *Journal of neural engineering*, 1(2):63–71, 2004.

D. Lewitus, K. L. Smith, W. Shain, and J. Kohn. Ultrafast resorbing polymers for use as carriers for cortical neural probes. *Acta Biomaterialia*, 7(6):2483–2491, 2011.

G. Li, G. Cui, N. S. Tzeng, S. J. Wei, T. Wang, M. L. Block, and J. S. Hong. Femtomolar concentrations of dextromethorphan protect mesencephalic dopaminergic neurons from inflammatory damage. *The FASEB Journal*, 19(6):489, 2005.

S. Li and J. D. Henry. Nonthrombogenic Approaches to Cardiovascular Bioengineering. July 2011.

P. Liesi and T. Kauppila. Induction of Type IV Collagen and Other Basement-Membrane-Associated Proteins after Spinal Cord Injury of the Adult Rat May Participate in Formation of the Glial Scar. *Experimental Neurology*, 173(1): 31–45, 2002.

G. Lind, C. E. Linsmeier, and J. Schouenborg. The density difference between tissue and neural probes is a key factor for glial scarring. *Scientific reports*, 3, 2013.

E. A. Ling. The origin and nature of microglia. *Advances in Cellular Neurobiology*, 2:33–82, 1981.

X. Liu, D. B. McCreery, R. R. Carter, L. a. Bullara, T. G. H. Yuen, and W. F. Agnew. Stability of the interface between neural tissue and chronically implanted intracortical microelectrodes. *IEEE transactions on Rehabilitation Engineering*, 7(3):315–326, Sept. 1999.

G. E. Loeb. Cochlear Prosthetics. *Annual Reviews in Neuroscience*, 13(1):357–371, 1990.

Y. Lu, D. Wang, T. Li, X. Zhao, Y. Cao, H. Yang, and Y. Y. Duan. Poly(vinyl alcohol)/poly(acrylic acid) hydrogel coatings for improving electrode-neural tissue interface. *Biomaterials*, 30(25):4143–4151, 2009.

K. A. Ludwig, J. D. Uram, J. Yang, D. C. Martin, and D. R. Kipke. Chronic neural recordings using silicon microelectrode arrays electrochemically deposited with a poly(3,4-ethylenedioxythiophene) (PEDOT) film. *Journal of Neural Engineering*, 3(1):59–70, 2006.

K. A. Ludwig, N. B. Langhals, M. D. Joseph, S. M. Richardson-Burns, J. L. Hendricks, and D. R. Kipke. Poly(3,4-ethylenedioxythiophene) (PEDOT) polymer coatings facilitate smaller neural recording electrodes. *Journal of Neural Engineering*, 8(1):14001, 2011.

A. Magnani, R. Barbucci, S. Lamponi, A. Chiumento, A. Paffetti, L. Trabalzini, P. Martelli, and A. Santucci. Two-step elution of human serum proteins from different glass-modified bioactive surfaces: A comparative proteomic analysis of adsorption patterns. *Electrophoresis*, 25(14):2413–2424, 2004.

E. Maisonhaute, B. A. Brookes, and R. G. Compton. Surface acoustic cavitation understood via nanosecond electrochemistry. 2. The motion of acoustic bubbles. *The Journal of Physical Chemistry B*, 106(12):3166–3172, 2002a.

E. Maisonhaute, C. Prado, P. C. White, and R. G. Compton. Surface acoustic cavitation understood via nanosecond electrochemistry. Part III: Shear stress in ultrasonic cleaning. *Ultrasonics sonochemistry*, 9(6):297–303, 2002b.

R. U. Margolis and R. K. Margolis. Distribution and metabolism of mucopolysaccharides and glycoproteins in neuronal perikarya, astrocytes, and oligodendroglia. *Biochemistry*, 13(14):2849–2852, 1974.

N. T. Markwardt, J. Stokol, and R. L. R. Ii. Sub-meninges implantation reduces immune response to neural implants. *Journal of neuroscience methods*, 2013.

S. P. Massia, M. M. Holecko, and G. R. Ehteshami. In vitro assessment of bioactive coatings for neural implant applications. *Journal of Biomedical Materials Research*, 68(1):177–186, Jan. 2004.

E. M. Maynard. Visual Prostheses. *Annual Reviews in Biomedical Engineering*, 3(1):145–168, 2001.

G. C. McConnell, T. M. Schneider, and R. V. Bellamkonda. Acute spatiotemporal changes in neuronal density surrounding microelectrode arrays implanted in rat motor cortex. In *Neural Engineering, 2007. CNE'07. 3rd International IEEE/EMBS Conference on*, pages 137–140. IEEE, 2007.

R. J. McKeon, M. J. Jurynec, and C. R. Buck. The chondroitin sulfate proteoglycans neurocan and phosphacan are expressed by reactive astrocytes in the chronic CNS glial scar. *The Journal of Neuroscience*, 19(24):10778–10788, 1999.

R. Michel, S. Pasche, M. Textor, and D. G. Castner. Influence of PEG architecture on protein adsorption and conformation. *Langmuir : the ACS journal of surfaces and colloids*, 21(26):12327–32, Dec. 2005.

R. Mohle, D. Green, M. A. S. Moore, R. L. Nachman, and S. Rafii. Constitutive production and thrombin-induced release of vascular endothelial growth factor by human megakaryocytes and platelets. *Proceedings of the National Academy of Sciences*, 94(2):663, 1997.

P. E. Mohr, J. J. Feldman, J. L. Dunbar, A. McConkey-Robbins, J. K. Niparko, R. K. Rittenhouse, and M. W. Skinner. The Societal Costs of severe to profound hearing loss in the United States. *International Journal of Technology Assessment in Health Care*, 16(04):1120–1135, 2001.

T. Moller, U. K. Hanisch, and B. R. Ransom. Thrombin-Induced Activation of Cultured Rodent Microglia. *Journal of Neurochemistry*, 75(4):1539–1547, 2000.

L. Muthusubramaniam, R. Lowe, W. H. Fissell, L. Li, R. E. Marchant, T. A. Desai, and S. Roy. Hemocompatibility of silicon-based substrates for biomedical implant applications. *Annals of biomedical engineering*, 39(4):1296–305, Apr. 2011.

E. J. H. Nathaniel and D. R. Nathaniel. The reactive astrocyte. *Adv Cell Neurobiol*, 2:249–301, 1981.

M. A. Nicolelis. Brain-machine interfaces to restore motor function and probe neural circuits. *Nat Rev Neurosci*, 4(5):417–422, 2003.

M. A. L. Nicolelis, D. Dimitrov, J. M. Carmena, R. Crist, G. Lehew, J. D. Kralik, and S. P. Wise. Chronic, multisite, multielectrode recordings in macaque monkeys. *Proceedings of the National Academy of Sciences*, 100(19):11041, 2003.

Y. Niu, A. Kumaraguru, R. Wang, and W. Sun. Hyperexcitability of inferior colliculus neurons caused by acute noise exposure. *Journal of neuroscience research*, 91(2):292–299, 2013.

M. Noble, J. Fok-Seang, and J. Cohen. Glia are a unique substrate for the in vitro growth of central nervous system neurons. *The Journal of neuroscience*, 4(7):1892–1903, 1984.

R. A. Normann, E. M. Maynard, P. J. Rousche, and D. J. Warren. A neural interface for a cortical vision prosthesis. *Vision Research*, 39(15):2577–2587, 1999.

W. T. Norton, T. Abe, S. E. Poduslo, and G. H. DeVries. The lipid composition of isolated brain cells and axons. *Journal of neuroscience research*, 1(1):57–75, 1975.

W. T. Norton, D. A. Aquino, I. Hozumi, F. C. Chiu, and C. F. Brosnan. Quantitative aspects of reactive gliosis: A review. *Neurochemical Research*, 17(9): 877–885, 1992.

J. S. O'Brien and E. L. Sampson. Lipid composition of the normal human brain: gray matter, white matter, and myelin. *Journal of lipid research*, 6(4): 537–544, 1965.

E. Okun, K. J. Griffioen, and M. P. Mattson. Toll-like receptor signaling in neural plasticity and disease. *Trends in neurosciences*, 34(5):269–281, 2011.

K. J. Otto, P. J. Rousche, and D. R. Kipke. Microstimulation in auditory cortex provides a substrate for detailed behaviors. *Hearing Research*, 210(1-2):112–117, 2005.

K. J. Otto, M. D. Johnson, and D. R. Kipke. Voltage pulses change neural interface properties and improve unit recordings with chronically implanted microelectrodes. *Biomedical Engineering, IEEE Transactions on*, 53(2):333–340, 2006.

E. Papavassiliou, N. Gogate, M. Proescholdt, J. D. Heiss, S. Walbridge, N. A. Edwards, E. H. Oldfield, and M. J. Merrill. Vascular Endothelial Growth Factor (Vascular Permeability Factor) Expression in Injured Rat Brain. *Journal of Neuroscience Research*, 49:451–460, 1997.

D. C. Pease. Polysaccharides associated with the exterior surface of epithelial cells: kidney, intestine, brain. *Journal of ultrastructure research*, 15(5):555–588, 1966.

M. Pekny and M. Nilsson. Astrocyte activation and reactive gliosis. *Glia*, 50 (4):427–434, 2005.

A. Pepe, P. Galliano, M. Aparicio, A. Durán, and S. Ceré. Sol-gel coatings on carbon steel: Electrochemical evaluation. *Surface and Coatings Technology*, 200(11):3486–3491, 2006.

A. L. Pierce, S. Sommakia, J. L. Rickus, and K. J. Otto. Thin-film silica sol-gel coatings for neural microelectrodes. *Journal of neuroscience methods*, 180(1): 106–110, May 2009.

V. S. Polikov, P. A. Tresco, and W. M. Reichert. Response of brain tissue to chronically implanted neural electrodes. *Journal of Neuroscience Methods*, 148 (1):1–18, Oct. 2005.

V. S. Polikov, M. L. Block, J.-M. M. Fellous, J.-S. S. Hong, and W. M. Reichert. In vitro model of glial scarring around neuroelectrodes chronically implanted in the CNS. *Biomaterials*, 27(31):5368–5376, Nov. 2006.

V. S. Polikov, E. C. Su, M. A. Ball, J.-S. Hong, and W. M. Reichert. Control protocol for robust in vitro glial scar formation around microwires: Essential roles of bFGF and serum in gliosis. *Journal of Neuroscience Methods*, 181(2): 170–177, 2009.

K. A. Potter, A. C. Buck, W. K. Self, M. E. Callanan, S. Sunil, and J. R. Capadona. The effect of resveratrol on neurodegeneration and blood brain barrier stability surrounding intracortical microelectrodes. *Biomaterials*, 2013.

A. Prasad and J. C. Sanchez. Quantifying long-term microelectrode array functionality using chronic in vivo impedance testing. *Journal of Neural Engineering*, 9(2):026028, Apr. 2012.

A. Prasad, Q.-S. Xue, V. Sankar, T. Nishida, G. Shaw, W. J. Streit, and J. C. Sanchez. Comprehensive characterization and failure modes of tungsten microwire arrays in chronic neural implants. *Journal of neural engineering*, 9(5), Oct. 2012.

D. Purves, G. Augustine, D. Fitzpatrick, W. Hall, A.-S. LaMantia, and L. White. *Neuroscience*. Sinauer Associates, Sunderland, Mass., 1997.

L. Qin, G. Li, X. Qian, Y. Liu, X. Wu, B. Liu, J.-S. Hong, and M. L. Block. Interactive role of the toll-like receptor 4 and reactive oxygen species in LPS-induced microglia activation. *Glia*, 52(1):78–84, 2005.

S. Radin and P. Ducheyne. Controlled release of vancomycin from thin sol-gel films on titanium alloy fracture plate material. *Biomaterials*, 28(9):1721–1729, 2007.

S. Radin, T. Chen, and P. Ducheyne. The controlled release of drugs from emulsified, sol gel processed silica microspheres. *Biomaterials*, 30(5):850–858, 2009.

H. Rakuman, W. Ferose, X. C. Ong, H. S. Tetikol, R. Khilwani, X. T. Cui, O. B. Ozdoganlar, G. K. Fedder, and P. J. Gilgunn. Ultra-compliant neural probes are subject to fluid forces during dissolution of polymer delivery vehicles. In *Engineering in Medicine and Biology Society (EMBC), 2013 35th Annual International Conference of the IEEE*, pages 1550–1553. IEEE, 2013.

M. S. Ramer, M. S.B., and J. V. Priestly. *Glial Cell Function*, chapter Axon regen, pages 621–639. Elsevier, 2001.

S. S. Rao, N. Han, and J. O. Winter. Polylysine-modified PEG-based hydrogels to enhance the neuro-electrode interface. *Journal of biomaterials science. Polymer edition*, 22(4-6):611–25, Jan. 2011.

M. Ravikumar, D. J. Hageman, W. H. Tomaszewski, G. M. Chandra, J. L. Skousen, J. R. Capadona, and Others. The Effect of Residual Endotoxin Contamination on the Neuroinflammatory Response to Sterilized Intracortical Microelectrodes. *J. Mater. Chem. B*, 2013.

S. M. Richardson-Burns, J. L. Hendricks, and D. C. Martin. Electrochemical polymerization of conducting polymers in living neural tissue. *Journal of Neural Engineering*, 4:L6, 2007.

L. S. Robblee, J. L. Lefko, and S. B. Brummer. Activated Ir: An Electrode Suitable for Reversible Charge Injection in Saline Solution. *Journal of The Electrochemical Society*, 130:731, 1983.

P. J. Rousche and R. A. Normann. Chronic recording capability of the Utah Intracortical Electrode Array in cat sensory cortex. *Journal of Neuroscience Methods*, 82(1):1–15, 1998.

P. J. Rousche, D. S. Pellinen, D. P. Pivin Jr, J. C. Williams, R. J. Vetter, D. P. Pivin, and D. R. Kipke. Flexible polyimide-based intracortical electrode arrays withbioactive capability. *Biomedical Engineering, IEEE Transactions on*, 48 (3):361–371, Mar. 2001.

Z. M. Ruggeri. Platelets in atherothrombosis. *Nat Med*, 8(11):1227–1234, 2002.

H. J. Salacinski, S. Goldner, A. Giudiceandrea, G. Hamilton, A. M. Seifalian, A. Edwards, and R. J. Carson. The mechanical behavior of vascular grafts: a review. *Journal of biomaterials applications*, 15(3):241–278, 2001.

T. Saxena, L. Karumbaiah, E. A. Gaupp, R. Patkar, K. Patil, M. Betancur, G. B. Stanley, and R. V. Bellamkonda. The impact of chronic blood–brain barrier breach on intracortical electrode function. *Biomaterials*, 2013.

L. Schilling and M. Wahl. Brain edema: pathogenesis and therapy. *Kidney International. Supplement*, 59:S69—-75, 1997.

L. Schilling and M. Wahl. Mediators of cerebral edema. *Advances in Experimental Medicine and Biology*, 474:123–141, 1999.

A. B. Schwarz. Cortical Neural Prosthetics. *Annual Review of Neuroscience*, 27:487–507, July 2004.

J. P. Seymour and D. R. Kipke. Neural probe design for reduced tissue encapsulation in CNS. *Biomaterials*, 28(25):3594–3607, 2007.

S. Sharma, R. W. Johnson, and T. A. Desai. Evaluation of the stability of nonfouling ultrathin poly(ethylene glycol) films for silicon-based microdevices. *Langmuir : the ACS journal of surfaces and colloids*, 20(2):348–56, Jan. 2004a.

S. Sharma, R. W. Johnson, and T. A. Desai. XPS and AFM analysis of antifouling PEG interfaces for microfabricated silicon biosensors. *Biosensors & bioelectronics*, 20(2):227–39, Sept. 2004b.

M. S. Shoichet, C. C. Tate, M. D. Baumann, and M. C. LaPlaca. *Indwelling Neural Implants: Strategies for Contending with the In Vivo Environment*, chapter Strategies for Regeneration and Repair in the Injured Central Nervous System. CRC Press, Boca Raton (FL), 2008.

J. L. Skousen, S. M. E. Merriam, O. Srivannavit, G. Perlin, K. D. Wise, and P. A. Tresco. Reducing surface area while maintaining implant penetrating profile lowers the brain foreign body response to chronically implanted planar silicon microelectrode arrays. *Progress in Brain Research*, 194:167, 2011.

G. M. Smith, U. Rutishauser, J. Silver, and R. H. Miller. Maturation of astrocytes in vitro alters the extent and molecular basis of neurite outgrowth. *Developmental biology*, 138(2):377–390, 1990.

R. L. Snyder, B. H. Bonham, and D. G. Sinex. Acute changes in frequency responses of inferior colliculus central nucleus (ICC) neurons following progressively enlarged restricted spiral ganglion lesions. *Hearing research*, 246 (1):59–78, 2008.

S. Sommakia, J. L. Rickus, and K. J. Otto. Effects of adsorbed proteins, an antifouling agent and long-duration DC voltage pulses on the impedance of silicon-based neural microelectrodes. In *Proceedings of the IEEE Engineering in Medicine and Biology Conference*, volume 2009, pages 7139–42. IEEE, Jan. 2009.

L. Spataro, J. Dilgen, S. Retterer, A. J. Spence, M. Isaacson, J. N. Turner, and W. Shain. Dexamethasone treatment reduces astroglia responses to inserted neuroprosthetic devices in rat neocortex. *Experimental Neurology*, 194(2):289–300, 2005.

O. Sporns, G. M. Edelman, K. L. Crossin, L. A. Krushel, and B. A. Cunningham. The neural cell adhesion molecule (N-CAM) inhibits proliferation in primary cultures of rat astrocytes. *Proceedings of the National Academy of Sciences of the United States of America*, 92(10):4323, 1995.

P. M. St. John, L. Kam, S. W. Turner, H. G. Craighead, M. Issacson, J. N. Turner, and W. Shain. Preferential glial cell attachment to microcontact printed surfaces. *Journal of Neuroscience Methods*, 75(2):171–177, Aug. 1997.

K. F. Standeven, R. A. S. Ariëns, and P. J. Grant. The molecular physiology and pathology of fibrin structure/function. *Blood Reviews*, 19(5):275–288, 2005.

W. R. Stauffer and X. T. Cui. Polypyrrole doped with 2 peptide sequences from laminin. *Biomaterials*, 27(11):2405–2413, 2006.

S. S. Stensaas and L. J. Stensaas. The reaction of the cerebral cortex to chronically implanted plastic needles. *Acta Neuropathol*, 35(3):187–203, 1976.

T. Stieglitz, M. Schuettler, J.-U. Meyer, et al. Micromachined, polyimide-based devices for flexible neural interfaces. *Biomedical Microdevices*, 2(4):283–294, 2000.

F. Strumwasser. Long-Term Recording from Single Neurons in Brain of Unrestrained Mammals. *Science*, 127(3296):469–470, 1958.

H. S. Suidan, C. D. Nobes, A. Hall, and D. Monard. Astrocyte spreading in response to thrombin and lysophosphatidic acid is dependent on the Rho GTPase. *Glia*, 21(2):244–252, 1997.

D. H. Szarowski, M. D. Andersen, S. Retterer, A. J. Spence, M. Isaacson, H. G. Craighead, J. N. Turner, and W. Shain. Brain responses to micro-machined silicon devices. *Brain Research*, 983(1-2):23–35, 2003.

F. Y. Tanga, N. Nutile-McMenemy, and J. A. DeLeo. The CNS role of Toll-like receptor 4 in innate neuroimmunity and painful neuropathy. *Proceedings of the National Academy of Sciences of the United States of America*, 102(16): 5856–5861, 2005.

M. F. Templin, D. Stoll, M. Schrenk, P. C. Traub, C. F. Vöhringer, and T. O. Joos. Protein microarray technology. *Drug Discovery Today*, 7(15):815–822, 2002.

L. W. Tien, F. Wu, M. D. Tang-Schomer, E. Yoon, F. G. Omenetto, and D. L. Kaplan. Silk as a multifunctional biomaterial substrate for reduced glial scarring around brain-penetrating electrodes. *Advanced Functional Materials*, 2013.

K. J. Tomaselli, K. M. Neugebauer, J. L. Bixby, J. Lilien, and L. F. Reichard. N-cadherin and integrins: two receptor systems that mediate neuronal process outgrowth on astrocyte surfaces. *Neuron*, 1(1):33–43, 1988.

G. Townsend, P. Peloquin, F. Kloosterman, J. F. Hetke, and L. S. Leung. Recording and marking with silicon multichannel electrodes. *Brain Research Protocols*, 9(2):122–129, 2002.

J. N. Turner, W. Shain, D. H. Szarowski, M. D. Andersen, S. Martins, M. Isaacson, H. G. Craighead, and M. Issacson. Cerebral Astrocyte Response to Micromachined Silicon Implants. *Experimental Neurology*, 156(1):33–49, 1999.

V. M. Tysseling-Mattiace, V. Sahni, K. L. Niece, D. Birch, C. Czeisler, M. G. Fehlings, S. I. Stupp, and J. A. Kessler. Self-assembling nanofibers inhibit glial scar formation and promote axon elongation after spinal cord injury. *J Neurosci*, 28(14):3814–3823, 2008.

S.-f. Tzeng, H.-y. Huang, T.-i. Lee, and J.-k. Jwo. Inhibition of Lipopolysaccharide-Induced Microglial Activation by Preexposure to Neurotrophin-3. 676:666–676, 2005.

S. Verhaverbeke and K. Christenson. Organic contamination removal. *Contamination-Free Manufacturing for Semiconductors and Other Precision Products*, pages 320–322, 2001.

R. J. Vetter, J. C. Williams, J. F. Hetke, E. A. Nunamaker, and D. R. Kipke. Chronic neural recording using silicon-substrate microelectrode arrays implanted in cerebral cortex. *Biomedical Engineering, IEEE Transactions on*, 51(6):896–904, 2004.

P. Vinaraphong, V. Krisdhasima, and J. McGuire. Elution of proteins from silanized silica surfaces by sodium dodecylsulfate and dodecyltrimethylammonium bromide. *Journal of colloid and interface science*, 174(2):351–360, 1995.

R. Wadhwa, C. F. Lagenaur, and X. T. Cui. Electrochemically controlled release of dexamethasone from conducting polymer polypyrrole coated electrode. *Journal of Controlled Release*, 110(3):531–541, 2006.

M. Wahl, A. Unterberg, A. Baethmann, and L. Schilling. Mediators of blood-brain barrier dysfunction and formation of vasogenic brain edema. *Journal of Cerebral Blood Flow & Metabolism Blood Flow Metab*, 8(5):621–634, 1988.

S. J. Wilks, S. M. Richardson-Burns, J. L. Hendricks, D. C. Martin, and K. J. Otto. Poly (3, 4-ethylenedioxythiophene) as a micro-neural interface material for electrostimulation. *Frontiers in Neuroengineering*, 2, 2009.

D. F. Williams, I. N. Askill, and R. Smith. Protein adsorption and desorption phenomena on clean metal surfaces. *Journal of Biomedical Materials Research*, 19(3):313–320, 1985.

J. C. Williams, R. L. Rennaker, and D. R. Kipke. Long-term neural recording characteristics of wire microelectrode arrays implanted in cerebral cortex. *Brain Research Protocols*, 4(3):303–313, 1999.

J. C. Williams, J. A. Hippensteel, J. Dilgen, W. Shain, and D. R. Kipke. Complex impedance spectroscopy for monitoring tissue responses to inserted neural implants. *Journal of Neural Engineering*, 4(4):410–423, 2007.

J. O. Winter, S. F. Cogan, and J. F. Rizzo. Neurotrophin-eluting hydrogel coatings for neural stimulating electrodes. *Journal of Biomedical Materials Research. Part B, Applied biomaterials*, 81(2):551–563, 2007.

K. D. Wise, J. B. Angell, and A. Starr. An integrated-circuit approach to extracellular microelectrodes. *IEEE Trans Biomed Eng*, 17(3):238–247, 1970.

A. J. Woolley, H. A. Desai, M. A. Steckbeck, N. K. Patel, and K. J. Otto. In situ characterization of the brain-microdevice interface using device-capture histology. *Journal of neuroscience methods*, 201(1):67–77, Sept. 2011.

A. J. Woolley, H. A. Desai, J. Gaire, A. L. Ready, and K. J. Otto. Intact histological characterization of brain-implanted microdevices and surrounding tissue. *Journal of visualized experiments : JoVE*, 72(15), 2012.

A. J. Woolley, H. A. Desai, and K. J. Otto. Chronic intracortical microelectrode arrays induce non-uniform, depth-related tissue responses. *Journal of neural engineering*, 10(2):026007, Feb. 2013.

Y. Wu, Q. Zheng, J. Du, Y. Song, B. Wu, and X. Guo. Self-assembled IKVAV peptide nanofibers promote adherence of PC12 cells. *Journal of Huazhong University of Science and Technology, Medical*, 26(5):594–596, 2006.

J. Yang and D. C. Martin. Microporous conducting polymers on neural microelectrode arrays II. Physical characterization. *Sensors & Actuators: A. Physical*, 113(2):204–211, 2004.

T. T. Yu and M. S. Shoichet. Guided cell adhesion and outgrowth in peptide-modified channels for neural tissue engineering. *Biomaterials*, 26(13):1507–1514, 2005.

T. G. H. Yuen and W. F. Agnew. Histological evaluation of polyesterimide-insulated gold wires in brain. *Biomaterials*, 16(12):951–956, 1995.

J. O. Zerbino, N. R. de Tacconi, and A. J. Arvia. The activation and deactivation of iridium electrodes in acid electrolytes. *Journal of The Electrochemical Society*, 125(8):1266–1276, 1978.

Z. Zhang, R. Yoo, M. Wells, T. P. Beebe, R. Biran, and P. A. Tresco. Neurite outgrowth on well-characterized surfaces: preparation and characterization of chemically and spatially controlled fibronectin and RGD substrates with good bioactivity. *Biomaterials*, 26(1):47–61, 2005.

Y. Zhong and R. V. Bellamkonda. Controlled release of anti-inflammatory agent α-MSH from neural implants. *Journal of Controlled Release*, 106(3): 309–318, 2005.

Y. Zhong and R. V. Bellamkonda. Dexamethasone-coated neural probes elicit attenuated inflammatory response and neuronal loss compared to uncoated neural probes. *Brain Research*, 1148:15–27, 2007.

VITA

VITA

Salah Sommakia

Education

- Ph.D., Biomedical Engineering, Purdue University, 2013.
  - *Dissertation:* "Effects of Dip-Coated Films on the Properties of Implantable Intracortical Microelectrodes".
  - *Advisors:* Kevin J. Otto and Jenna L. Rickus.
- M.S., Biomedical Engineering, Rutgers University, 2007.
  - *Thesis:* "Electrical and Topographical Characterization of Thin Film Transistors based on a novel organic semiconductor for Biosensing Applications".
  - *Advisor:* Yves J. Chabal
- B.S., Electronic Engineering/Computer Engineering, University of Aleppo, Syria, 2005.

Teaching Experience

- BME595: Regulatory Compliance for Medical Devices — Fall 2013
- BME405: Senior Design Laboratory — Spring 2008, Spring 2012
- BME305: Bioinstrumentation Laboratory — Fall 2007, Fall 2011
- BME206: Biomaterials & Biomechanics Laboratory — Spring 2011

Publications

- **S. Sommakia**, J.L. Rickus, , and K.J. Otto "DC voltage biasing for the restoration of electrode impedance of neural microelectrodes", In Preparation
- **S. Sommakia**, J.L. Rickus, , and K.J. Otto "Polyethylene glycol preserves electrical properties of neural microelectrodes and modulates glial response to foreign objects *in vitro*" *Journal of Neural Engineering*. In revision.

- **S. Sommakia**, J.L. Rickus, , and K.J. Otto "Effects of adsorbed proteins, an antifouling agent long-duration DC voltage pulses on the impedance of silicon-based neural microelectrodes." *Proceedings of the 31st Annual IEEE EMBC International Conference*. 2009.
- A.L. Pierce, **S. Sommakia**, J.L. Rickus, , and K.J. Otto "Thin-film silica sol-gel coatings for neural microelectrodes." *Journal of Neuroscience Methods*, Vol. 180(1):106-10, 2009.

Awards & Invited Talks

- Bilsland Dissertation Fellowship, 2012–2013
- Purdue Research Foundation (PRF) Fellowship, 2008–2009.
- Joe Bourland Travel Award to attend BMES Annual Fall Meeting 2008.
- 2nd place, Best Oral Presentation at 1st IBE regional conference, 2009, West Lafayette, IN.
- **S. Sommakia**, J.L. Rickus, K.J. Otto, "Effects of adsorbed proteins, an antifouling agent and long-duration DC voltage pulses on the impedance of silicon-based neural microelectrodes". Podium Presentation, 31st Annual IEEE EMBC International Conference, September 2009, Minneapolis, MN.
- **S. Sommakia**, J.L. Kuske, S.L. Voytik-Harbin, J.L. Rickus, K.J. Otto. "An in vitro brain injury model for implantable neural prostheses". Podium Presentation, BMES Annual Fall Meeting, October 2008, St. Louis, MO

Poster Presentations

- **S. Sommakia**, J.L. Rickus, K.J. Otto, "Quantitative Assessment of Effects of Poly(ethylene Glycol) on Responses of Primary Cortical Cells to Microwire In Vitro". Poster presentation, October 2011, BMES Annual Fall Meeting, Hartford, CT.
- **S. Sommakia**, J.L. Rickus, K.J. Otto, "Poly(ethylene glycol) as a neurointegrative treatment for intracortical microelectrodes". Poster presentation. 3rd Annual meeting of the Indiana Clinical and Translational Sciences Institute (CTSI), April 2011, Indianapolis, IN.
- **S. Sommakia**, J.L. Rickus, K.J. Otto, "Cellular response of mixed cortical primary cultures to PEG, sol-gel silica coated microwire". Poster Presentation, Society for Neuroscience Annual Meeting, November 2010, San Diego, CA.
- **S. Sommakia**, J.L. Rickus, K.J. Otto, "Potential strategy for the modulation of protein adsorption onto neural microelectrodes". Poster Presen-

tation, Society for Neuroscience Annual Meeting, October 2009, Chicago, IL.

- **S. Sommakia**, A.L. Pierce, J.L. Rickus, K.J. Otto. "Novel silica sol-gel thin film coatings for implantable neural electrodes". Neural Interfaces Conference, June 2008, Cleveland, OH.
- **S. Sommakia**, A.L. Pierce, J.L. Rickus, K.J. Otto. "Validation and Characterization of silica-sol gel coated implantable neural probes". Sigma Xi Annual Poster Competition, Purdue University. February 2008.

Professional Activities

- Biomedical Engineering Society: 2008–present
- Society for Neuroscience: 2009–present